

**UCGE Reports
Number 20341**

Department of Geomatics Engineering

**Remote sensing-based determination of deciduous and
understory phenology over boreal forest**

(URL: <http://www.geomatics.ucalgary.ca/graduatetheses>)

by

Kazi Mahmudur Rahman

September 2011



UNIVERSITY OF CALGARY

Remote sensing-based determination of deciduous and understory phenology

over boreal forest

by

Kazi Mahmudur Rahman

A THESIS

SUBMITTED TO THE FACULTY OF GRADUATE STUDIES

IN PARTIAL FULFILMENT OF THE REQUIREMENTS FOR THE

DEGREE OF MASTER OF SCIENCE

DEPARTMENT OF GEOMATICS ENGINEERING

CALGARY, ALBERTA

SEPTEMBER, 2011

© Kazi Mahmudur Rahman 2011

Abstract

Phenology of the deciduous trees and understory grasses are the vegetation developmental stages influenced by the climatic variables. The study of the deciduous and understory phenology is important in understanding plant growth, net ecosystem CO₂ exchange, forest flammability, forest hydrology, risk of insect infestation, etc. The objective of the study was to determine the phenological stages of deciduous [i.e., deciduous leaf out (DLO), deciduous leaf fall (DLF)] and understory grass green-up [i.e., green grass stage (GGS)] over the boreal forested region in the Canadian province of Alberta. In this study, the MODIS-based 8-day: (i) surface temperature (T_S)-images to derive the equivalent air temperature (\bar{T}_a ; used to determine DLF), (ii) surface reflectances for calculation of normalized difference water index (NDWI: used to determine DLO and GGS) and (iii) accumulated growing degree days (AGDD: a favourable temperature regime for plant growth: used to determine DLO and GGS). The temporal dynamics of AGDD, \bar{T}_a and NDWI was analysed, in conjunction with *in-situ* DLO, DLF and GGS observations in determining the optimal thresholds for DLO in 2006 (i.e., 80 degree-days and NDWI 0.325), DLF in 2006-2007 (i.e., 4 °C) and GGS in 2006 (i.e., 90 degree-days and NDWI 0.45). The implementation of these thresholds revealed reasonable agreements [i.e., on an average (91.9% of the DLO and 94.2% of the GGS for AGDD) and (65% of both DLO and GGS for NDWI) within ± 2 periods or ± 16 days of deviations during 2007-2008; and 77.4% of the DLF for \bar{T}_a within same deviations during 2008)] with compare to the *in-situ* observed data.

Preface

In the scope of this thesis, I have developed methods in determining the deciduous and understory vegetation phenological stages over the boreal forested regions in Alberta. Some of the findings of this research were highlighted in the following publications:

Peer-reviewed Journal Article

- [1] Rahman, K. M., and Hassan, Q. K. 2011. Applicability of remote sensing-based surface temperature regimes in determining the deciduous phenology over boreal forest. *Journal of Plant Ecology*, [In review].

Abstract

- [2] Rahman, K. M., Hassan, Q. K., Sekhon, N. S. 2011. Use of remote sensing in delineating deciduous phenology. *CGU-CSAFM 2011 Scientific Meeting held on May 15-18, 2011 at Banff, AB, Canada.*

Acknowledgements

I have had the good fortune to have enormous guidance from my supervisor, Dr. Quazi K. Hassan where his enormous support, ideas, motivation and helpful instructions gave me to make the successful completion of my thesis work. I am also thankful to my co-supervisor, Dr. Anis Haque for his cooperation. I am very happy to have the members of examining committee, Dr. Janaka Ruwanpura, Dr. Michael Collins, and Dr. Gopal Achari in my thesis defence and would like to thank them for their valuable time and the discerning input to my thesis work.

I would like to acknowledge the different financial supports of: (i) Dr. Quazi K. Hassan's various research grants, (ii) Faculty of Graduate Studies Scholarship Award, (iii) Differential fees and Teaching Assistantships, and (iv) the travel grant of Schulich School of Engineering to attend a conference.

I am very much grateful and would like to thank the following agencies for providing the data free of charge: (i) NASA for providing MODIS data; (ii) Alberta Sustainable Resource Development for providing *in-situ* vegetation phenological observation data; and (iii) Environment Canada for providing air temperature data.

I am lucky to have many wonderful friends in my "Earth Observation for Environment Laboratory" group and thankful to all the group members for their support. I also want to thank to my beloved family members for their encouragement and greatly appreciated

and pleased to my dear wife, Musa. Shammi Akther for her enormous help and inspiration during the program to make it achievable. .

Dedication

To the loving memory

of

My Parents

Table of Contents

Approval Page.....	ii
Abstract.....	iii
Preface.....	iv
Acknowledgements.....	v
Dedication.....	vii
Table of Contents.....	viii
List of Tables.....	x
List of Figures and Illustrations.....	xii
List of Symbols.....	xv
List of Abbreviations and Nomenclature.....	xvi
CHAPTER 1: INTRODUCTION.....	1
1.1 Background.....	1
1.2 Vegetation phenology.....	2
1.3 Problem statement.....	4
1.4 Research objectives.....	5
1.5 Thesis structure.....	5
CHAPTER 2: LITERATURE REVIEW.....	7
2.1 Definition of the deciduous phenological stages.....	7
2.2 Definition of the understory grass green-up phenological stages.....	8
2.3 Factors influencing the vegetation phenology.....	8
2.4 Methods of determining deciduous phenology.....	9
2.5 Methods of determining understory phenology.....	15
2.6 Description of MODIS data.....	19
CHAPTER 3: STUDY AREA AND DATA REQUIREMENTS.....	22
3.1 Description of the study area.....	22
3.2 Data requirements.....	28
3.2.1 Satellite data.....	28
3.2.2 In-situ phenological and air temperature data.....	28
CHAPTER 4: METHODOLOGY.....	31
4.1 Data pre-processing.....	33
4.1.1 In-situ phenological and air temperature data.....	33
4.1.2 Satellite data.....	34
4.1.2.1 Data downloading.....	34
4.1.2.2 Data Reprojection.....	35
4.1.2.3 Image Mosaicking.....	37
4.1.2.4 Generating EVI maps.....	38
4.1.2.5 Generating NDWI maps.....	39
4.1.2.6 Correcting cloud contamination of the satellite images.....	39
4.1.2.7 Generating GDD maps.....	40

4.2. Determining threshold for DLO, DLF and GGS.....	42
4.2.1 Determining threshold for DLO and GGS.....	42
4.2.2 Determining threshold for DLF.....	43
4.3 Validation	44
4.4 Generating spatial dynamics for DLO, DLF and GGS	44
 CHAPTER 5: RESULTS AND DISCUSSION.....	 45
5.1 Relation between MODIS-based T_s and air temperature.....	45
5.2 Determination of thresholds values and its validation.....	46
5.2.1 Determination of the threshold-value for DLO.....	46
5.2.1.1 Determination of AGDD threshold for DLO and its validation.....	46
5.2.1.2 Determination of NDWI threshold for DLO and its validation	52
5.2.2 Determination of the temperature threshold for DLF and its validation.....	57
5.2.3 Determination of the threshold-value for GGS.....	62
5.2.3.1 Determination of AGDD threshold for GGS and its validation.....	62
5.2.3.2 Determination of NDWI threshold for GGS and its validation.....	67
5.3 Discussion.....	71
5.4 Spatial dynamics of DLO, DLF and GGS.....	74
5.4.1 Spatial dynamics of DLO.....	75
5.4.2 Spatial dynamics of DLF.....	79
5.4.3 Spatial dynamics of GGS.....	83
 CHAPTER 6: CONCLUSIONS AND FUTURE WORK.....	 87
6.1 Summary.....	87
6.2 Contributions.....	88
6.3 Further considerations.....	88
 REFERENCES.....	 90
 Appendix.....	 106
Appendix-I.....	107
Appendix-II.....	108

List of Tables

Table 2.1: Characteristics of MODIS spectral bands	21
Table 3.1: Characteristics of natural regions of Alberta	24
Table 4.1: Time periods of MODIS 8-day composites data	38
Table 5.1: Implementation of different AGDD thresholds in determining the optimal threshold.....	49
Table 5.2: Relation between observed and predicted DLO periods at each of the lookout tower sites during 2007-2008using threshold of 70.....	50
Table 5.3: Relation between observed and predicted DLO periods at each of the lookout tower sites during 2007-2008.....using threshold of 80	51
Table 5.4: Relation between observed and predicted DLO periods at each of the lookout tower sites during 2007-2008.....using threshold of 90	52
Table 5.5: Implementation of different NDWI thresholds in determining the optimal threshold.....	54
Table 5.6: Relation between observed and predicted DLO periods at each of the lookout tower sites during 2007-2008.....using NDWI threshold 0.30	55
Table 5.7: Relation between observed and predicted DLO periods at each of the lookout tower sites during 2007-2008.....using NDWI threshold 0.325	56
Table 5.8: Relation between observed and predicted DLO periods at each of the lookout tower sites during 2007-2008.....using NDWI threshold 0.35	56
Table 5.9: Implementation of different \bar{T}_a thresholds in determining the optimal threshold.....	59
Table 5.10: Relation between observed and predicted DLF periods at each of the lookout tower sites during 2008...using threshold of 3.5 °C.....	60
Table 5.11: Relation between observed and predicted DLF periods at each of the lookout tower sites during 2008...using threshold of 4 °C.....	61
Table 5.12: Relation between observed and predicted DLF periods at each of the lookout tower sites during 2008...using threshold of 4.5 °C.....	61

Table 5.13: Implementation of different AGDD thresholds to determine the best AGDD threshold for predicting GGS during 2006.....	64
Table 5.14: Relation between in-situ observed and AGDD-based predicted GGS periods at eachusing AGDD threshold 75.....	65
Table 5.15: Relation between in-situ observed and AGDD-based predicted GGS periods at eachusing AGDD threshold 90.....	66
Table 5.16: Relation between in-situ observed and AGDD-based predicted GGS periods at eachusing AGDD threshold 105.....	66
Table 5.17: Implementation of different NDWI thresholds to determine the best NDWI threshold for predicting GGS stage during 2006	69
Table 5.18: Relation between <i>in-situ</i> observed and NDWI-based predicted GGS periods at eachusing NDWI threshold 0.40	70
Table 5.19: Relation between <i>in-situ</i> observed and NDWI-based predicted GGS periods at eachusing NDWI threshold 0.45	70
Table 5.20: Relation between <i>in-situ</i> observed and NDWI-based predicted GGS periods at eachusing NDWI threshold 0.50	71

List of Figures and Illustrations

Figure 1.1: The extent of the boreal forest region over Canada	2
Figure 2.1: The spectral reflectance curves of green and dry vegetation and soil along with the spectral wavelengths	11
Figure 3.1: a) Location of Alberta in Canada, b) Natural regions of Alberta	23
Figure 3.2: Location of deciduous stands (i.e., gray shades); and the DLO, DLF lookout tower sites (i.e., black circles)	25
Figure 3.3: Location of forest dominant areas (i.e., gray shades); and the lookout tower sites (i.e., black circles) where GGS	27
Figure 3.4: Location of the Environment Canada weather stations across Alberta, where the daily average air temperatures were	30
Figure 4.1: Schematic diagram of the methodology of determining DLO, DLF and (GGS)	32
Figure 4.2: MODIS T_s in HDF format for the period of 13 (i.e., 97 DOY; within 48 °N and 115 °W)	35
Figure 4.3: MRT Reprojection processing tool box upon up-loading the HDF file as input with the required parameters and	36
Figure 4.4: Process of Mosaicking the reprojected Geo-TIFF image for all the MODIS data and clipping them at the coverage area of Alberta	37
Figure 5.1: (a) Relation between MODIS-based surface temperature and air temperature obtained from Environment Canada in 2006; (b)	46
Figure 5.2: Determination of DLO threshold; (a) an averaged temporal trends of growing degree days (GDD) and accumulated GDD (AGDD) during 2006, (b) relative frequency distribution	48
Figure 5.3: Determination of NDWI threshold for DLO; (a) an average temporal trends of NDWI; (b) relative frequency distribution of NDWI at all of the lookout tower sites	53
Figure 5.4: Determination of DLF threshold; (a) an averaged temporal trends of equivalent 8-day air temperature (\bar{T}_a) during 2006-2007; (b) relative frequency distribution of all of the \bar{T}_a values	58
Figure 5.5: Determination of GGS threshold; (a) an average temporal trends of GDD and AGDD at all of the <i>in-situ</i> lookout tower sites during 2006; (b) relative frequency distribution of AGDD at lookout tower sites	63

Figure 5.6: Determination of NDWI threshold for GGS; (a) an average temporal trends of NDWI at all of the in-situ lookout tower sites in 2006;; (b) relative frequency distribution of NDWI at lookout tower sites.....	68
Figure 5.7: Spatial dynamics for the timing of DLO and its relative frequency during 2006.....	76
Figure 5.8: Spatial dynamics for the timing of DLO and its relative frequency during 2007.....	77
Figure 5.9: Spatial dynamics for the timing of DLO and its relative frequency during 2008.....	78
Figure 5.10: Spatial dynamics for the timing of DLF and its relative frequency, during 2006.....	80
Figure 5.11: Spatial dynamics for the timing of DLF and its relative frequency, during 2007.....	81
Figure 5.12: Spatial dynamics for the timing of DLF and its relative frequency, during 2008.....	82
Figure 5.13: Spatial dynamics for the timing of GGS occurrence and its relative frequency distribution during 2006.....	84
Figure 5.14: Spatial dynamics for the timing of GGS occurrence and its relative frequency distribution during 2007.....	85
Figure 5.15: Spatial dynamics for the timing of GGS occurrence and its relative frequency distribution during 2008.....	86
Figure AII.1: Graphical interface for Mosaicking Geo-TIFF images.....	109
Figure AII.2: Graphical interface for generating layer-stack images.....	111
Figure AII.3: Graphical interface for converting to binary number.....	113
Figure AII.4: Graphical interface for calculating total cloud free number	114
Figure AII.5: Graphical interface for calculating mean & sum of mean deviation	116
Figure AII.6: Graphical interface for calculating average mean deviation	118
Figure AII.7: Graphical interface for estimating the corrected gap-filled pixel values due to cloud contamination.....	120
Figure AII.8: Graphical interface for converting T_s into \bar{T}_a	122

Figure AII.9: Graphical interface for GDD calculation.....	124
Figure AII.10: Graphical interface for enhancing 1 km GDD into 500 m spatial resolution.....	126
Figure AII.11: Graphical interface for cumulative AGDD calculation	128
Figure AII.12: Graphical interface for calculating the stack min on the basis of AGDD threshold	130
Figure AII.13: Graphical interface for indexing on the basis of stack min	132
Figure AII.14: Graphical interface for generating the spatial dynamics for DLO and GGS.....	134
Figure AII.15: Graphical interface for calculating the stack min on the basis of \bar{T}_a threshold.....	136
Figure AII.16: Graphical interface for Indexing on the basis of stack min for DLF.....	138
Figure AII.17: Graphical interface for generating the spatial dynamics for DLF	140
Figure AII.18: Classified map of generating the spatial dynamics	142

List of Symbols

Symbol

\bar{T}_a

ρ

T_a

T_{base}

T_s

Definition

Average air temperature

Surface Reflectance

Air Temperature

Base temperature

Surface Temperature

List of Abbreviations and Nomenclature

Abbreviation	Definition
AGDD	Accumulated growing degree days
ANOVA	One-way analysis of variance
CCB	Coniferous closed bud
CGS	Cured grass stage
CNF	Coniferous needle flush
COB	Coniferous open bud
DCB	Deciduous closed bud
DCC	Deciduous color change
DLO	Deciduous leaf out
DOB	Deciduous open bud
DOY	Day of Year
ETM	Enhanced Thematic Mapper
EVI	Enhanced Vegetation Index
FFMT	Forest Fire Management Terms
GDD	Growing degree days
GGS	Green grass stage
HDF	Hierarchical Data Format
LAI	Leaf area Index
LP DAAC	Land processes distributed active archive center
MIR	Middle-infrared
MODIS	Moderate Resolution Imaging Spectroradiometer
NASA	National Aeronautics and Space Administration
NDVI	Normalized Difference Vegetation Index
NDMI	Normalized difference moisture index
NDSI	Normalized difference snow index
NDWI	Normalized difference water index
NIR	Near infrared
PAR	Photosynthetically active radiation
PFD	Photon flux density
PVI	Perpendicular vegetation index
SAVI	Soil adjusted vegetation index
SGN	Snow gone
SOG	Snow on ground
SPG	Snow patches on ground
SPOT	Satellites Pour l'Observation de la Terre
SR	Simple ratio
SRD	Sustainable Recourse Development
SWIR	Shortwave infrared
TIFF	Tagged Image File Format
TGS	Transition grass stage

UTM
VARI
WDRVI

Universal Transverse Mercator
Visible atmospherically resistant index
Wide dynamic range vegetation index

CHAPTER 1: INTRODUCTION

This chapter describes the introductory information about the research work. Those include brief discussion about background of the study, importance of studying vegetation phenology, problem statement, research objectives, and finally structure of the thesis.

1.1 Background

Canada has approximately 10% of the world's forest, which contains 397.3 million hectares of forest, other wooded land and other land with tree covers. It covers 30% of the world's boreal forest (NRC 2010). The Canadian boreal forest contains approximately 35% of its landmass and 77% of total forested area. Figure 1.1 shows the extent of boreal region (i.e., light gray shades with taiga ecozone and dark gray shades with boreal ecozone) over Canada.

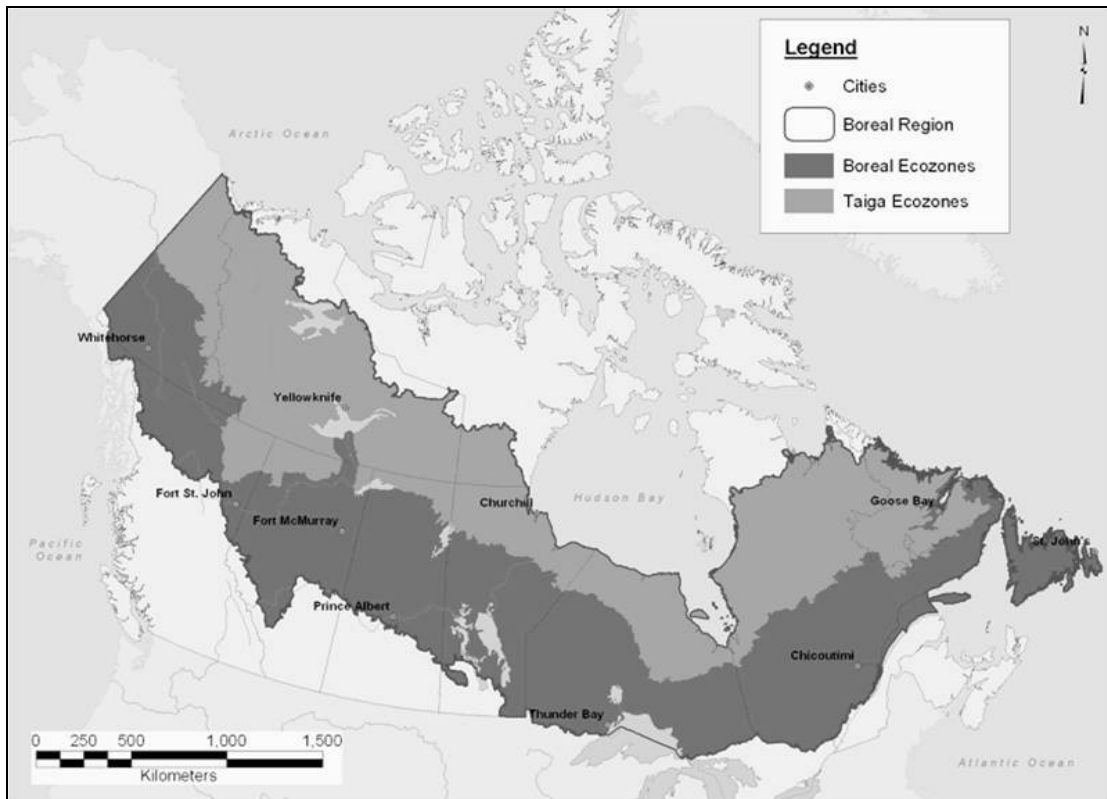


Figure 1.1: The extent of the boreal forest region (i.e., dark shaded area) over Canada (modified after CBI 2011).

1.2 Vegetation phenology

Vegetation phenology is the science of understanding the periodic/cyclic events associated with the plant developmental stages; and mainly associated with climatic regimes (Delpierre et al. 2009, Morisette et al. 2009). In general, the climatic variables (i.e., temperature, incident solar radiation, precipitation, etc.) are mainly responsible for both of the seasonal and inter-annual variability observed in the phenological events (e.g., vegetation green-up, bud flashing, budburst, leaf out, leaf coloring, leaf fall, leaf

senescence, etc.) at local, regional, and global-levels (Cleland et al. 2007, Morisette et al. 2009).

In the context of boreal forested regions, the vegetation phenology can be categorized into four groups (FFMT 1999):

- i. snow stage [e.g., snow on ground (SOG), snow patches on ground (SPG), snow gone (SGN)],
- ii. conifer stage [e.g., coniferous closed bud (CCB), coniferous open bud (COB), coniferous needle flush (CNF),
- iii. deciduous stage [e.g., deciduous closed bud (DCB), deciduous open bud (DOB), deciduous leaf out (DLO), deciduous color change (DCC), deciduous leaf fall (DLF)], and
- iv. understory stage [e.g., cured grass stage (CGS), transition grass stage (TGS), green grass stage (GGS)].

In this thesis, the phenological stages associated with both deciduous (i.e., DLO and DLF) and understory grass green-up stages (i.e., GGS) are considered. In particular to deciduous phenology, these stages provide valuable information regarding: (i) plant growth (Lechowicz and Koike 1995, Vitasse et al. 2009, Hari and Nojd 2009); (ii) plants' ability of exchanging atmospheric carbon-di-oxide (Cleland et al. 2007, Barr et al. 2009, Gryning et al. 2009); (iii) flammability of the plants in the event of forest fire (Peckham et al. 2008, Serbin et al. 2009); (iv) forest ecohydrology, e.g. evapotranspiration, precipitation, soil moisture, canopy moisture etc. (Wilson and Baldocchi 2000); and (v)

risk of insect infestation (Hogg 1999) among others. On the other hand, understory grass stages also play significant roles in: (i) micro-climatic environment, composition and diversity of plant community (Macdonald and Fenniak 2007, Chavez and Macdonald 2010, Lu et al. 2011), (ii) overstory succession and nutrient cycling (Roberts 2004, Hart and Chen 2006, Gilliam 2007), (iii) sources of food and habitat for wildlife species/animals (Nilsson and Wardle 2005), (iv) determining the forest fire risk and fire behavior in the event of fire occurrences, etc.

1.3 Problem statement

In Alberta, the department of Sustainable Resource Development (SRD) has been acquiring some of the key phenological stages including DLO, DLF, and GGS data since early 1970's at approximately 120 lookout tower sites across the forested landscape. These data are being used in predicting forest fire behaviour in the event of their occurrences (Lawson and Armitage 2008). In fact, these data provide accurate assessment for the phenological stage of interest. However, these suffer from some limitations, such as, (i) these provide site specific information over relatively smaller geographical extent (several hundreds of m²), (ii) highly depend on the skill of the operator as these are based on visual assessment, and (iii) lack of spatial variability as employing more operators are very costly. Thus it requires exploring alternate methods in order to address the above mentioned limitations. Such an alternate method is the use of remote sensing-based techniques, which is already proven as an effective technological advancement in determining various phenological stages over various biomes across the world (Delbart et al. 2006, Cleland et al. 2007, Reed et al. 2009, White et al. 2009, Morisette et al. 2009).

1.4 Research objectives

In the thesis, the overall goal was to delineate the deciduous and understory phenological stages over forest-dominant regions in Alberta primarily using remotely sensed data. The specific objectives were to determine:

- (i) Deciduous phenological stages (i.e., DLO and DLF) associated with trembling aspen (*Populus tremuloides*) over the deciduous-dominant stands;
- (ii) Understory phenological stage (i.e., GGS) over both conifer and deciduous stands.

1.5 Thesis structure

This thesis consists of six chapters. Chapter one (i.e., this one) describes the background of the research, problem statement, and also objectives of the research.

Chapter two provides the literature review with brief description of different phenological stages. It also provides the in-situ (i.e., ground)-based and remote sensing-based methods of determining the vegetation phenology.

Chapter three describes the study area used in this research. It also provides the brief description of the ground-based and satellite-based datasets required in this research.

Chapter four illustrates the methodology of the study. It includes the determination of DLO, DLF, and GGS.

Chapter five provides the results of this research. It also includes brief discussion on the findings.

Chapter six summarizes the key findings of the research along with the scientific contribution of the research, and the future works.

CHAPTER 2: LITERATURE REVIEW

This chapter provides brief description in six sections regarding deciduous and understory vegetation phenology definitions, the methods associated with their determination, etc., which includes: (i) definition of the deciduous phenological stages, (ii) definition of the understory grass green-up phenological stages, (iii) the factors influencing the vegetation phenology, (iv) methods of determining deciduous phenology, (v) methods of determining understory phenology, (vi) description of the MODIS data.

2.1 Definition of the deciduous phenological stages

In general, the deciduous phenological stages occur during spring to late fall season. These stages are defined by Alberta forest division (FFMT 1999) for the species of trembling aspen and described as follows:

- DCB: the time when 75% or more of the buds for the species of interest in the surrounding area of a lookout tower sites are still closed.
- DOB: the time when 75% or more of the buds for the species of interest in the surrounding area of a lookout tower sites have swollen to the green leaf parts are visible but the leaves have not yet opened.
- DLO: the time when 75% or more of the leaves would open with a length of at least 1.25 cm in diameter for the species of interest in the surrounding area of a lookout tower sites.

- DCC: as the time when 50% or more of the leaves for the species of interest have changed their color from green to fall color in the surrounding area of a lookout tower sites.
- DLF: the time when 50% or more of the leaves would fall down for the species of interest in the surrounding area of a lookout tower sites.

2.2 Definition of the understory grass green-up phenological stages

In general, the understory grass green-up phenological stages occur during spring season. These stages are defined by Alberta forest division (FFMT 1999) and described as follows:

- CGS: the time when 75% to 100% of the understory grass in the surrounding area of a lookout tower sites is cured (i.e., < 25% of the grass is green).
- TGS: the time when 50% to 75% of the understory grass in the surrounding area of a lookout tower sites is cured.
- GGS: the time when 75% of the understory grass in the surrounding area of a lookout tower sites) is green.

2.3 Factors influencing the vegetation phenology

Vegetation phenological stages are mainly influenced by the seasonal and inter-annual variations of the climatic conditions (McCloy 2010, Reed et al. 2009). These climatic variables include light availability, temperature, air humidity, precipitation, soil moisture, etc. (Hart and Chen 2006, Cleland et al. 2007, Hassan and Bourque 2009, Liang and Schwartz 2009, Gu et al. 2010). The other factors that influence the vegetation phenology

are soil nutrients, pH, vegetation types (i.e., deciduous, coniferous and understory), composition and density, and some physical characteristics of the litter layer (Hart and Chen 2006, Barbier et al. 2008).

2.4 Methods of determining deciduous phenology

The most accurate and widely used method of determining the deciduous phenological stages is the employment of *in-situ* (i.e., ground) observations. For example:

- Pellikka (2001) used ground-based measurements of leaf area index [LAI: defined as the one-sided green leaf area per unit ground area; (Hassan and Bourque, 2010)] and photosynthetically active radiation (PAR) to determine canopy closure increment in spring and canopy closure decrement in autumn over deciduous forests in German Alps;
- Fisher et al. (2007) employed ground-measured air temperature records in determining the spring onset over deciduous forests in New England, USA; and
- Beaubien and Hamman (2011) described the development of a database regarding spring phenology for the common plants in Canada on the basis of integrating the visual observation of the volunteers.

Despite its accuracy, it only provides site specific information over relatively smaller geographical extent (in the order of several hundreds of m²). Thus, other methods are required to address the spatial variability, and remote sensing-based methods can be

considered as a viable one due to its continuous coverage of the earth surface (Delbart et al. 2006, Cleland et al. 2007, Reed et al. 2009).

In most of the instances, remote sensing-based vegetation and water indices are commonly used ones in determining various vegetation developmental stages, e.g., green up, maturity, etc. over different forested regions. These indices are calculated from the surface reflectance of the spectral bands which are acquired by the satellite sensors. For example; the spectral signature curves, used to detect the different phenomenon such as green and dry vegetation, and soil, are shown in Figure 2.1 by the effective reflectances. The reflectance of vegetation have tow general forms of green/wet (i.e., photosynthetic) and dry (i.e., non-photosynthetic). Here, it shows that the reflectance of green vegetation (Figure 2.1) has a unique spectral signature which enables it to be distinguished readily from other types of reflectances. It is low in both the blue and red regions of the spectrum (i.e., 0.4 - 0.6 μm), due to absorption by chlorophyll for photosynthesis and it has a small peak at the green region (i.e., 0.5 μm). Also the reflectance of green vegetation is much higher in the near infrared (NIR) region than that in the visible band due to the cellular structure in the leaves. The spectrum of the dry non-photosynthetic vegetation shows the absorptions due to cellulose, lignin, and nitrogen presence. In the green vegetation, these absorptions are seems week due to the stronger presence of water bands. On the other hand, due to montmorillonite, the spectrum of the soil shows a weak reflectance signature at 2.2 μm .

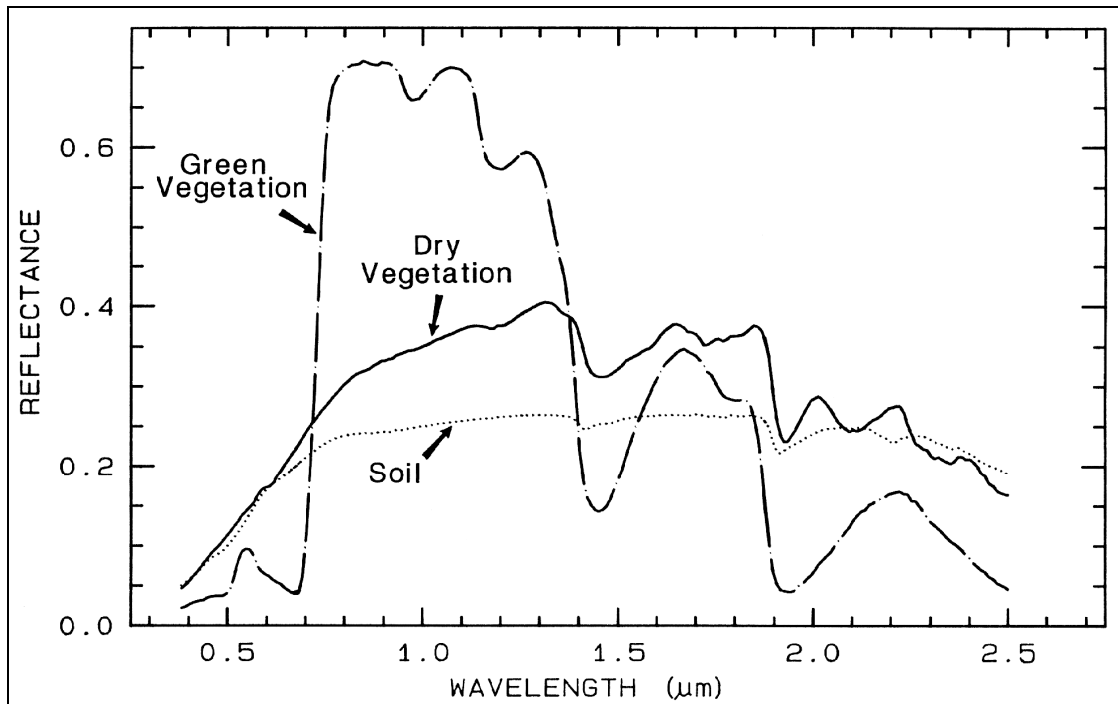


Figure 2.1: The spectral reflectance curves of green and dry vegetation and soil along with the spectral wavelengths (after Clark et al. 1999).

Based on the spectral signatures, the remote sensing-based indices were estimated which include the application of:

- Normalized difference vegetation index [NDVI: a measure of vegetation greenness (Parviainen et al. 2010)] in determining the onset of green-up over: (a) temperate deciduous broadleaf forests in France (Duchemin et al. 1999, Soudani et al. 2008) and; (b) boreal forest in northern Eurasia (Delbart et al. 2006); The NDVI was calculated using the following expression (Rouse et al. 1974):

$$NDVI = \frac{\rho_{NIR} - \rho_{Red}}{\rho_{NIR} + \rho_{Red}} \quad (1)$$

where, ρ is the surface reflectance for the NIR (near-infrared) and red spectral bands.

- Enhanced vegetation index [EVI: a measure of vegetation greenness and canopy structure; (Huete et al. 2002)] in determining the onset of green-up over: (a) deciduous broadleaf forest in Wisconsin, USA (Ahl et al. 2006, Liang et al. 2011a); (b) boreal forested regions in Alberta, Canada (Sekhon et al. 2010); The EVI was calculated using the following expression (Huete et al 2002):

$$EVI = 2.5 * \frac{\rho_{NIR} - \rho_{Red}}{\rho_{NIR} + \rho_{Red} - \rho_{Blue} + 1} \quad (2)$$

where, ρ is the surface reflectance for the near-infrared, red and blue spectral bands.

- LAI in defining the vegetation maturity over mixed temperate deciduous forest in Wisconsin, USA and the LAI was obtained from Moderate Resolution Imaging Spectroradiometer (MODIS) satellite (Hanes and Schwartz 2010); and
- Normalized difference water index [NDWI: a measure of water/moisture in the canopy; (Chen et al. 2005)] in defining the deciduous leaf out over boreal forest in

central Siberia (Delbert et al. 2005); among others. The NDWI was calculated according to the following equation (Gao 1996):

$$NDWI = \frac{\rho_{NIR} - \rho_{SWIR}}{\rho_{NIR} + \rho_{SWIR}} \quad (3)$$

where, ρ is the surface reflectance for the near-infrared and short wave infrared (SWIR) spectral bands.

The temporal trends of these indices are used for detecting the changes in biophysical and/or biochemical characteristics of the vegetation on transformation of the phenological stage (Xiao et al. 2009, McCloy 2010). In the literature, it is found that the application of both NDVI and EVI in predicting the spring onset induces uncertainty due to the presence of snow on the ground over the boreal-dominant regions in particular (Delbert et al. 2006, Sekhon et al. 2010). Thus, we may assume that the application of another vegetation index of LAI also may be affected in a similar fashion. On the other hand, the implementation of NDWI reveals that it is capable of determining the vegetation developmental phases independent of the snow conditions (Delbart et al. 2006, Reed et al. 2009, Sekhon et al. 2010). In general, the temporal trends of these indices are able to determine several phenological stages, such as, onset, maturity, and end of the growing season depending on the type of the forested ecosystems (Zhang et al. 2003, Delbart et al. 2005). However, some of the intermediate phenological stages (e.g., DLO and DLF) during the growing season may require further investigation.

In general, the responses of vegetation are largely controlled by the climatic variables (Hassan and Bourque 2009); thus remote sensing-based surface temperature (T_S) is also experimented in determining the deciduous phenology, however in a limited capacity.

For example:

- Hanes and Schwartz (2010) determined the dynamics of leaf out in a deciduous-dominant mixed temperate forest as a function of accumulated growing degree days (GDD: defined as the favourable temperature regime for plant growth);
- Zhang et al. (2004) determined the green-up onset as a function of accumulated chilling days (i.e., days with temperatures experiencing less than a threshold-value).

In both of the above cases, MODIS-based T_S products were directly used without transforming them into equivalent daily average air temperature. As, for the calculation of GDD and chilling days, it would be very common to use such average air temperature measured near the surface (Delbert et al. 2008, Li et al. 2010). In this context, the GDD mapping methods (as described in Hassan et al. 2007a, b, Akther and Hassan 2011) using MODIS-based T_S products in conjunction with ground-based air temperature measurements would be a viable alternate.

2.5 Methods of determining understory phenology

The most commonly used method to study understory phenology is the use of ground-based methods. For example:

- Richardson and O'Keef (2009) analyzed the long term Harvard forest phenology record to investigate differences in spring and autumn phenology between understory species (i.e., shrub and herbs) and canopy species. They used accumulated transmitted PAR as ground measurement to predict budburst of different understory and over story species in central Massachusetts, USA;
- Butler et al. (2008) performed a one-way analysis of variance (ANOVA) to observe the understory species (i.e., woody and herbaceous vegetation) richness and abundance within each individual plantation area using the ground-based measurements of tree density, % canopy openness, etc. over north-eastern Costa Rica;
- Kudo et al. (2008) investigated the flowering stage of understory species (i.e., herbaceous) during spring, early-summer, and late-summer bloomers using ground-based air temperature, photon flux density (PFD) among others over Tomakomai Experimental Forest of Hokkaido University in northern Japan;
- Liang et al. (2011b) used ground-based air temperature, relative humidity and digital photographs to measure spring time understory (i.e., grasses and herbs) greenness over Chequamegon National Forest in northern Wisconsin, USA; and
- In Alberta, understory grass greening stages over the boreal dominant forested regions are recorded using visual observations at approximately 120 lookout tower sites across the landscape. These dataset are used to predict the forest fire

behaviour in the event of fire occurrences during the growing/fire season (FFMT 1999).

Though the ground-based methods can provide information accurately, it may not be useful to determine the dynamics over a large area. In this context, remote sensing-based methods can be used to delineate the spatial dynamics of the understory vegetation. For example:

- Tuanmu et al. (2010) reported mapping of understory vegetation (i.e., bamboo) using phenological characteristics derived from remotely sensed MODIS-based 16-day composites of surface reflectance data. The employed vegetation index was wide dynamic range vegetation index (WDRVI) to determine start of season, end of season, mid of season over Chinese Wolong Nature Reserve; The WDRVI was calculated according to the following equation (Gitelson 2004):

$$WDRVI = \alpha * \frac{\rho_{NIR} - \rho_{Red}}{\rho_{NIR} + \rho_{Red}} \quad (4)$$

where, ρ is the surface reflectance for the near-infrared and red spectral bands and α is a weighting coefficient set as 0.25 (Henebry et al. 2004).

- Yauschew-Raguenes et al. (2008) used SPOT/VEGETATION-derived perpendicular vegetation index (PVI) to observe the seasonal changes of the herbaceous understory vegetation (over the large maritime pine forest area in

south-western France. The PVI was found to be related with the ground-based measurements of fraction of absorbed photosynthetically active radiation (fAPAR) over understory vegetation; The PVI was calculated as follows (Richardson and Wiegand 1977):

$$PVI = \frac{\rho_{NIR} - \alpha\rho_{Red} - \beta}{\sqrt{(\alpha^2 + 1)}} \quad (5)$$

where, ρ is the surface reflectance for the near-infrared and red spectral bands and α, β [(i.e., $\alpha = 1.253, \beta = 0.030$, (Baret et al. 1995)] are soil line parameters.

- Eriksson et al. (2006) developed a reflectance model based on LANDSAT ETM+ to investigate the impact of the understory vegetation (i.e., grasses, herbs, ferns, mosses and small bushes) on the forest canopy of LAI over southern Sweden. They observed that the understory vegetation coverage would be higher in coniferous than deciduous stands having the same LAI;
- Wilfong et al. (2009) used LANDSAT ETM+-based NDVI and other vegetation indices [i.e., simple ratio (SR), EVI, visible atmospherically resistant index (VARI), soil adjusted vegetation index (SAVI), normalized difference moisture index (NDMI), etc.] to characterize the seasonal changes (i.e., greenness, leaf senescence, leaf abscission, etc.) of understory vegetation (i.e., shrub) in south-

western Ohio and Indiana, USA. The calculations of the indices are as follows (Huete 1988, Wang et al. 2007):

$$SR = \frac{\rho_{NIR}}{\rho_{Red}} \quad (6)$$

where, ρ is the surface reflectance for the near-infrared and red spectral bands

$$VARI = \frac{\rho_{Green} - \rho_{Red}}{\rho_{Green} + \rho_{Red} - \rho_{Blue}} \quad (7)$$

where, ρ is the surface reflectance for the green, red and blue spectral bands.

$$SAVI = \frac{\rho_{NIR} - \rho_{Red}}{\rho_{NIR} + \rho_{Red} + L} * (1 + L) \quad (8)$$

where, ρ is the surface reflectance for the near-infrared and red spectral bands and L is the soil brightness correction factor (i.e., L = 0.5).

$$NDMI = \frac{\rho_{NIR} - \rho_{MIR}}{\rho_{NIR} + \rho_{MIR}} \quad (9)$$

where, ρ is the surface reflectance for the near-infrared and middle-infrared (MIR) spectral bands

However, some of the remote sensing-based indices (e.g., WDRVI, PVI, and LAI) would have uncertainty due to the heterogeneity in the forested landscape (Colombo et al. 2003, Urgenson et al. 2009, Tuanmu et al. 2010). In case of both NDVI and EVI, it was also demonstrated their limited capability over boreal forested regions to determine vegetation phenology due to the presence of snow during early spring (Delbart et al. 2005, Sekhon et al. 2010). On the other hand, it was found that the implementation of normalized difference water index (i.e., NDWI) has better prediction capacity in determining the vegetation green up stages independent of the snow conditions (Delbart et al. 2005, Sekhon et al. 2010). However, the applicability of NDWI in determining understory phenology was so far not reported elsewhere, thus it might be worthwhile to evaluate its performance.

As climatic variables (in particular to temperature) largely control vegetation growth, thus remote sensing-based surface temperature regimes have also been used in vegetation phenological studies. Some of examples have also been mentioned in the previous section “2.4 Methods of determining deciduous phenological phenology”. As the implementation of temperature-derived predictors was not widely found, we opted to apply the GDD-based method in understanding the understory phenology.

2.6 Description of MODIS data

For the last decade, scientists are using widely the standard MODIS data products due to its high temporal (i.e., at daily-level for the most of the parts of the world) and low to medium spatial resolution (i.e., 250 m to 1 km) to study global change from a variety of

disciplines, including oceanography, biology, and atmospheric science. The MODIS data (e.g., vegetation indices, surface reflectance, surface temperature, land cover types, forest fires, etc.) have been designed to provide improved monitoring and understanding of global dynamics and processes.

MODIS is a key sensor on board of both Terra and Aqua satellites, launched on 18 December 1999 and 4 May 2002 respectively by National Aeronautics and Space Administration (NASA). Terra's orbit passes around the Earth from north to south across the equator in the morning (10:30 am) in a descending orbit, while Aqua passes south to north over the equator in the afternoon (1:30 pm) in an ascending orbit. Both the satellites placed in 705-km polar, sun-synchronous orbits. MODIS Terra and Aqua are viewing swath width of 2,330 km (cross track) by 10 km (along track at nadir) and views the entire surface of the Earth every one to two days. The Scan Mirror Assembly of the instruments uses continuously rotating double-sided scan mirror to scan ± 55 degrees. It is driven by a motor encoder which is built to operate at 100 percent duty cycle during the 6-year design life. Its detectors measure 36 spectral bands ranging the wavelength from 0.4 μm to 14.4 μm with high radiometric sensitivity (12 bit) and acquire data in three native spatial resolutions: (i) bands 1-2 at 250 m, (ii) bands 3-7 at 500 m, and (iii) bands 8-36 at 1000 m and the temporal resolutions are: daily, 8-day, 16-day, monthly, quarterly, and yearly (see Table 2.1 for more details).

Table 2.1: Characteristics of MODIS spectral bands.

Band No.	Reflected range (µm)	Emitted range (µm)	Key use	Pixel size (m)
1	0.620–0.670	-	Absolute land cover transformation, vegetation chlorophyll	250
2	0.841–0.876	-	Cloud amount, vegetation land cover transformation	250
3	0.459–0.479	-	Soil/vegetation differences	500
4	0.545–0.565	-	Green vegetation	500
5	1.230–1.250	-	Leaf/canopy differences	500
6	1.628–1.652	-	Snow/cloud differences	500
7	2.105–2.155	-	Cloud & land properties	500
8	0.405–0.420	-	Chlorophyll	1000
9	0.438–0.448	-	Chlorophyll	1000
10	0.483–0.493	-	Chlorophyll	1000
11	0.526–0.536	-	Chlorophyll	1000
12	0.546–0.556	-	Sediments	1000
13	0.662–0.672	-	Atmosphere, sediments	1000
14	0.673–0.683	-	Chlorophyll fluorescence	1000
15	0.743–0.753	-	Aerosol properties	1000
16	0.862–0.877	-	Aerosol & atmospheric properties	1000
17	0.890–0.920	-	Aerosol & atmospheric properties	1000
18	0.931–0.941	-	Aerosol & atmospheric properties	1000
19	0.915–0.965	-	Aerosol & atmospheric properties	1000
20	-	3.660–3.840	Sea surface temperature	1000
21	-	3.929–3.989	Forest fires & volcanoes	1000
22	-	3.929–3.989	Cloud & surface temperature	1000
23	-	4.020–4.080	Cloud & surface temperature	1000
24	-	4.433–4.498	Cloud fraction, troposphere temperature	1000
25	-	4.482–4.549	Cloud fraction, troposphere temperature	1000
26	1.360–1.390	-	Cloud fraction, troposphere temperature	1000
27	-	6.535–6.895	Mid troposphere humidity	1000
28	-	7.175–7.475	Upper troposphere humidity	1000
29	-	8.400–8.700	Surface temperature	1000
30	-	9.580–9.880	Total ozone	1000
31	-	10.780–11.280	Cloud/surface temp., forest fires, volcanoes	1000
32	-	11.770–12.270	Cloud Height, forest fires & volcanoes, surface temperature	1000
33	-	13.185–13.485	Cloud fraction, cloud height	1000
34	-	13.485–13.785	Cloud fraction, cloud height	1000
35	-	13.785–14.085	Cloud fraction, cloud height	1000
36	-	14.085–14.385	Cloud fraction, cloud height	1000

CHAPTER 3: STUDY AREA AND DATA REQUIREMENTS

This chapter provides a brief description regarding the study area and data requirements. In terms of data requirements, the description about the satellite data and *in-situ* phenological and air temperature data are also discussed.

3.1 Description of the study area

The study area is Alberta, which lies in between 49-60 °N latitude, and 110-120 °W longitude (see Figure 3.1). Topographically, it is variable in the range 150-3650 m above the mean sea level. Climatically, it experiences relatively humid conditions (i.e., annual precipitation in the range 260-1710 mm) with short summers, long and cold winters (where the average annual temperature in the range -7.1 °C to 6 °C) (Dowing and Pettapiece 2006). The province is divided into 6 natural regions on the basis of climate, soil, and vegetation types; and their brief descriptions are provided in Table 3.1 (Dowing and Pettapiece 2006). The natural regions are: boreal, rocky mountain, foothills, Canada shield, parkland and grassland (see Figure 3.1).

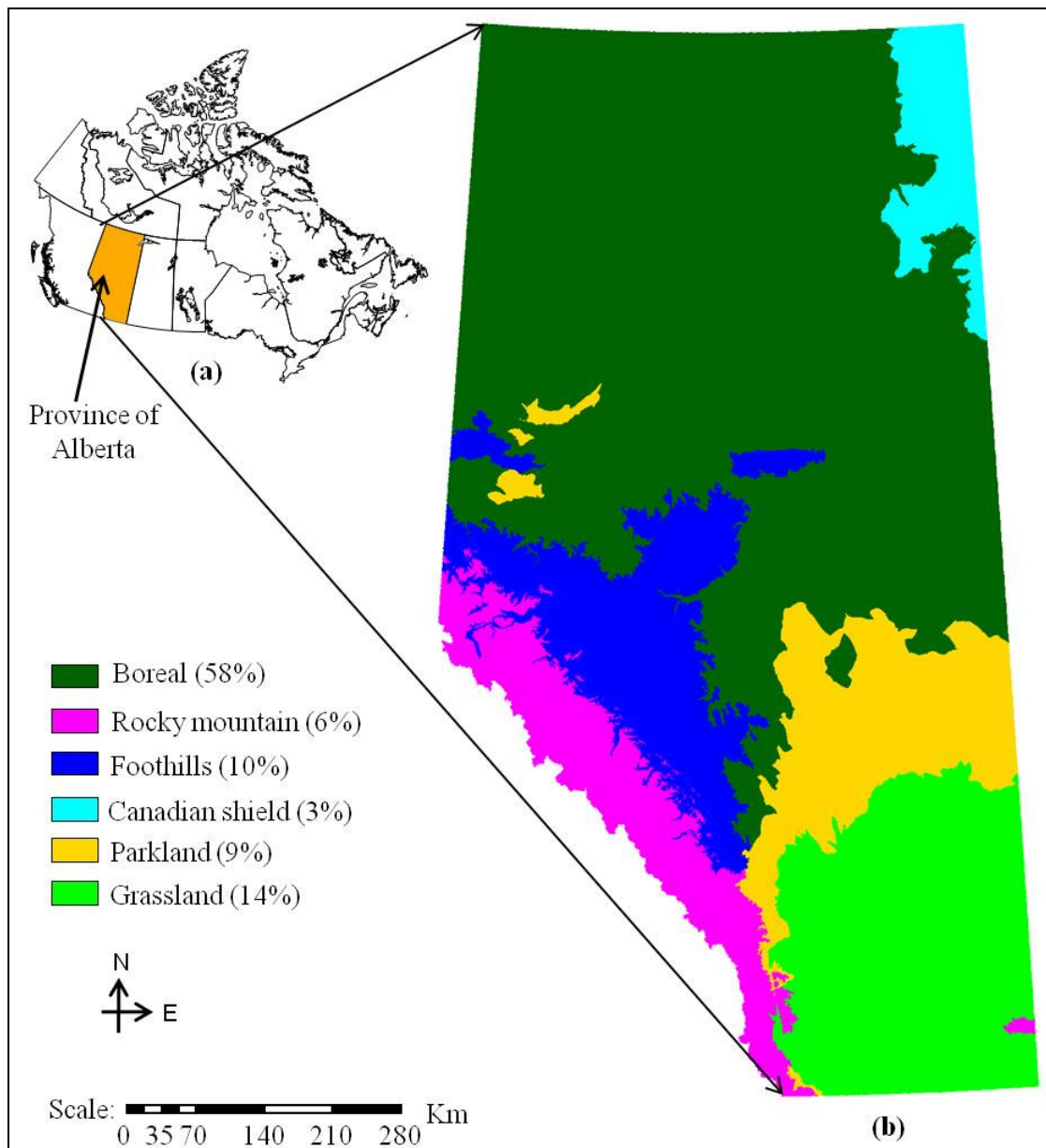


Figure 3.1: a) Location of Alberta in Canada, b) Natural regions of Alberta (i.e., within 49-60 °N and 110-120 °W).

Table 3.1: Characteristics of natural regions of Alberta.

Natural Region No.	Natural Region Name	% of Alberta	Mean annual Temp. (°C)	Mean annual precip. (mm)	Main vegetation coverage
I	Boreal	58	-0.2	469	Mixedwood: dominant-aspen, white spruce & black spruce, shrubby understories, jack pine
II	Canadian Shield	3	-2.6	380	Rock barrens (mixed with; aspen, open jack pine, birch), dry jack pine forests, dunes largely unvegetated
III	Foothills	10	1.7	603	Mainly closed coniferous forests (aspen-lodgepole pine, lodgepole pine-black spruce, white spruce)
IV	Parkland	9	2.3	447	Aspen forests with grass lands
V	Rocky Mountain	6	-0.4	798	Mixed aspen & conifer forests (lodgepole pine, white spruce, douglas fir)
VI	Grassland	14	4	374	Grasslands (blue grama, needle and thread), shrublands

Figure 3.2 shows the location of deciduous species stands (i.e., gray shades); and the lookout tower sites (i.e., black circles) where deciduous leaf out and deciduous leaf fall *in-situ* observations were acquired. In terms of forest the most dominant deciduous species are trembling aspen and balsam poplar (*Populus balsamifera*) (Barr et al. 2004, Li et al. 2010). Their spatial distributions were obtained from Alberta SRD and the dynamics of DLO and DLF were only determined within the deciduous-dominant stands.

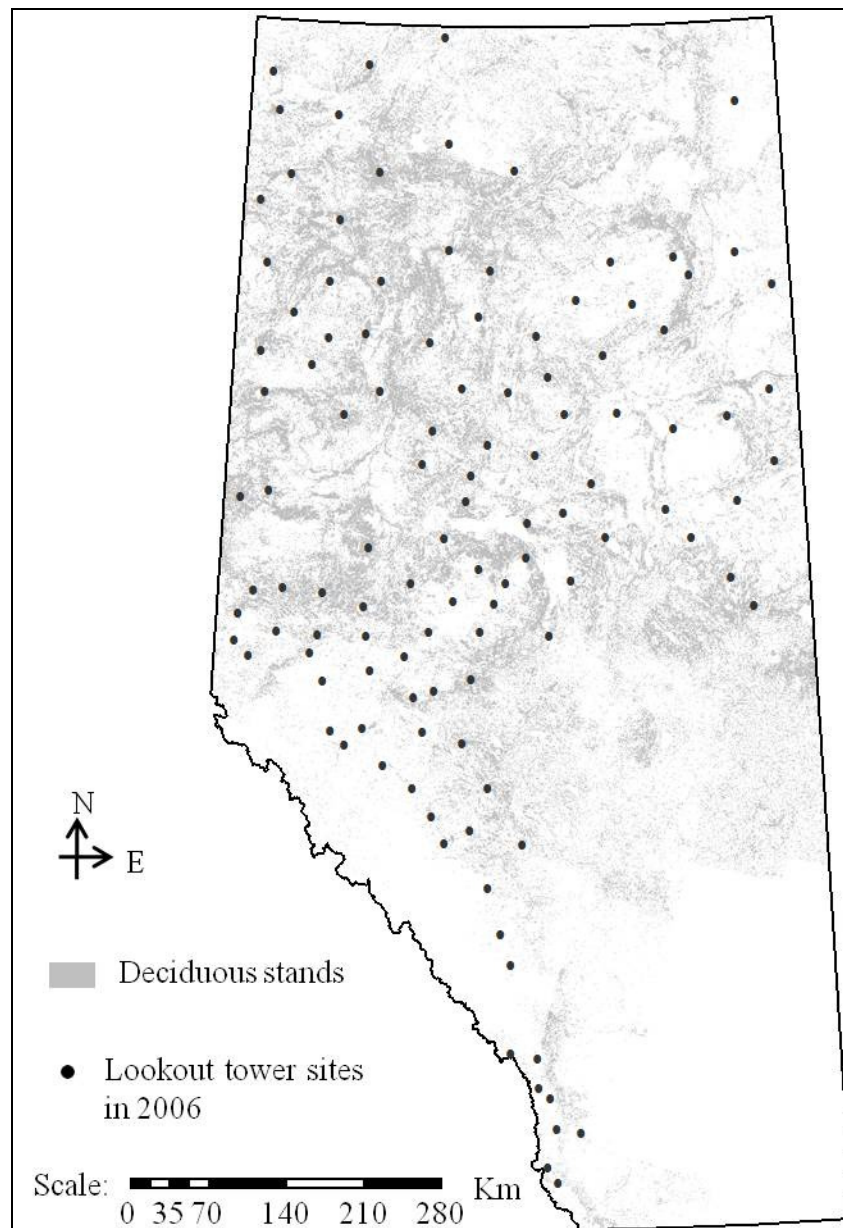


Figure 3.2: Location of deciduous stands (i.e., gray shades); and the lookout tower sites (i.e., black circles) where deciduous leaf out (DLO) and deciduous leaf fall (DLF) *in-situ* observations were acquired in Alberta (i.e., within 49-60 °N and 110-120 °W).

Figure 3.3 shows the extent of the forest dominant areas (i.e., mainly deciduous and coniferous) in the study area derived from MODIS-based land cover map at a spatial resolution of 500 m with the locations of operating lookout tower sites during 2006 (where the GGS were observed). Alberta has a wide variety of land covers having various types of understory (i.e., shrubs-herbs, lichen, sphagnum, beaked hazelnut, willow, grouse-berry, dogwood, Labrador tea, etc.) with deciduous and coniferous forests intersperse (Dowing and Pettapiece 2006).

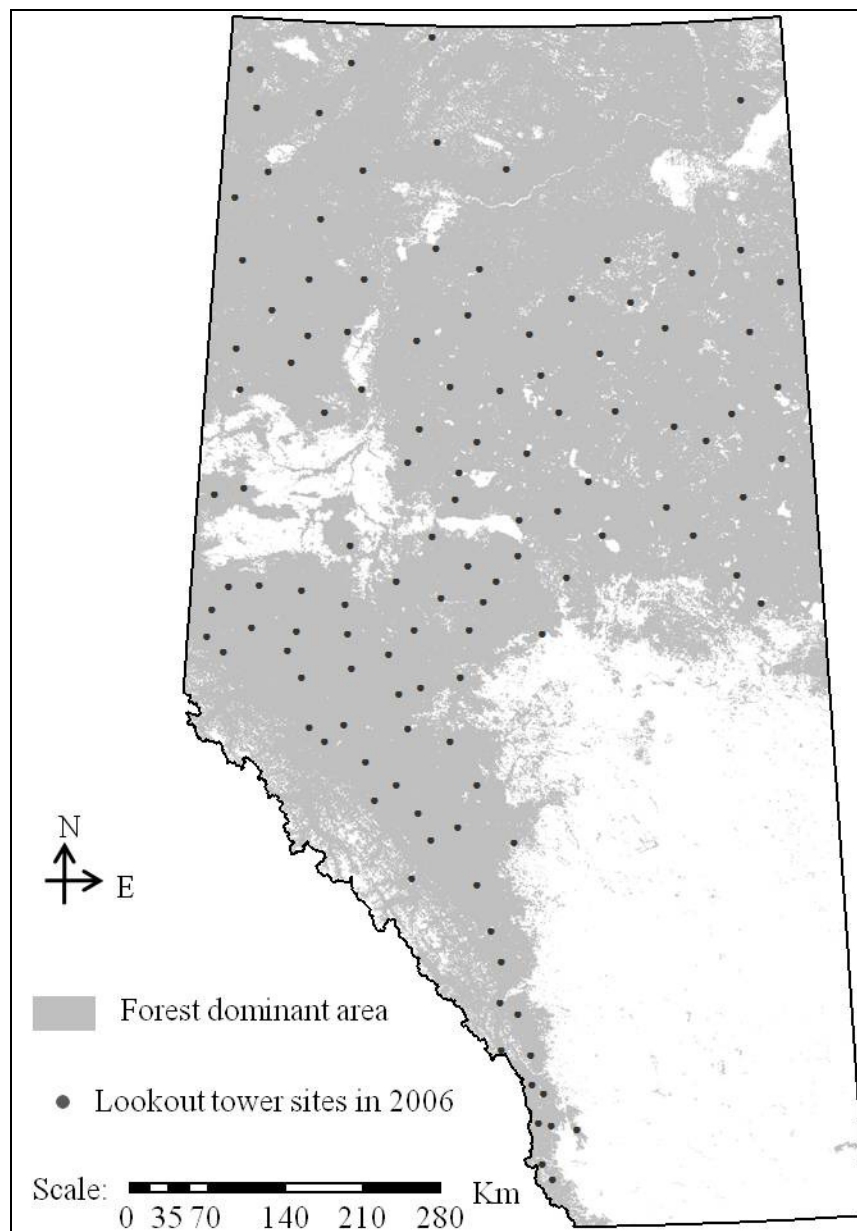


Figure 3.3: Location of forest dominant areas (i.e., gray shades); and the lookout tower sites (i.e., black circles) where GGS *in-situ* observations were acquired in Alberta (i.e., within 49-60 °N and 110-120 °W).

3.2 Data requirements

3.2.1 Satellite data

In this study, the MODIS-based data were used freely available from the Land Processes Distributed Active Archive Center of NASA (LP DAAC 2010) during the growing seasons (i.e., April-October) for the years 2006-2008. Those included: (i) 8-day composites of T_s (i.e., MOD11A2 V.005) at 1 km spatial resolution, (ii) eighty one (81) 8-day composites of surface reflectance data (MOD09A1 V.005) at 500 m spatial resolution to calculate EVI and NDWI; (iii) annual land cover map (MCD12Q1 V.005) at 500 m resolution for the year 2006-2008 used to define the forested regions.

3.2.2 In-situ phenological and air temperature data

The *in-situ* phenological data for DLO, DLF, and GGS at the lookout tower sites (see Figure 3.2 and 3.3 for location information) were obtained available from Alberta SRD during the period 2006-2008. The number of lookout tower sites was found to be approximately 115 per year for both DLO and GGS. On the other hand, the operational numbers of lookout tower sites for DLF were relatively small, e.g., 15 in 2006, 6 in 2007, and 31 in 2008. The rationale behind the smaller number of observation sites for DLF was that most of the lookout towers happened to cease their operation before the occurrence of the DLF stages due to the significant drop of the forest fire events (Michael Kakoullis, SRD, personal communication). In general, it was observed that the timing of DLO, DLF and GGS were found to be influenced by elevation, and/or latitude. For example: the timing of occurrence for DLO/GGS was increased from low to high latitudes and/or elevations; and the opposite for DLF.

Apart from the phenological dataset, daily average air temperature acquired at 1.2-2 m above the surface at 182 weather stations were also obtained (see Figure 3.4 for location information) during the years 2006-2008, available from Environment Canada (EC 2010).

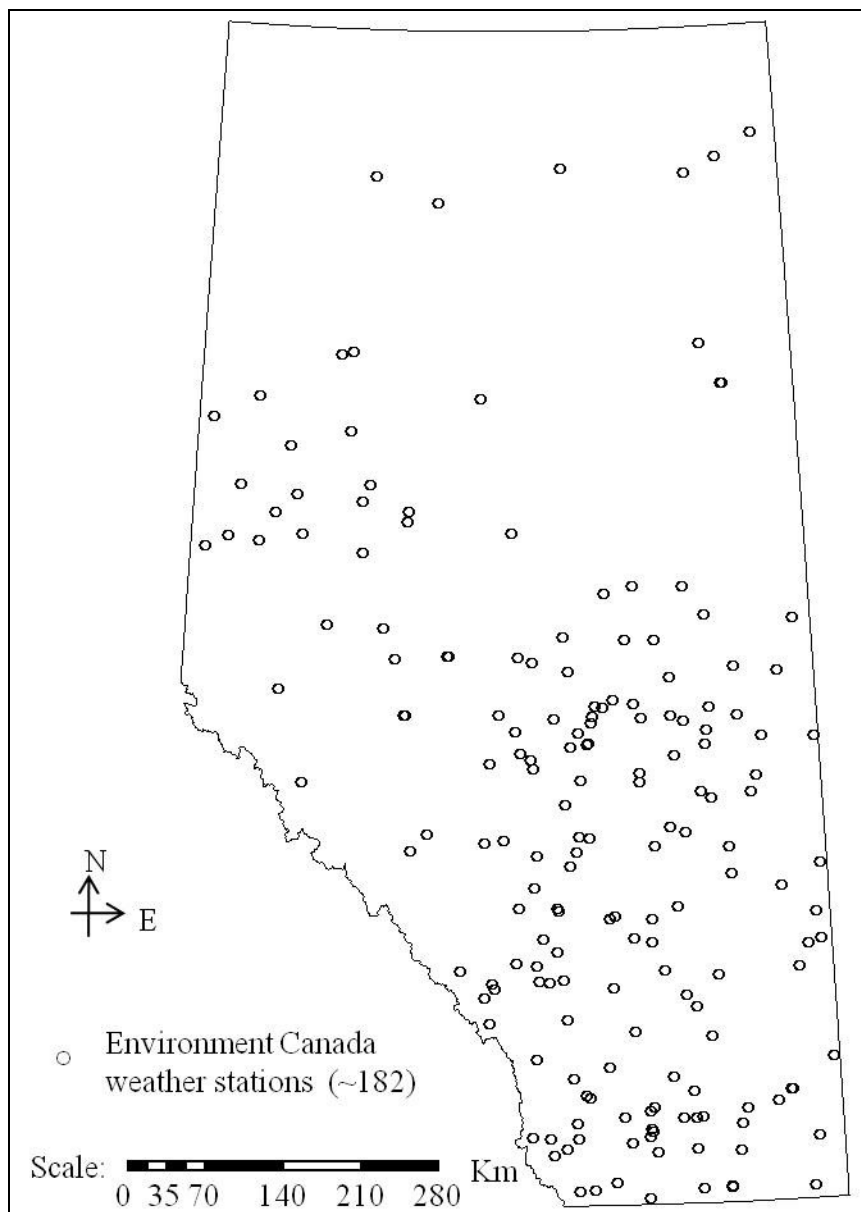


Figure 3.4: Location of the Environment Canada weather stations across Alberta (i.e., within 49-60 °N and 110-120 °W), where the daily average air temperatures were acquired at a height between 1.2-2 m above the ground-surface.

CHAPTER 4: METHODOLOGY

This chapter describes the methodology of this research work. There are mainly four steps involved, such as, (i) data pre-processing, (ii) determining threshold for DLO, DLF and GGS, (iii) validation schema for DLO, DLF and GGS, and (iv) generating spatial dynamics for DLO, DLF, and GGS; and briefly described in Figure 4.1.

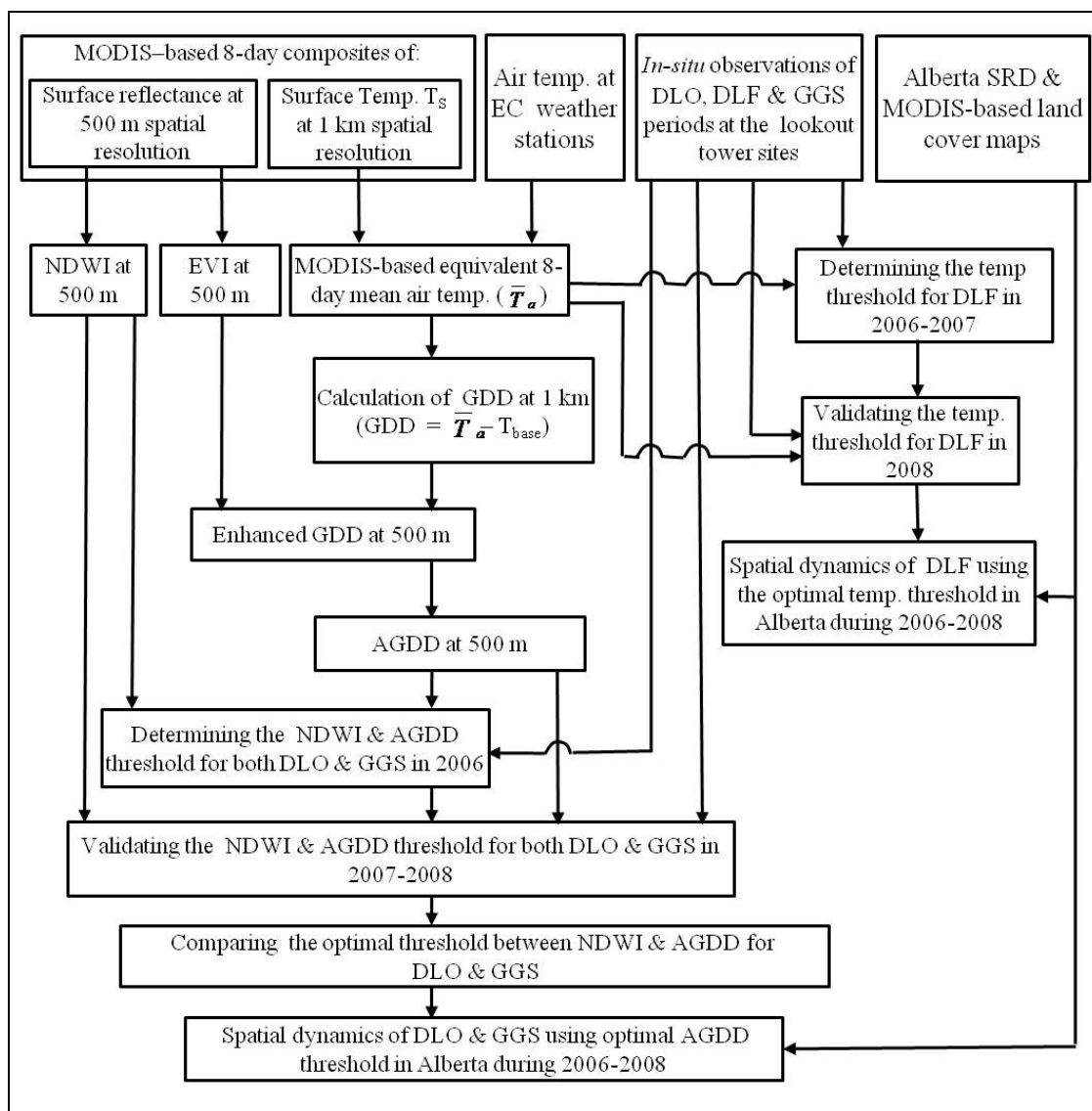


Figure 4.1: Schematic diagram of the methodology of determining DLO, DLF and GGS.

4.1 Data pre-processing

4.1.1 *In-situ phenological and air temperature data*

In-situ phenological data was used in this study as ground based measurements which were compared with the satellite data applied in the study area. These phenology data has been collected by the lookout personnel at the lookout tower sites, placed mostly in the forested areas over Alberta. There were a large number of lookout towers sites found in Alberta which were approximately 120 per year to observe the vegetation phenology occurrences. These data were recorded in the form of day of year (DOY: 1 to 365 or 366 depending on the leap year), thus those were transformed into equivalent 8-day period coinciding with that of MODIS 8-day composites using the following expression (Sekhon et al. 2010):

$$P = \left(\frac{DOY - 1}{8} \right) + 1 \quad (10)$$

where, P (=1 to 46) is the equivalent no. of periods that falls during the MODIS 8day composites.; and always it will be an integer (e.g., P = 24 if the Eq. 1 produces values in the range 24.125-24.875. Upon implementation, it was observed that the average period of DLO, GGS, and DLF were during 18, 19, and 34 periods respectively for the years 2006-2008.

The air temperature data were averaged at 8-day intervals, which also had to coincide with the MODIS 8-day composites. All of these phenological and air temperature

datasets were employed in calibrating and validating MODIS-based estimations of DLO, DLF and GGS stages.

4.1.2 Satellite data

4.1.2.1 Data downloading

The MODIS data (i.e., surface temperature, surface reflectance, and land cover type) used in this research were obtained in Hierarchical Data Format (HDF: MOD11A2.A2006097.h10v04.005.2008108231826.hdf; for example, see Figure 4.2) from NASA (LP DAAC 2010). These data were ordered through the Land Processes Distributed Active Archive Centre, NASA (LP DAAC 2010) within the geographical locations of: (i) 48 °N to 115 °W, (ii) 52 °N to 120 °W, (iii) 55 °N to 116 °W, and (iv) 55 °N to 98 °W) to cover whole Alberta (i.e., within 49-60 °N and 110-120 °W) from 2006-2008 during the growing season (i.e., April to October) at each 8-day intervals. So, for each of the data set, the ordering request was four times for each year and in total the request was done for 36 times for three years. For each of the T_s and surface reflectance images, it was 324 files for three years. On the other hand, the land cover images were having 4 scenes per year, which was an annual composite.

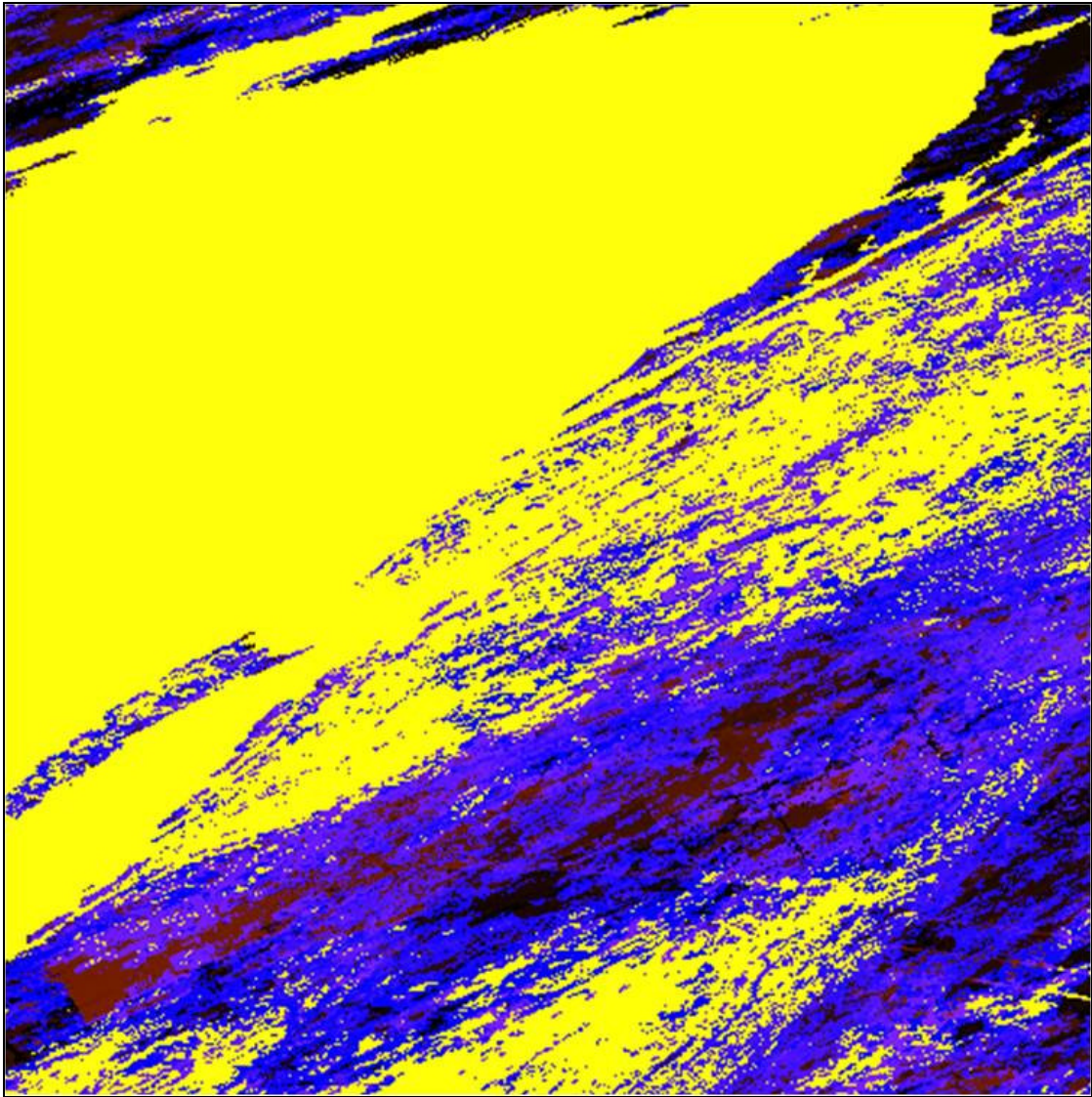


Figure 4.2: MODIS T_s in HDF format for the period of 13 (i.e., 97 DOY; within 48 °N and 115 °W).

4.1.2.2 Data Reprojection

The MODIS-based T_s and surface reflectance, and land cover type data were acquired as raw data were originally provided in sinusoidal projection. These data were re-projected

into UTM Zone 12 NAD 83 using MODIS Reprojection Tool (MRT, 2010: see Figure 4.3 for its interface); and the output images were produced in Geo-TIFF format.

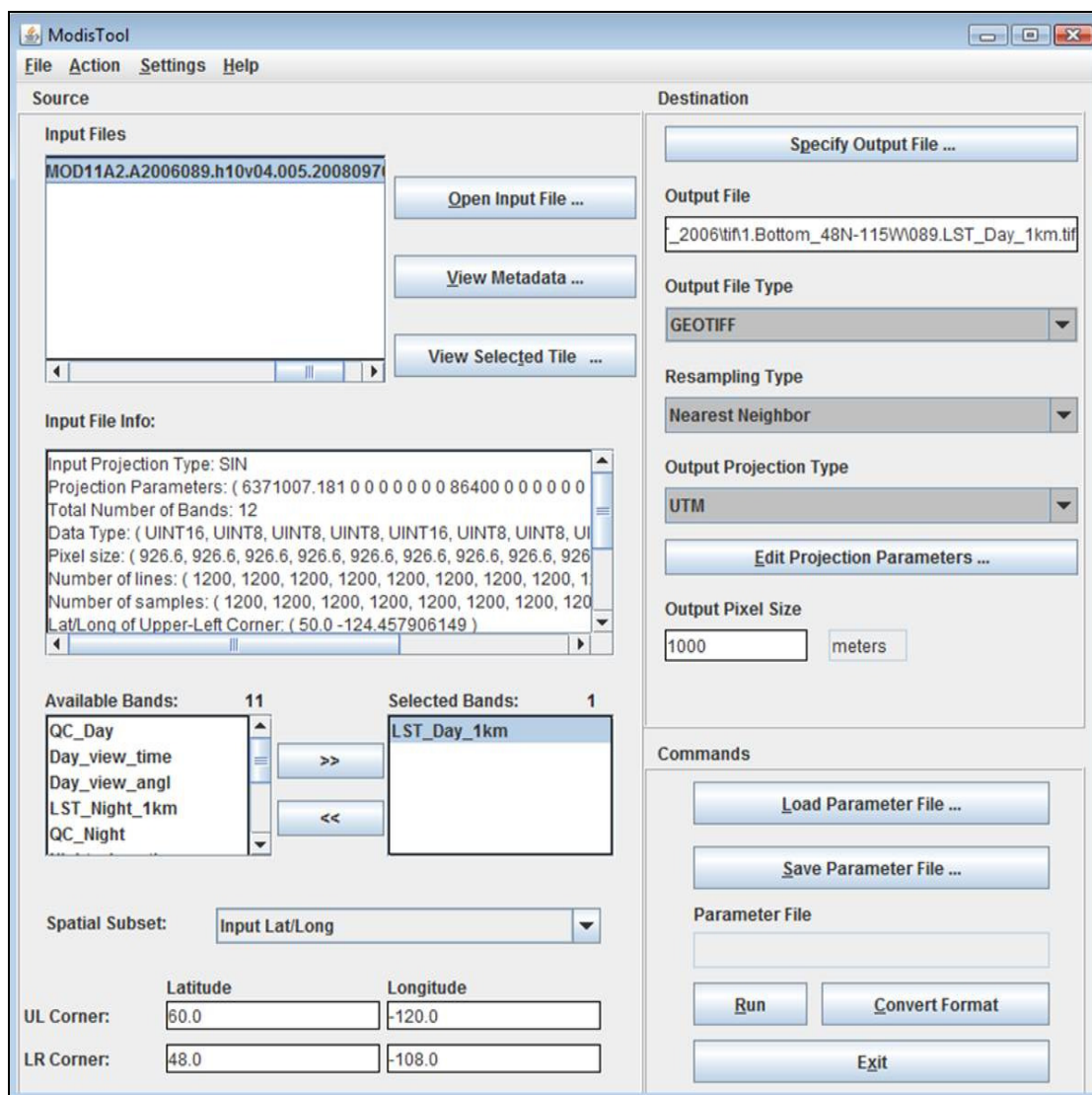


Figure 4.3: MRT Reprojection processing tool box upon up-loading the HDF file as input with the required parameters and reprojected Geo-TIFF image as output for MODIS T_S for the period of 12 (i.e., 89 DOY; within 48-60 °N and 108-120 °W).

4.1.2.3 Image Mosaicking

The four scenes of GEOTIFF images per period (i.e., 8-day composites of 27 periods during April-October, see Table 4.1) for each of the data set were then mosaicked together to create the respective final images of the data sets and then clipped them into Alberta shape (e.g., see Figure 4.4). Then, all the images were again re-projected to 10TM (Ten Degree Transverse Mercator) NAD 83 AEP Forest (usually used projection system by the Alberta Government). This projection system is suitable to span over the whole area of Alberta (Akther and Hassan 2011). Finally it was found 81 images for each of T_s , EVI, and NDWI and 3 images for land cover type for 2006-2008.

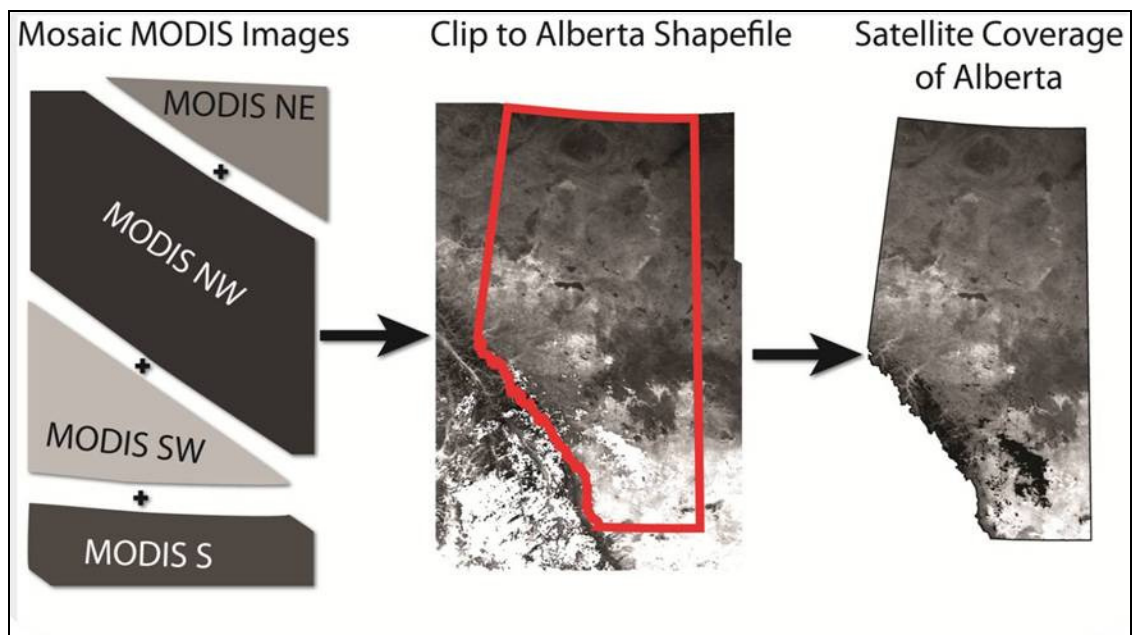


Figure 4.4: Process of mosaicking the reprojected TIFF image for all the MODIS data and clipping them at the coverage area of Alberta.

Table 4.1: Time periods of MODIS 8-day composites data.

Periods	DOY	Start dates in 2006/2007	Start dates in 2008	Periods	DOY	Start dates in 2006/2007	Start dates in 2008
12	89-96	30-Mar-07	29-Mar-08	26	201-208	20-Jul-07	19-Jul-08
13	97-104	07-Apr-07	06-Apr-08	27	209-216	28-Jul-07	27-Jul-08
14	105-112	15-Apr-07	14-Apr-08	28	217-224	05-Aug-07	04-Aug-08
15	113-120	23-Apr-07	22-Apr-08	29	225-232	13-Aug-07	12-Aug-08
16	121-128	01-May-07	30-Apr-08	30	233-240	21-Aug-07	20-Aug-08
17	129-136	09-May-07	08-May-08	31	241-248	29-Aug-07	28-Aug-08
18	137-144	17-May-07	16-May-08	32	249-256	06-Sep-07	05-Sep-08
19	145-152	25-May-07	24-May-08	33	257-264	14-Sep-07	13-Sep-08
20	153-160	02-Jun-07	01-Jun-08	34	265-272	22-Sep-07	21-Sep-08
21	161-168	10-Jun-07	09-Jun-08	35	273-280	30-Sep-07	29-Sep-08
22	169-176	18-Jun-07	17-Jun-08	36	281-288	08-Oct-07	07-Oct-08
23	177-184	26-Jun-07	25-Jun-08	37	289-296	16-Oct-07	15-Oct-08
24	185-192	04-Jul-07	03-Jul-08	38	297-305	24-Oct-07	23-Oct-08
25	193-200	12-Jul-07	11-Jul-08				

4.1.2.4 Generating EVI maps

The MODIS-based 8-day composites of surface reflectance data were used to calculate enhanced vegetation index using the Equation (2) described in the earlier section 2.4. The EVI images were preferred to calculate at 8-day intervals to match the temporal resolution of the T_s images instead of MODIS EVI products (i.e., MOD13Q1 V.005, only available in the form of 16-day composites). Then from the calculation the EVI maps were generated at 500 m spatial resolution throughout the growing season during 2006-2008.

4.1.2.5 Generating NDWI maps

The MODIS-based 8-day composites of surface reflectance data were used to calculate NDWI using the Equation (3) described in the earlier section 2.4 where the short wave infrared spectral band was 2.13 μm . It was revealed that $\text{NDWI}_{2.13\mu\text{m}}$ was found to be the best indices of interest for determining vegetation green up phenology (Sekhon et al. 2010). From the calculation the NDWI maps were generated at 500 m resolution throughout the growing season during 2006-2008.

4.1.2.6 Correcting cloud contamination of the satellite images

It was observed that the satellite images (i.e., T_s , EVI, and NDWI) were contaminated by cloud where the clouds obstacle might cause problems to understand the dynamics for the variable of interest. To fill the cloud contaminated pixels, the concept of image correction proposed by Hassan et al. (2007a) was used. The involved equations are as follows:

$$Y = \frac{\sum_{i=1}^{i=n} X(i) - X(i)}{m}, \text{ and} \quad (11)$$

$$Z_n = \bar{X}(n) - Y, \quad (12)$$

where,

$\bar{X}(i)$ is the mean value of T_s /EVI/NDWI for each of 27 8-day composites of T_s /EVI/NDWI for a specific year for the whole image [where i ($=1,2,3,\dots,n$) is the 8-day

period of interest and n = the total number of 8-day composite images (i.e. $n = 27$)] over the year,

$X(i)$ is the T_S /EVI/NDWI of every time series individual pixels values which are counted as cloud free composites, m is the total number of cloud-free 8-day composites,

Y is the average temporal deviation of T_S /EVI/NDWI from $\bar{X}(i)$ for a specific cloud-contaminated pixel of interest, and

Z_n is the estimated T_S /EVI/NDWI that was filled into cloud contaminated pixels of 8-day period.

4.1.2.7 Generating GDD maps

Both of the datasets (i.e., T_S and EVI) were used to calculate GDD by adopting the empirical methods described in Akther and Hassan (2011). It consisted of several steps:

- Step 1: The MODIS-based instantaneous 8-day composites of T_S were extracted at each of the single pixels (i.e., acquired between 10:30-12:00 local time) at the 182 weather stations; and compared them with the 8-day average air temperature (\bar{T}_a) during 2006 (see Figure 5.1a).
- Step 2: In order to validate the observed relation in Step 1, it was used at the sites of the same 182 weather stations during the years 2007-2008; and compared with the \bar{T}_a (see Figure 5.1b).

- Step 3: then the observed relation was applied (see in Figure 5.1b) in converting the MODIS-based T_s images into equivalent \overline{T}_a . These were then used to calculate GDD maps at 1 km spatial resolution using the following expression (Heidi and Ari 2008, Hassan and Bourque 2009):

$$GDD = \overline{T}_a - T_{base} \quad (13)$$

where, T_{base} is the base temperature (= 278.15 K), which is considered to be the minimum requirement for plant growth in our study area (Dowing and Pettapiece 2006, Hassan et al 2007a).

- Step 4: a data fusion technique was implemented which was initially described in Hassan et al. (2007b) in enhancing the spatial resolution of GDD maps from 1 km to 500 m using EVI images as a basis of fusion. It was possible as GDD and EVI were found to be linearly correlated (i.e., $r^2=0.87$; Hassan et al. 2007a). Mathematically, the data fusion process could be expressed as follows (Hassan et al. 2007b):

$$GDD_{500m} = \frac{EVI_{ins}}{EVI_{avg}} \times GDD_{1km} \quad (14)$$

where, EVI_{ins} is the instantaneous value of EVI at the centre of a 3 x 3 moving window; EVI_{avg} is the average value of all of the EVI values within the moving

window. The ratio between EVI_{ins} and EVI_{avg} acts as a weighted-function in the calculation of GDD at 500 m resolution.

- Step 5: At each of the period, the accumulated GDD (AGDD) were calculated using the following expression:

$$AGDD = \sum_{i=1}^n (8 \times GDD_{500m}) \quad (15)$$

where, i is the first 8-day period of the growing season; and n (=1 to 27) is the 8-day period of interest during the growing season.

4.2 Determining threshold for DLO, DLF and GGS

4.2.1 Determining threshold for DLO and GGS

The temporal trends of both GDD (AGDD) and NDWI were first extracted at the lookout tower sites location with the obtained *in-situ* DLO and GGS periodic records during the years of 2006-2008. Then in order to determine the best fitted threshold value of AGDD and NDWI for DLO and GGS occurring stage, these datasets were divided into two groups as calibration and validation phases. For calibration, ~34% data points which is the dataset in the year 2006 were considered and the remaining ~66% data points were used in validation purposes (i.e., during 2007-2008). The following steps were performed for DLO and GGS stage in the calibration purposes:

- Calculated an average and a standard deviation value of AGDD and NDWI-value at the lookout tower sites location during the *in-situ* DLO and GGS periods. Then

these values were considered as an initial threshold value for DLO and GGS where equal or greater amount of AGDD and NDWI would be the least requirement for DLO and GGS occurrence.

- On the basis of average and standard deviation value, a sensitivity analysis was performed for both of the initial threshold of AGDD and NDWI in determining the DLO and GGS stage within a range of “initial threshold ± 1 standard deviation” in the interval of one-third standard deviation. In terms of illustrating the early and delayed predictions with compare to the *in-situ* DLO and GGS observation periods, the signs of “-” and “+” deviations were used respectively throughout the thesis.

4.2.2 Determining thresholds for DLF

During the years of 2006-08, the temporal trends of MODIS-derived equivalent \bar{T}_a was extracted at those sites with available *in-situ* DLF records. For the determination of thresholds for DLF, the respective dataset were divided into calibration and validation datasets. In calibration, ~40% data points (i.e., during 2006-2007) were used for DLF. The inclusion of 2007 data in the calibration of DLF was due to the fact that 2006 data only represented ~29% of the entire dataset. The remaining data points were used in validation purposes in 2008. The calibration for DLF was performed in two distinct steps:

- Calculated the average and standard deviation of \bar{T}_a during the average *in-situ* DLF observation period. The observed average \bar{T}_a -value was then considered as

an initial “threshold” for DLF determination (i.e., either equal or less to the \bar{T}_a -value would be the minimum requirement for DLF occurrence);

- Performed sensitivity analysis for the initial threshold in determining the DLF stage in the range “initial threshold ± 1 standard deviation” in the interval of one-third standard deviation.

4.3 Validation

In the scope of validation, it was predicted the periods for: (i) DLO and GGS during the years 2007-2008, and (ii) DLF during 2008; using their respective optimal thresholds observed in the calibration phase as discussed above. Then the deviations were calculated between the predicted and observed DLO, DLF and GGS periods in determining the agreements between the datasets (see results and discussion chapter for more details).

4.4 Generating spatial dynamics for DLO, DLF and GGS

Between the two predictors (i.e., NDWI and AGDD), the best predictor threshold value was used to determine DLO and GGS. On the other hand, the best predictor threshold value of temperature was used to determine DLF. Thus the optimal threshold values were used to generate the spatial dynamics of DLO, DLF and GGS over the areas as shown in Figure 3.2 & 3.3.

CHAPTER 5: RESULTS AND DISCUSSION

This chapter illustrates all the results and discussion of this thesis work, which includes (i) the relation between MODIS-based T_s and air temperature, (ii) determination of thresholds values for DLO, DLF, and GGS and their validation, (iii) spatial dynamics of DLO, DLF and GGS, and (iv) discussion.

5.1 Relation between MODIS-based T_s and air temperature

The relation between MODIS-based instantaneous 8-day composites of T_s and 8-day average air temperature (\bar{T}_a) during 2006 revealed reasonably strong relations (i.e., $r^2 \approx 0.69$ with a slope of 0.61 ± 0.01 and intercept of 103.66 ± 3.55 at 95% confidence level for the regression line with p value < 0.0001 ; see Figure 5.1a). The relation observed in 2006, found to have similar relations (i.e., $r^2 \approx 0.70$ with a slope of 0.78 ± 0.01 and intercept 63.17 ± 3.05 at 95% confidence level for the regression line with p value < 0.0001 ; see Figure 5.1b) for approximately 97% of the cases during 2007-2008 period. The remaining 2.87% of the data points (i.e., 254 out of 8848) were found to be in southern Alberta, where the land cover is primarily agriculture area was excluded from the above mentioned analysis. Note that similar agreements (i.e., $r^2 \approx 0.70$) were also observed in other studies (Akther and Hassan 2011).

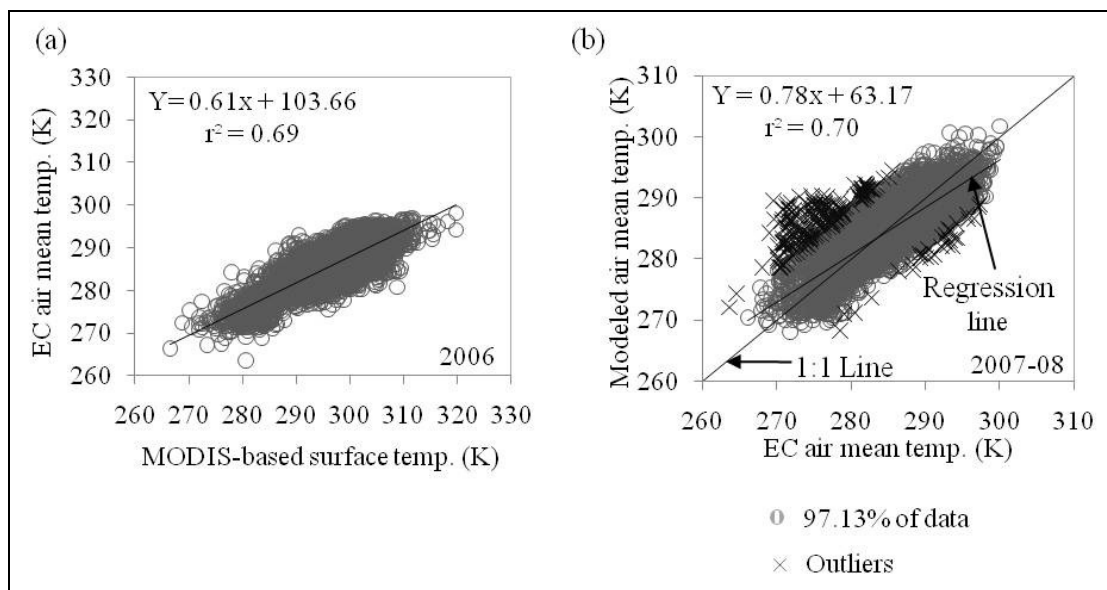


Figure 5.1: (a) relation between MODIS-based 8-day composites of instantaneous surface temperature (acquired between 10:30-12:00 local time) and 8-day average air temperature obtained from Environment Canada in 2006 ($n = 4561$; F-statistics = 10071.80 with p -value < 0.0001); (b) validation of the relationship as seen in (b) during 2007-2008 ($n = 8594$; F-statistics = 20288.79 with p -value < 0.0001).

5.2 Determination of thresholds values and its validation

5.2.1 Determination of the threshold-value for DLO

5.2.1.1 Determination of AGDD threshold for DLO and its validation

Figure 5.2a illustrates the averaged temporal trends of GDD and AGDD during 2006 upon considering all of the 115 lookout tower sites. It was found that the initial AGDD threshold was 101 degree-days with a standard deviation of ± 40 degree-days during the period of *in-situ* DLO as shown with the vertical dotted-line in Figure 5.2a. Then the distribution of the individual AGDD thresholds (see Figure 5.2b) was analyzed and $\sim 83\%$

of the cases were found to be in the range 60-140 degree-days (i.e., \sim initial threshold ± 1 standard deviation). Due to the observed variability's in the individual AGDD thresholds, a sensitivity analysis was performed in the range 60-140 degree-days (see Table 5.1) in the interval of 10 AGDD (i.e., \sim one-third of standard deviation). It was decided that the threshold of 80 would be the optimal selection; which yielded 35.7%, 86.1%, and 98.3% agreements at 0, ± 1 , and ± 2 periods of deviations respectively. Note that AGDD threshold of 90 had the highest agreements at 0 period of deviation (i.e., 39.1% of the cases); however, relatively less for both ± 1 (i.e., 80.9%) and ± 2 (i.e., 94.8%) periods of deviations. On the other hand, both of the AGDD thresholds of 60 and 70 were having greater agreements (i.e., 87.4%) at ± 1 period of deviation, but relatively less at 0 period of deviation (i.e., $\sim 31\%$) with compare to the threshold of 80. Thus the observed optimal AGDD threshold of 80 degree days would be reasonable for DLO.

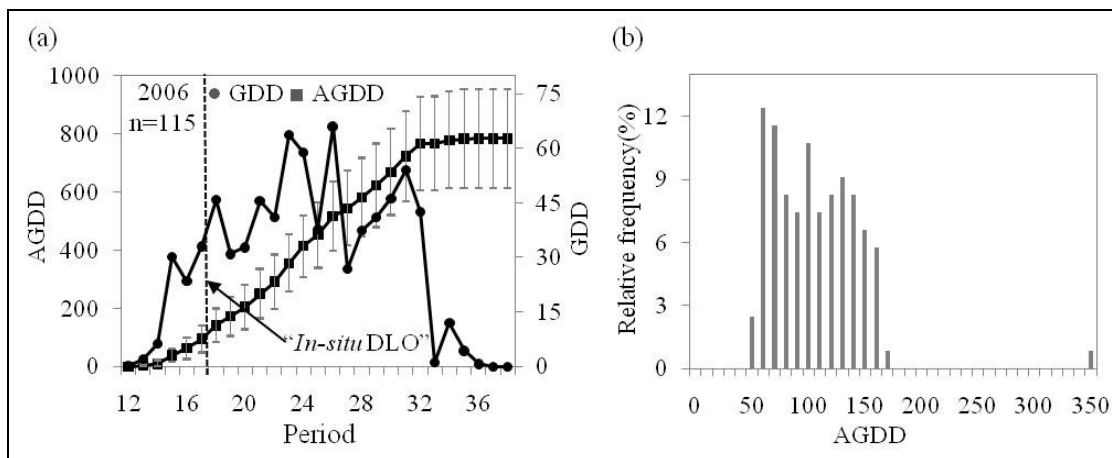


Figure 5.2: Determination of DLO threshold; (a) an averaged temporal trends of growing degree days (GDD), accumulated GDD (AGDD) along with its ± 1 standard deviation during 2006 at the lookout tower sites, and the average *in-situ* DLO observation period; (b) relative frequency distribution of all of the AGDD values at each individual lookout tower sites.

Table 5.1: Implementation of different AGDD thresholds in determining the optimal threshold by evaluating the deviations between observed and predicted DLO periods at each of the lookout tower sites using the data from 2006.

% out of 115 lookout towers (2006)								
AGDD	Deviations (in periods)							
Threshold	0	± 1	± 2	± 3	± 4	± 5	± 6	± 7
60	30.4	87.8	98.3	99.1	99.1	99.1	99.1	100
70	31.3	87.8	98.3	99.1	99.1	99.1	100	100
80	35.7	86.1	98.3	99.1	99.1	99.1	100	100
90	39.1	80.9	94.8	99.1	99.1	99.1	100	100
100	34.8	73.9	92.2	98.3	99.1	99.1	100	100
110	33.0	67.8	87.0	96.5	99.1	99	100	100
120	27.8	60.9	81.7	93.0	98.3	98	100	100
130	20.9	53.9	77.4	91.3	97.4	97	100	100
140	13.9	47.0	68.7	89.6	97.4	97	100	100

The optimal AGDD threshold (i.e., 80 degree-days) and other two nearby thresholds (i.e., 70 and 90 degree-days) were applied during the years 2007-2008 at the lookout tower sites (see Tables 5.2, 5.3, and 5.4). It was found that the deviations were ± 2 periods for significant amount of the cases for each of the AGDD thresholds, such as, (i) 88.2% in

2007, 85.8% in 2008, and 87.0% in 2007-2008 on an average for the AGDD threshold of 70 (see Table 5.2 for detail information); (ii) 94.5% in 2007, 89.4% in 2008, and 91.9% in 2007-2008 on an average for the AGDD threshold of 80 (see Table 5.3 for detail information); and (iii) 90.9% in 2007, 87.6% in 2008, and 89.2% in 2007-2008 on an average for the AGDD threshold of 90 (see Table 5.4 for detail information). Thus, the selection of the optimal AGDD threshold of 80 degree-days was proven to be the best one.

Table 5.2: Relation between observed and predicted DLO periods at each of the lookout tower sites during 2007-2008 using the optimal AGDD threshold of 70 degree days. The ‘+ve’ and ‘-ve’ signs represent positive (i.e., delayed) and negative (i.e., early) predictions respectively.

Year	No. of lookout tower sites	Deviations (in periods) on the basis of AGDD 70 degree-days						
		0	±1	±2	±3	±4	±5	≥ ±6
2007	110	33.6	73.6	88.2	95.5	96.4	100	100
2008	113	33.6	78.8	85.8	92.9	97.3	99.1	100
2007-2008	223	33.6	76.2	87.0	94.2	96.9	99.6	100

Table 5.3: Relation between observed and predicted DLO periods at each of the lookout tower sites during 2007-2008 using the optimal AGDD threshold of 80 degree days. The '+ve' and '-ve' signs represent positive (i.e., delayed) and negative (i.e., early) predictions respectively.

Year	No. of lookout tower sites	Deviations (in periods) on the basis of AGDD 80 degree-days						
		0	±1	±2	±3	±4	±5	±6
2007	110	30.9	78.2	94.5	98.2	99.1	100	100
2008	113	37.2	81.4	89.4	93.8	97.3	98.2	100
2007-2008	223	34.1	79.8	91.9	96.0	98.2	99.1	100

Table 5.4: Relation between observed and predicted DLO periods at each of the lookout tower sites during 2007-2008 using the optimal AGDD threshold of 90 degree days. The ‘+ve’ and ‘-ve’ signs represent positive (i.e., delayed) and negative (i.e., early) predictions respectively.

Year	No. of lookout tower sites	Deviations (in periods) on the basis of AGDD 90 degree-days						
		0	±1	±2	±3	±4	±5	±6
2007	110	22.7	69.1	90.9	96.4	99.1	100	100
2008	113	30.1	72.6	87.6	93.8	97.3	98.2	100
2007-2008	223	26.5	70.9	89.2	95.1	98.2	99.1	100

5.2.1.2 Determination of NDWI threshold for DLO and its validation

Figure 5.3a shows the averaged temporal trend of extracted NDWI-values at all the 115 lookout tower sites during 2006 along with the averaged *in-situ* DLO observed period using a vertical dotted line. The initial NDWI threshold was found to be 0.39 with a standard deviation of 0.16 that matched with the average *in-situ* DLO period. Further analysis of the distribution of the individual NDWI threshold values revealed that were analyzed; and ~83% of the cases were found in the range of 0.30-0.60 (i.e., ~initial threshold ± 1 standard deviation) (see Figure 5.3b). So thus, a sensitivity analysis of the NDWI thresholds was conducted in the range of 0.30-0.60 to determine the best NDWI

threshold (see Table 5.5). This analysis showed that a NDWI threshold of 0.325 would be the best selection, where it had better agreements with 20%, 55%, and 70% agreements at 0, ± 1 , and ± 2 periods of deviations respectively. Another NDWI threshold (i.e., 0.30) also revealed similar agreements (i.e. 18%, 55%, and 74% of the cases at 0, ± 1 , and ± 2 periods of deviations respectively). However, the NDWI threshold value of 0.325 had better agreement at the zero deviations compare to other thresholds values. Thus the NDWI threshold value of 0.325 was selected as the optimal NDWI threshold that was also relatively close to the initial NDWI threshold of 0.39.

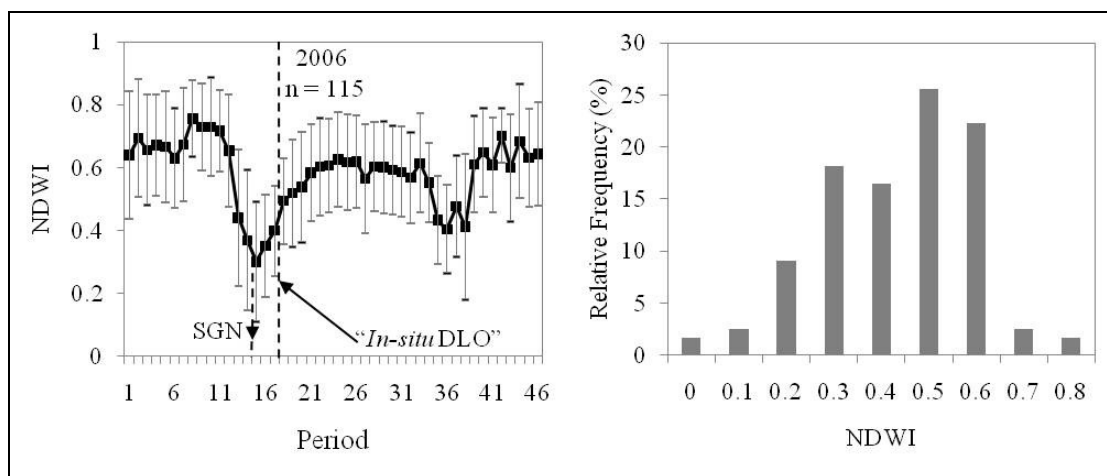


Figure 5.3: Determination of NDWI threshold for DLO; (a) an average temporal trends of NDWI along with its ± 1 standard deviation at all of the in-situ lookout tower sites in 2006; and the dotted line shows the averaged *in-situ* DLO period and n = total number of observed lookout tower stations in 2006; (b) relative frequency distribution of NDWI at all of the lookout tower sites.

Table 5.5: Implementation of different NDWI thresholds in determining the optimal threshold by evaluating the deviations between observed and predicted DLO periods at each of the lookout tower sites using the data from 2006.

% out of 121 lookout towers (2006)

NDWI Threshold	Deviations (in periods)								
	0	±1	±2	±3	±4	±5	±6	±7	> ±7
0.30	18	55	74	88	93	96	98	98	100
0.325	20	55	70	82	91	94	97	98	100
0.35	17	57	70	84	91	93	95	98	100
0.375	17	55	69	81	89	92	94	98	100
0.4	17	53	72	83	89	90	90	95	100
0.425	14	46	68	81	88	91	93	96	100
0.45	14	49	64	78	87	91	93	96	100
0.475	9	40	59	70	80	85	91	92	100
0.5	8	37	60	74	85	90	94	95	100
0.525	10	28	55	67	83	88	92	96	100
0.55	8	21	48	64	77	86	91	97	100
0.575	9	18	41	61	73	83	87	92	100
0.60	14	19	42	61	72	80	87	93	100

Table 5.6, 5.7, and 5.8 show the implementation of the optimal NDWI threshold (i.e., 0.325) along with other two nearby thresholds (i.e., 0.30, and 0.35) during the years 2007-2008 at the lookout tower sites. It revealed that the deviations were better for the NDWI threshold of 0.325 in relation to *in-situ* periods (i.e., ± 2 periods of deviation for 63% of the cases in 2007, 68% of the cases in 2008; and 65% of the cases in 2007-2008 on an average) in comparison to other two thresholds.

Table 5.6: Relation between observed and predicted DLO periods at each of the lookout tower sites during 2007-2008 using the optimal NDWI threshold 0.30. The ‘+ve’ and ‘-ve’ signs represent positive (i.e., delayed) and negative (i.e., early) predictions respectively.

Year	No. of lookout tower sites	Deviations (in periods) on the basis of NDWI 0.30								
		0	± 1	± 2	± 3	± 4	± 5	± 6	± 7	$> \pm 7$
2007	115	10	32	57	78	87	96	97	99	100
2008	119	23	55	73	83	92	99	99	100	100
2007-08	234	16	44	65	81	90	97	98	100	100

Table 5.7: Relation between observed and predicted DLO periods at each of the lookout tower sites during 2007-2008 using the optimal NDWI threshold 0.325. The ‘+ve’ and ‘-ve’ signs represent positive (i.e., delayed) and negative (i.e., early) predictions respectively.

Year	No. of lookout tower sites	Deviations (in periods) on the basis of NDWI 0.325								
		0	±1	±2	±3	±4	±5	±6	±7	> ±7
2007	115	10	39	63	82	90	96	98	99	100
2008	119	19	50	68	76	88	97	97	100	100
2007-08	234	15	45	65	79	89	96	98	100	100

Table 5.8: Relation between observed and predicted DLO periods at each of the lookout tower sites during 2007-2008 using the optimal NDWI threshold 0.35. The ‘+ve’ and ‘-ve’ signs represent positive (i.e., delayed) and negative (i.e., early) predictions respectively.

Year	No. of lookout tower sites	Deviations (in periods) on the basis of NDWI 0.35								
		0	±1	±2	±3	±4	±5	±6	±7	> ±7
2007	115	7	36	63	78	89	94	99	99	100
2008	119	13	42	65	71	87	94	97	100	100
2007-08	234	10	39	64	75	88	94	98	100	100

5.2.2 Determination of the temperature threshold for DLF and its validation

Figure 5.4a illustrates the averaged temporal trend of equivalent \bar{T}_a during the years 2006-2007 upon considering all of the 21 lookout tower sites. It was found that the initial \bar{T}_a threshold was 4.4 °C with a standard deviation of ± 1.46 °C during the period of *in-situ* DLF as shown with the vertical dotted-line in Figure 5.4a. The distribution of the individual \bar{T}_a thresholds (see Figure 5.4b) was found to be in the range 3-6 °C (i.e., \sim initial threshold ± 1 standard deviation) for $\sim 80\%$ of the cases. Within this range, it was decided that threshold of 4 °C would be the optimal selection; which yielded 23.8%, 81.0%, 90.5% agreements at 0, ± 1 , and ± 2 periods of deviations respectively (see Table 5.9). The \bar{T}_a thresholds of 4.5 and 5 °C were having greater agreements at 0 deviation (i.e., 28.6% and 38.1% for 4.5 and 5 °C respectively); however, relatively less for both ± 1 (i.e., 66.7%) and ± 2 (i.e., 76.2%) periods of deviations. Thus the observed optimal \bar{T}_a threshold of 4 °C would be reasonable.

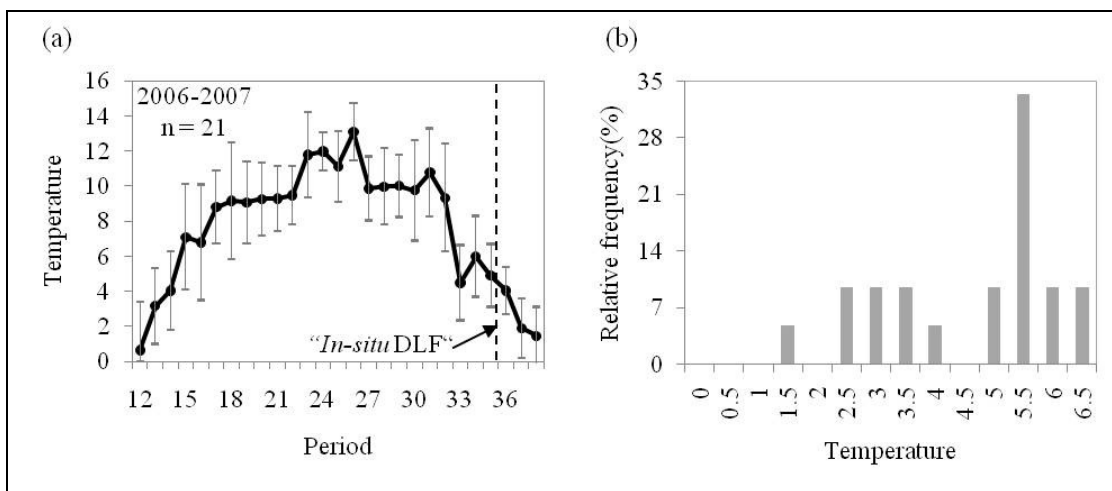


Figure 5.4: Determination of DLF threshold; (a) an averaged temporal trends of equivalent 8-day air temperature (\bar{T}_a) along with its ± 1 standard deviation during 2006-2007, and the average *in-situ* DLF observation period; (b) relative frequency distribution of all of the \bar{T}_a values at each individual lookout tower sites.

Table 5.9: Implementation of different \bar{T}_a thresholds in determining the optimal threshold by evaluating the deviations between observed and predicted DLF periods at each of the lookout tower sites using the data from 2006-2007.

% out of 21 lookout towers (2006-2007)									
Temperature	Deviations (in periods)								
Threshold	0	± 1	± 2	± 3	± 4	± 5	± 6	± 7	$> \pm 7$
3	9.5	57.1	71.4	100	100	100	100	100	100
3.5	14.3	71.4	85.7	100	100	100	100	100	100
4	23.8	81.0	90.5	100	100	100	100	100	100
4.5	28.6	66.7	76.2	90	95	100	100	100	100
5	38.1	52.4	71.4	90.5	90.5	90.5	95	95	100
5.5	19.0	42.9	52.4	66.7	71.4	76	86	86	100
6	9.5	33.3	57.1	61.9	66.7	66.7	76.2	85.7	100

The optimal \bar{T}_a threshold (i.e., 4 °C) with other two nearby thresholds (i.e., 3.5 °C and 4.5 °C) were applied during the 2008 at the lookout tower sites (see Table 5.10, 5.11, & 5.12). It was found that the deviations were ± 2 periods for reasonable amount of cases for each of the \bar{T}_a thresholds during 2008, such as (i) 71.0% for the \bar{T}_a threshold of 3.5 °C (see Table 5.10 for detail information); (ii) 77.4% for the \bar{T}_a threshold of 4 °C (see Table 5.11 for detail information); and (iii) 74.2% for the \bar{T}_a threshold of 4.5 °C (see Table

5.12 for detail information). Thus, the selection of the optimal \bar{T}_a threshold of 4 °C was proven to be the best one. The level of agreements in validation phases was relatively less in comparison to that of the calibration phase (i.e., 90.5% of the cases for ± 2 periods of deviations for the \bar{T}_a threshold 4 °C). It might be associated with the relatively less number of *in-situ* DLF data points (i.e., 52 in total for the years 2006-2008) available for this study.

Table 5.10: Relation between observed and predicted DLF periods at each of the lookout tower sites during 2008 using the optimal 8-day air temperature (\bar{T}_a) threshold of 3.5 °C. The '+ve' and '-ve' signs represent positive (i.e., delayed) and negative (i.e., early) predictions respectively.

Year	No. of lookout tower sites	Deviations (in periods) on the basis of 3.5 °C					
		0	± 1	± 2	± 3	± 4	± 5
2008	31	19.4	41.9	71.0	83.9	87.1	100

Table 5.11: Relation between observed and predicted DLF periods at each of the lookout tower sites during 2008 using the optimal 8-day air temperature (\bar{T}_a) threshold of 4 °C. The '+ve' and '-ve' signs represent positive (i.e., delayed) and negative (i.e., early) predictions respectively.

Year	No. of lookout tower sites	Deviations (in periods) on the basis of 4 °C					
		0	±1	±2	±3	±4	±5
2008	31	19.4	51.6	77.4	87	94	100

Table 5.12: Relation between observed and predicted DLF periods at each of the lookout tower sites during 2008 using the optimal 8-day air temperature (\bar{T}_a) threshold of 4.5 °C. The '+ve' and '-ve' signs represent positive (i.e., delayed) and negative (i.e., early) predictions respectively.

Year	No. of lookout tower sites	Deviations (in periods) on the basis of 4.5 °C					
		0	±1	±2	±3	±4	±5
2008	31	12.9	48.4	74.2	87.1	90.3	100

5.2.3 Determination of the threshold-value for GGS

5.2.3.1 Determination of AGDD threshold for GGS and its validation

Figure 5.5 shows the averaged temporal trends of GDD and AGDD considering all of the 121 lookout tower sites during 2006; and also the distribution of the individual AGDD thresholds. During the average *in-situ* period of GGS (as shown with the vertical dotted-line in Figure 5.5a), it was found that an AGDD threshold of 128 degree-days with a standard deviation of ± 48 degree-days. It would be interesting to note that ~89% of the cases were found in the AGDD threshold range of 60-195 degree-days (i.e., ~initial threshold ± 1 standard deviation) in the interval of 15 AGDD (i.e., ~one-third of standard deviation). In this particular range of the AGDD thresholds, a sensitivity analysis was performed (see Table 5.13 for more information). It revealed that the AGDD threshold of 90 degree-days would be the best selection, which produced reasonable agreements (i.e., 31.4%, 71.9%, and 90.1% agreements at 0, ± 1 , and ± 2 periods of deviations respectively) in comparison to the *in-situ* GGS observations. The AGDD thresholds of both 75 and 105 degree-days were also having reasonable agreements at ± 2 period of deviations (i.e. 83.5-86.8% of the cases), however these had relatively less agreements at 0 period of deviations (i.e., 24.0-27.3% of the cases), and ± 1 period of deviations (i.e., 64.2-65.0% of the cases). Thus the observed optimal AGDD threshold of 90 degree days would be reasonable for GGS.

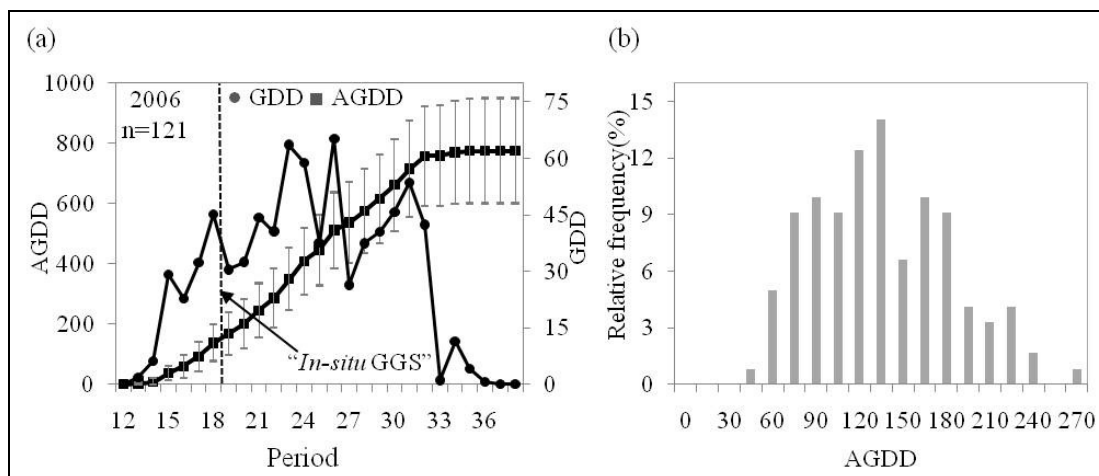


Fig. 5.5: Determination of GGS threshold; (a) an average temporal trends of GDD and AGDD along with its ± 1 standard deviation at all of the *in-situ* lookout tower sites during 2006; and the dotted line shows the averaged *in-situ* GGS period and n = total number of observed lookout tower stations in 2006; (b) relative frequency distribution of AGDD at each individual lookout tower sites.

Table 5.13: Implementation of different AGDD thresholds to determine the best AGDD threshold for predicting GGS during 2006.

% out of 121 lookout towers (2006)

AGDD Threshold	Deviations (in periods)							
	0	±1	±2	±3	±4	±5	±6	±7
60	19.0	53.7	79.3	94.2	100	100	100	100
75	24.0	64.2	83.5	97.5	100	100	100	100
90	31.4	71.9	90.1	98.3	100	100	100	100
105	27.3	65.0	86.8	97.5	99.2	100	100	100
120	24.0	67.8	86.0	93.4	99.2	100	100	100
135	16.5	62.0	84.3	91.7	98.3	99.2	100	100
150	19.8	56.2	78.5	89.3	96.7	99.2	100	100
165	14.0	47.9	71.1	86.0	95.0	99.2	100	100
180	9.1	41.3	63.6	82.6	92.6	99.2	100	100
195	6.6	34.7	53.7	76.0	88.4	97.5	99.2	100

The optimal AGDD threshold (i.e., 90 degree-days) and other two nearby thresholds (i.e., 75 and 105 degree-days) were then applied to determine the predicted GGS periods during the years 2007-2008 at the lookout tower sites (see Table 5.14, 5.15, and 5.16). It was found that the agreements between the AGDD-derived and *in-situ* GSS observations

were reasonable at ± 2 periods of deviations for each of the AGDD thresholds, such as, (i) 89.3% in 2007, 88.3% in 2008, and 88.8% in 2007-2008 for the threshold AGDD 75 on an average (see Table 5.14 for detail information); (ii) 94.3% in 2007, 94.2% in 2008, and 94.2% in 2007-2008 for the threshold AGDD 90 on an average (see Table 5.15 for detail information; and (iii) 90.2% in 2007, 90.0% in 2008, and 90.1% in 2007-2008 for the threshold AGDD 105 on an average (see Table 5.16 for detail information). Thus, the selection of the optimal AGDD threshold of 90 degree-days was proven to be the best one.

Table 5.14: Relation between *in-situ* observed and AGDD-based predicted GGS periods at each of the lookout tower sites during 2007-2008 using the optimal AGDD threshold of 75 degree days. The ‘+ve’ and ‘-ve’ signs represent positive (i.e., delayed) and negative (i.e., early) predictions respectively.

Year	No. of lookout tower sites	Deviations (in periods) on the basis of AGDD 75 degree-days					
		0	± 1	± 2	± 3	± 4	± 5
2007	122	30.3	72.1	89.3	95.1	99.2	100
2008	120	28.3	65.0	88.3	95.8	100	100
2007-2008	242	29.3	68.6	88.8	95.5	100	100

Table 5.15: Relation between *in-situ* observed and AGDD-based predicted GGS periods at each of the lookout tower sites during 2007-2008 using the optimal AGDD threshold of 90 degree days. The '+ve' and '-ve' signs represent positive (i.e., delayed) and negative (i.e., early) predictions respectively.

Year	No. of lookout tower sites	Deviations (in periods) on the basis of AGDD 90 degree-days					
		0	±1	±2	±3	±4	±5
2007	122	44.3	79.5	94.3	96.7	98.4	100
2008	120	35.8	73.3	94.2	99.2	100	100
2007-2008	242	40.1	76.4	94.2	97.9	99.2	100

Table 5.16: Relation between *in-situ* observed and AGDD-based predicted GGS periods at each of the lookout tower sites during 2007-2008 using the optimal AGDD threshold of 105 degree days. The '+ve' and '-ve' signs represent positive (i.e., delayed) and negative (i.e., early) predictions respectively.

Year	No. of lookout tower sites	Deviations (in periods) on the basis of AGDD 105 degree-days						
		0	±1	±2	±3	±4	±5	±6
2007	122	32.8	70.5	90.2	95.1	96.7	100	100
2008	120	30.8	73.3	90.0	95.8	97.5	99.2	100
2007-2008	242	31.8	71.9	90.1	95.5	97.1	100	100

5.2.3.2 Determination of NDWI threshold for GGS and its validation

Fig. 5.6a shows the averaged temporal trend of extracted NDWI-values at all of the 121 GGS lookout tower sites during 2006 along with the averaged *in-situ* GGS observed period (as shown using a vertical dotted line). The initial NDWI threshold was found to be 0.48 with a standard deviation of 0.16 that coincided with the average *in-situ* DLO period. In addition, the frequency distribution of the individual NDWI threshold values were found to be in the range of 0.30-0.65 (i.e., \sim initial threshold ± 1 standard deviation) for $\sim 86\%$ of the cases (see Figure 5.6b). Thus, a sensitivity analysis of the NDWI thresholds was performed in this range of thresholds to determine the optimal one (see Table 5.17 for more details). It was found that the NDWI threshold of 0.45 would be the best selection, which produced better agreements (i.e., 21.5%, 56.2%, 69.4% of the cases at 0, ± 1 , and ± 2 periods of deviations respectively). The other thresholds of both 0.40 and 0.50 also produced similar agreements (i.e. 15.7-24.0%, 50.4-51.2%, and 65.3-68.6% of the cases at 0, ± 1 , and ± 2 periods of deviations respectively). Thus the NDWI threshold value of 0.45 was selected as the optimal NDWI threshold that was also relatively close to the initial NDWI threshold of 0.48.

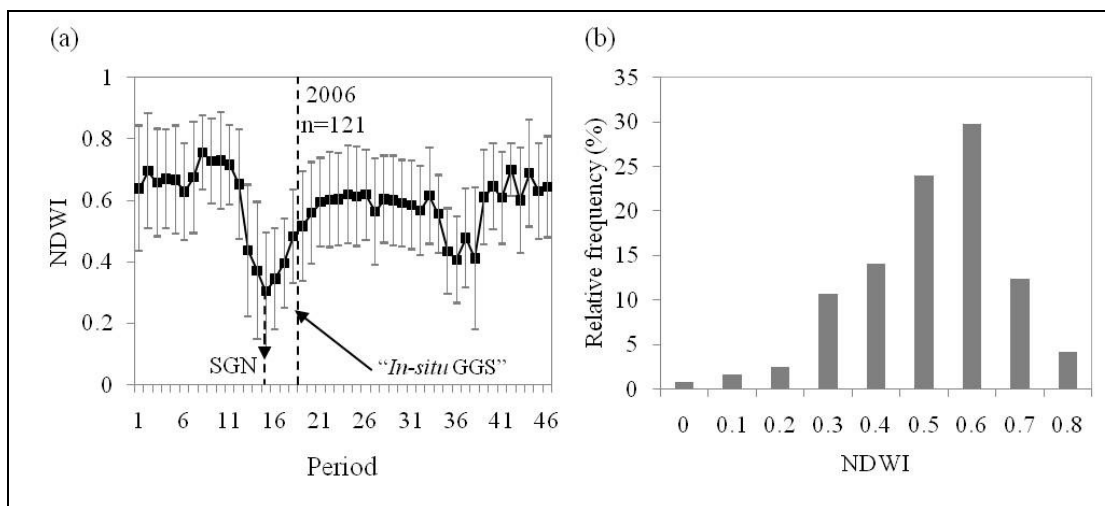


Fig. 5.6: Determination of NDWI threshold for GGS; (a) an average temporal trends of NDWI along with its ± 1 standard deviation at all of the in-situ lookout tower sites in 2006; and the dotted line shows the averaged *in-situ* GGS period and n = total number of observed lookout tower stations in 2006; (b) relative frequency distribution of NDWI at all of the lookout tower sites.

Table 5.17: Implementation of different NDWI thresholds to determine the best NDWI threshold for predicting GGS during 2006.

% out of 121 lookout towers (2006)

NDWI Threshold	Deviations (in periods)								
	0	±1	±2	±3	±4	±5	±6	±7	> ±7
0.3	13.2	50.4	66.9	85.1	92.6	95.9	98.3	100	100
0.35	9.9	49.6	67.8	81.0	90.9	95.9	96.7	99.2	100
0.4	15.7	50.4	68.6	83.5	88.4	90.9	94.2	97.5	100
0.45	21.5	56.2	69.4	78.5	85.1	90.1	97.5	98.3	100
0.5	24.0	51.2	65.3	77.7	86.0	91.7	95.9	98.3	100
0.55	24.0	43.8	57.0	65.3	81.0	90.1	95.9	100	100
0.6	13.2	33.1	54.5	62.8	73.6	83.5	95.0	99.2	100
0.65	13.2	33.1	45.5	62.0	72.7	84.3	94.2	97.5	100

Table 5.18, 5.19, and 5.20 show the implementation of the optimal NDWI threshold (i.e., 0.45) along with other two nearby thresholds (i.e., 0.40, and 0.50) during the years 2007-2008 at the lookout tower sites and compared with the *in-situ* GGS observations. It revealed that the deviations were better for the NDWI threshold of 0.45 in relation to *in-situ* periods (i.e., ±2 periods of deviation for 63.1% of the cases in 2007, 65.8% of the cases in 2008; and 64.5% of the cases in 2007-2008 on an average) in comparison to other two thresholds.

Table 5.18: Relation between *in-situ* observed and NDWI-based predicted GGS periods at each of the lookout tower sites during 2007-2008 using the optimal NDWI threshold of 0.40. The '+ve' and '-ve' signs represent positive (i.e., delayed) and negative (i.e., early) predictions respectively.

Year	No. of lookout tower sites	Deviations (in periods) on the basis of NDWI 0.40						
		0	±1	±2	±3	±4	±5	±6
2007	122	10.7	40.2	62.3	77.0	89.3	95.9	100
2008	120	9.2	40.0	63.3	79.2	90.8	95.0	100
2007-08	242	9.9	40.1	62.8	78.1	90.1	95.5	100

Table 5.19: Relation between *in-situ* observed and NDWI-based predicted GGS periods at each of the lookout tower sites during 2007-2008 using the optimal NDWI threshold of 0.45. The '+ve' and '-ve' signs represent positive (i.e., delayed) and negative (i.e., early) predictions respectively.

Year	No. of lookout tower sites	Deviations (in periods) on the basis of NDWI 0.45						
		0	±1	±2	±3	±4	±5	±6
2007	122	18.9	48.4	63.1	79.5	90.2	98.4	100
2008	120	16.7	43.3	65.8	79.2	88.3	95.8	100
2007-08	242	17.8	45.9	64.5	79.3	89.3	97.1	100

Table 5.20: Relation between *in-situ* observed and NDWI-based predicted GGS periods at each of the lookout tower sites during 2007-2008 using the optimal NDWI threshold of 0.50. The ‘+ve’ and ‘-ve’ signs represent positive (i.e., delayed) and negative (i.e., early) predictions respectively.

Year	No. of lookout tower sites	Deviations (in periods) on the basis of NDWI 0.50						
		0	±1	±2	±3	±4	±5	≥ ±6
2007	122	6.6	31.1	47.5	63.9	83.6	95.9	100
2008	120	12.5	34.2	54.2	66.7	81.7	92.5	100
2007-08	242	9.5	32.6	50.8	65.3	82.6	94.2	100

5.3 Discussion

During the calibration phase for the DLO, DLF, and GGS determination, the following variability's associated with the variable of interest (i.e., AGDD, NDWI, and \bar{T}_a) were found:

- AGDD thresholds varied in between 60-140 degree-days for ~83% of the cases for DLO (see Table 5.1), and 60-195 degree-days for ~89% of the cases for GGS (see Table 5.13);
 - NDWI thresholds varied in the range of 0.30-0.60 for ~83% of the cases for DLO (see Table 5.5), and 0.30-0.65 for ~86% of the cases for GGS (see Table 5.17);
- and

- \bar{T}_a thresholds were found to be in between 3-6 °C for ~80% of the cases for DLF (see Table 5.9).

The above mentioned variability's might be related with one or more of the following causes:

- apart from the temperature regimes, the phenological stages would also be influenced by other climatic variables, e.g., photosynthetically active radiation and water regimes; which were not considered in the scope of this study.
- some other climatic condition during the prior winter season, i.e., the fulfillment of the chilling requirements would also a critical parameter (Morin et al. 2009);
- it would be possible that the optimal amount of nutrient might not be available for all of the lookout tower sites;
- biological factors, such as, the inter and intra-species competition were not take into consideration; and
- the differences in genetic compositions among the inter and intra-species might differ in terms of their growth requirements observed in other studies (Li et al. 2010); among others.

In terms of determined thresholds, the AGDD threshold of 80 degree-days for DLO was found to be similar (i.e., in the range 80-100 degree-days) with compare to other studies conducted over western Canadian boreal forests (Parry et al. 1997, Barr et al. 2004). On the other hand, it was not possible to compare the AGDD threshold for GGS

determination as there were no similar studies found in the literature so far. In addition, in the context of NDWI thresholds, no studies were so far to found for both DLO and GGS for comparison purposes. In terms of \bar{T}_a threshold for determining DLF, the optimal threshold of 4 °C) would be reasonable as plants would cease the biological activities below 5 °C in general (Hassan and Bourque 2009).

During the DLO, DLF, and GGS validation phase, the relatively high deviations (i.e., > ± 2 periods) between the MODIS-predicted and *in-situ* observations were found as follows:

- ~10% and 6% of the cases for DLO and GGS using AGDD thresholds;
- ~35% of the cases for both DLO and GGS using NDWI thresholds; and
- ~23% of the cases for DLF using \bar{T}_a threshold.

The above mentioned deviations might be attributed due to one or combination of the following causes:

- the *in-situ* measurements were on the basis of visual observations, thus the operators' interpretation skills would be critical (Sekhon et al. 2010);
- at each of the lookout tower sites, ~20 to 100 trees were sampled to define the occurrence of the phenological stage of interest (Dylan Heerema: a veteran lookout tower operator, personal communication). Thus, it would be possible that the spatial resolution of the *in-situ* observations might not have similar dimension as of MODIS data for some cases.

- one global threshold might not be able to delineate the entire spatial dynamics across the study area (Li et al. 2010); and
- the relatively less number of *in-situ* DLF data points (i.e., 52 in total for the years 2006-2008) would not be sufficient enough.

5.4 Spatial dynamics of DLO, DLF and GGS

Between the two predictors of AGDD and NDWI, the analysis revealed that the AGDD thresholds were produced better results for determining both DLO and GGS. Thus, respective AGDD thresholds (i.e., 80 and 90 degree-days for DLO and GGS respectively) were used to generate the spatial dynamics for both DLO and GGS. On the other hand, the \bar{T}_a threshold of 4 °C was used to generate the spatial dynamics of DLF.

5.4.1 Spatial dynamics of DLO

Figure 5.7, 5.8 and 5.9 shows the spatial dynamics of DLO over the deciduous-dominant stands across Alberta during 2006-2008 upon applying the observed optimal threshold of AGDD. It revealed that the DLO occurred during the periods of 17-19 (i.e., 9 May-1 June in 2006 and 2007; and 8 May-31 May in 2008) for most of the times (i.e., ~65%, 82%, and 85% of the cases in 2006, 2007, and 2008 respectively (see Figures 5.7, 5.8. and 5.9). In general, the period of DLO occurrence was increasing in the northward directions and decreasing in the southward directions. It could be explained with the fact that temperature regimes decrease in the northward directions and in the high elevated/mountain areas in the northern hemisphere (Hassan et al. 2007a, Sekhon et al. 2010).

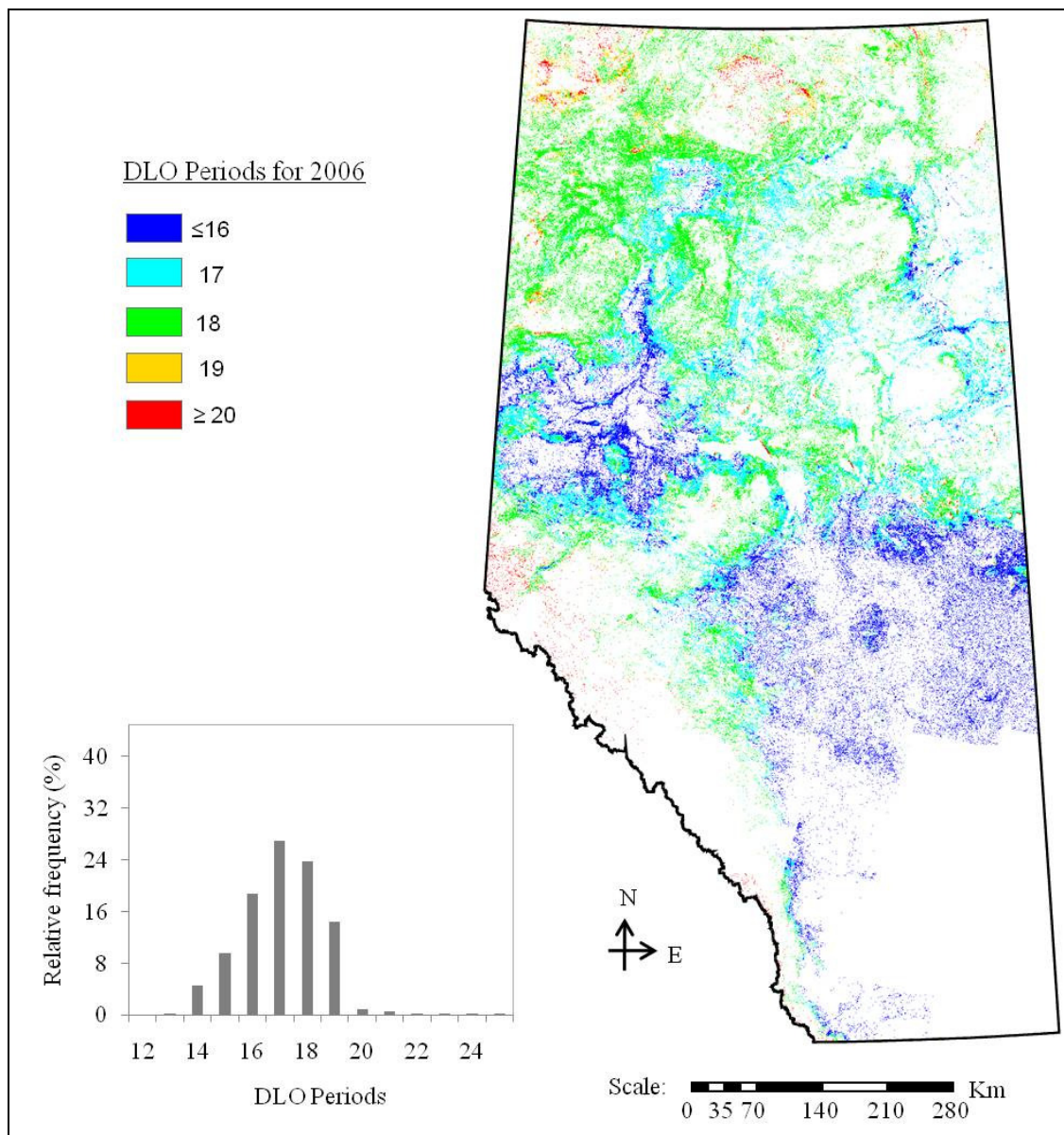


Figure 5.7: Spatial dynamics for the timing of DLO and its relative frequency during 2006.

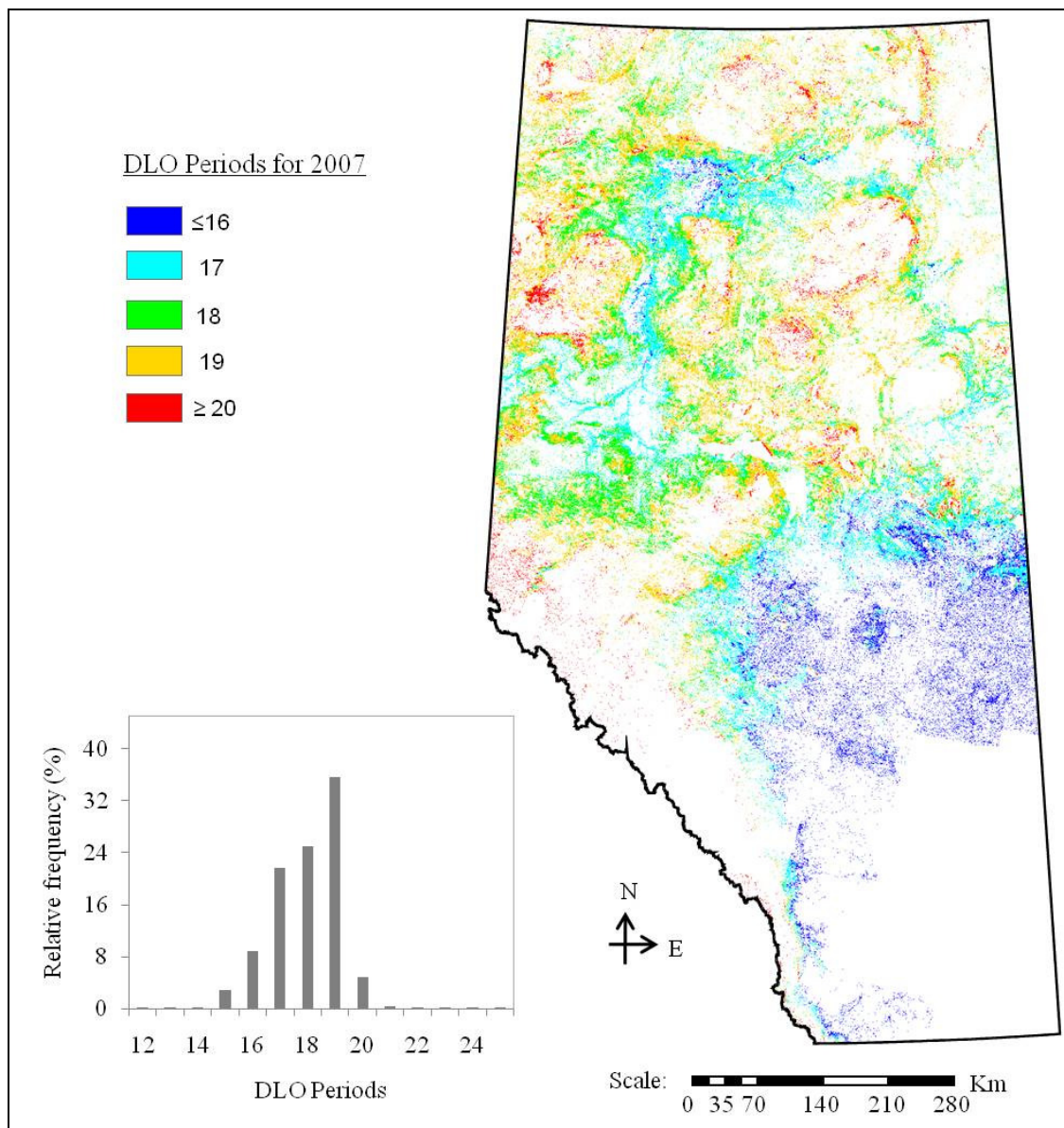


Figure 5.8: Spatial dynamics for the timing of DLO and its relative frequency during 2007.

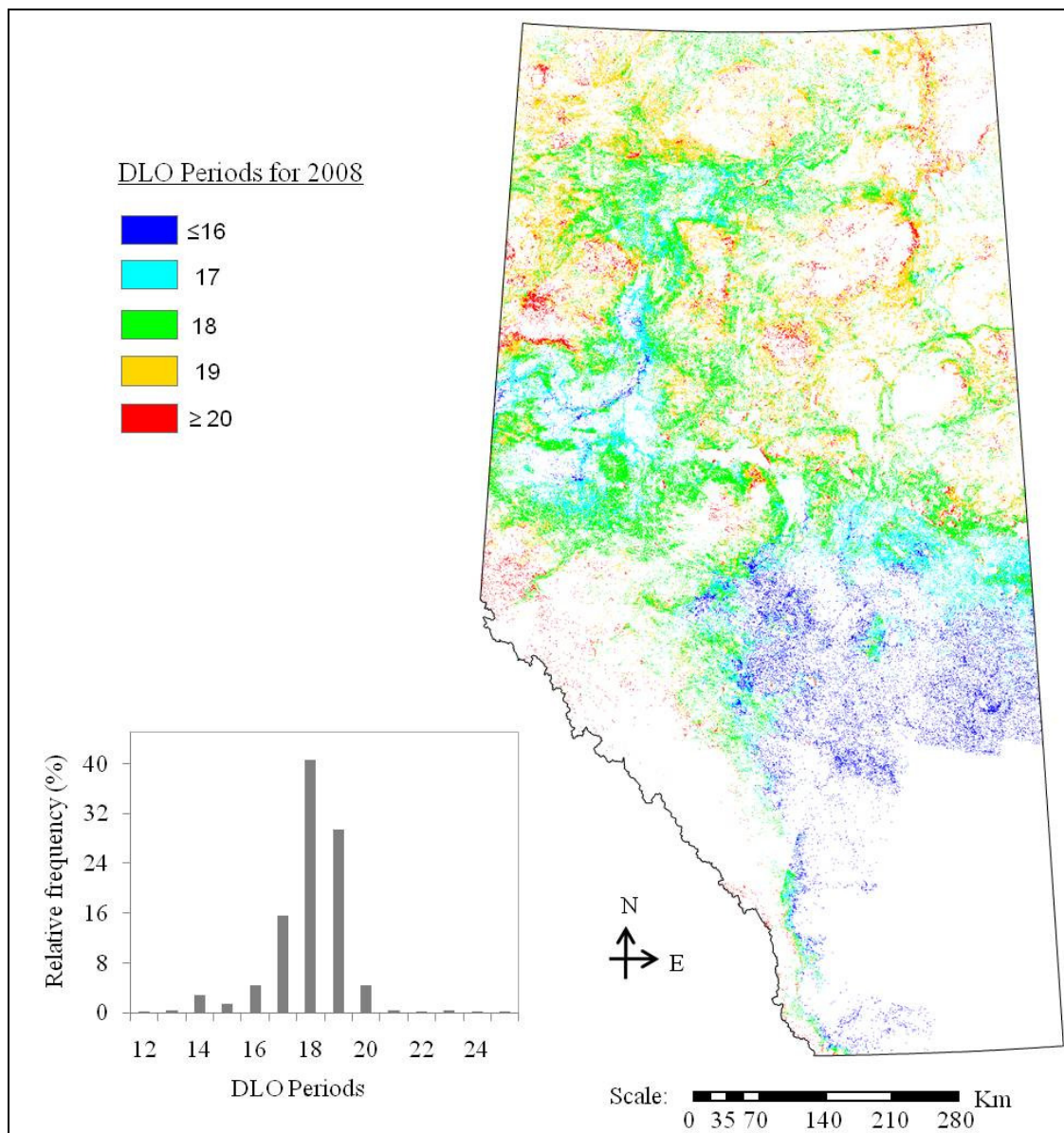


Figure 5.9: Spatial dynamics for the timing of DLO and its relative frequency during 2008.

5.4.2 Spatial dynamics of DLF

Figure 5.10, 5.11 and 5.12 shows the spatial dynamics of DLF over the deciduous-dominant stands across Alberta during 2006-2008 upon applying the observed optimal threshold of \bar{T}_a . It revealed that the DLF occurred during the periods of 32-36 (i.e., 6 Sep.-15 Oct. in 2006 and 2007; and 5 Sep.-14 Oct. in 2008) for most of the times (~88%, 73%, and 75% of the cases in 2006, 2007, and 2008 respectively (see Figures 5.9, 5.10, and 5.11). In general, the occurrences happened opposite for DLF with compare to DLO (i.e., DLF occurrence was increasing in the southward directions). It could be explained with the fact that discussed above in section 5.4.1.

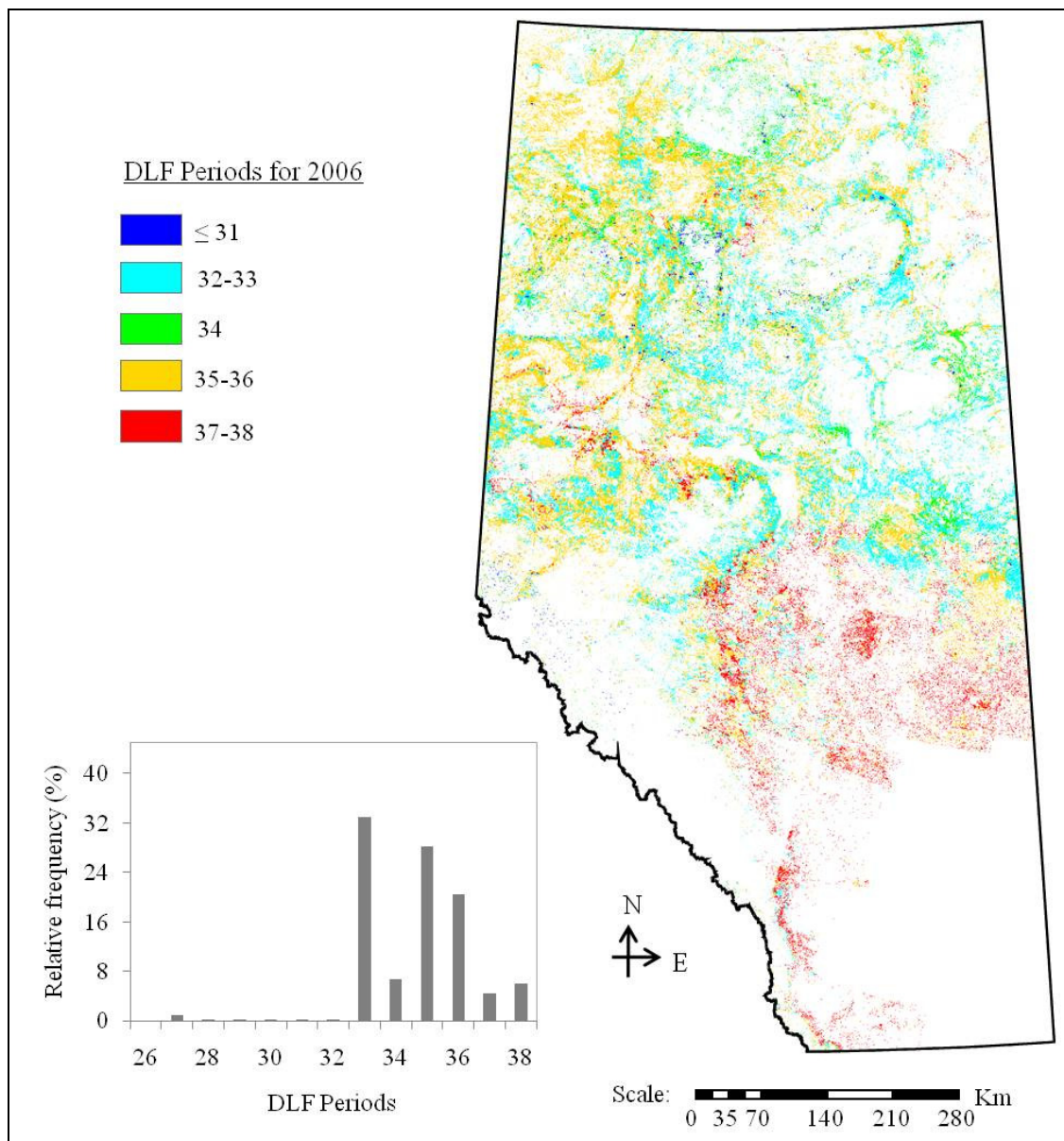


Figure 5.10: Spatial dynamics for the timing of DLF and its relative frequency during 2006.

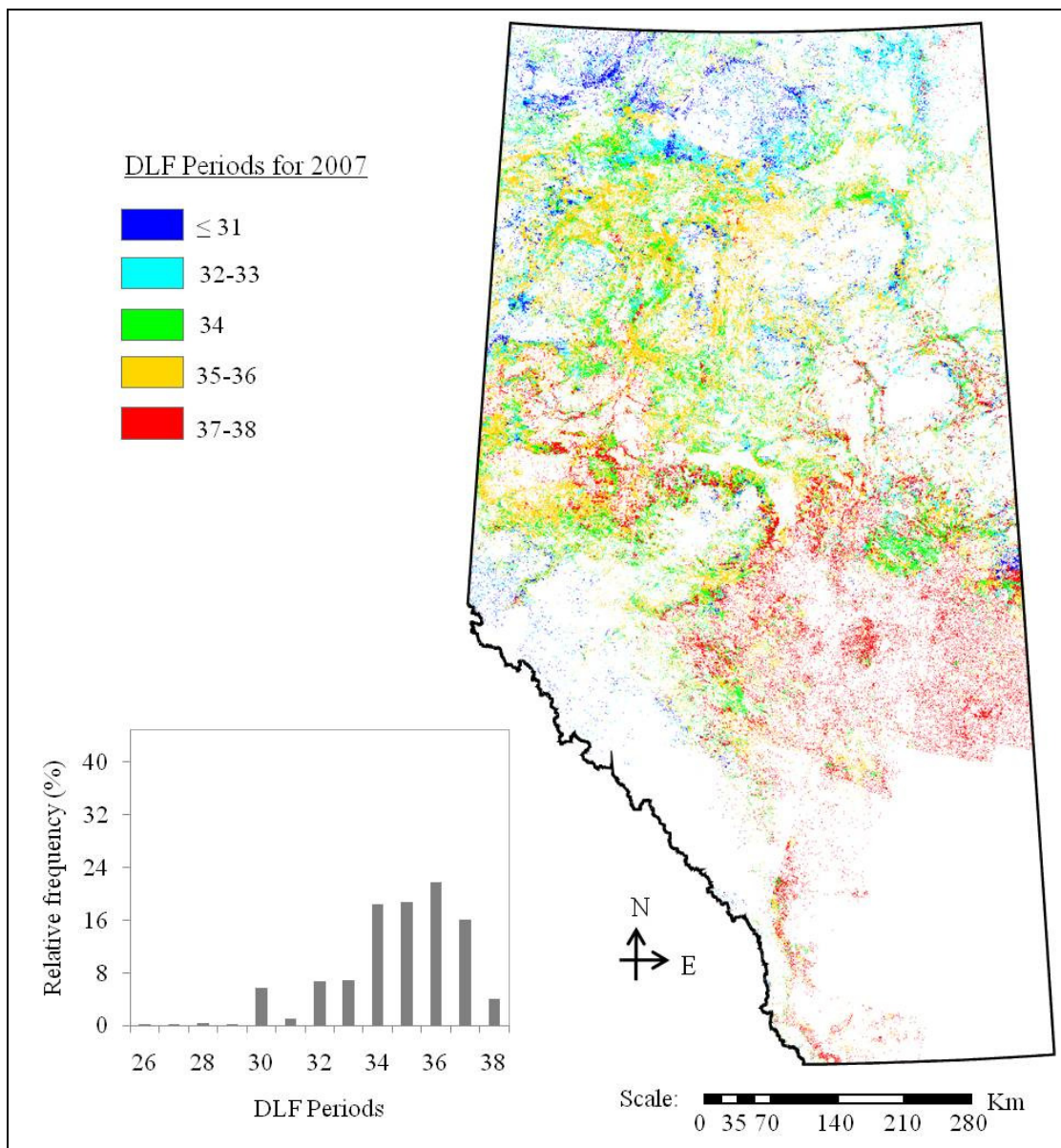


Figure 5.11: Spatial dynamics for the timing of DLF and its relative frequency during 2007.

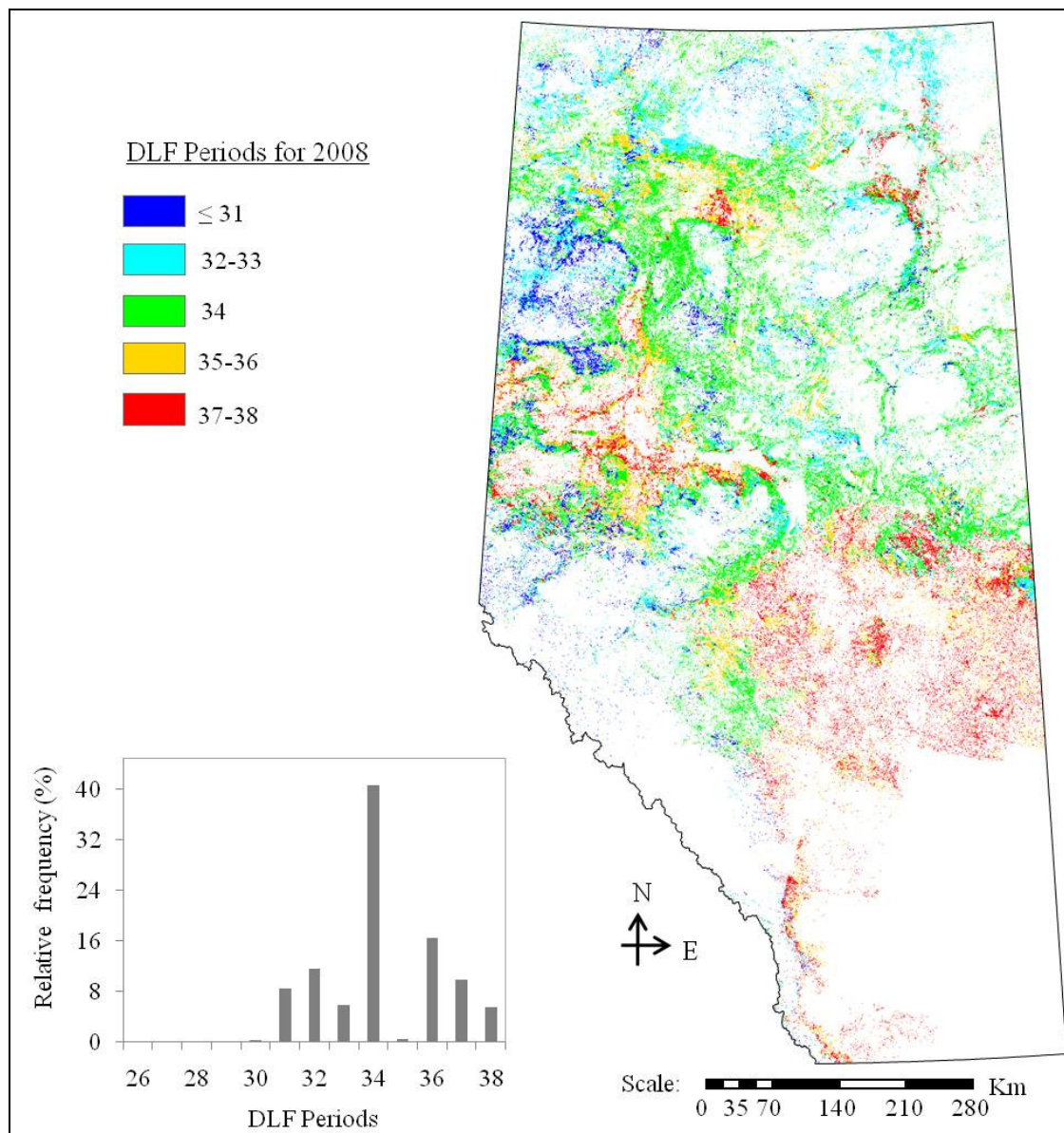


Figure 5.12: Spatial dynamics for the timing of DLF and its relative frequency during 2008.

5.4.3 Spatial dynamics of GGS

Figure 5.13, 5.14 and 5.15 shows the spatial dynamics of GGS over the forest dominant areas across Alberta during 2006-2008 upon applying the observed optimal threshold of AGDD. It revealed that the GGS occurred during the periods of 18-19 (i.e., 17 May-1 June in 2006 and 2007; and 16 May-31 May in 2008) for most of the times (i.e., ~56%, 66%, 72% of the cases in 2006, 2007, and 2008 respectively (see Figures 5.12, 5.13, and 5.14). In general, it was observed that the period of GGS occurrence was increasing in the northward directions and in the high elevated/mountain areas. These could be explained with the fact that discussed above in the earlier section of 5.4.1.

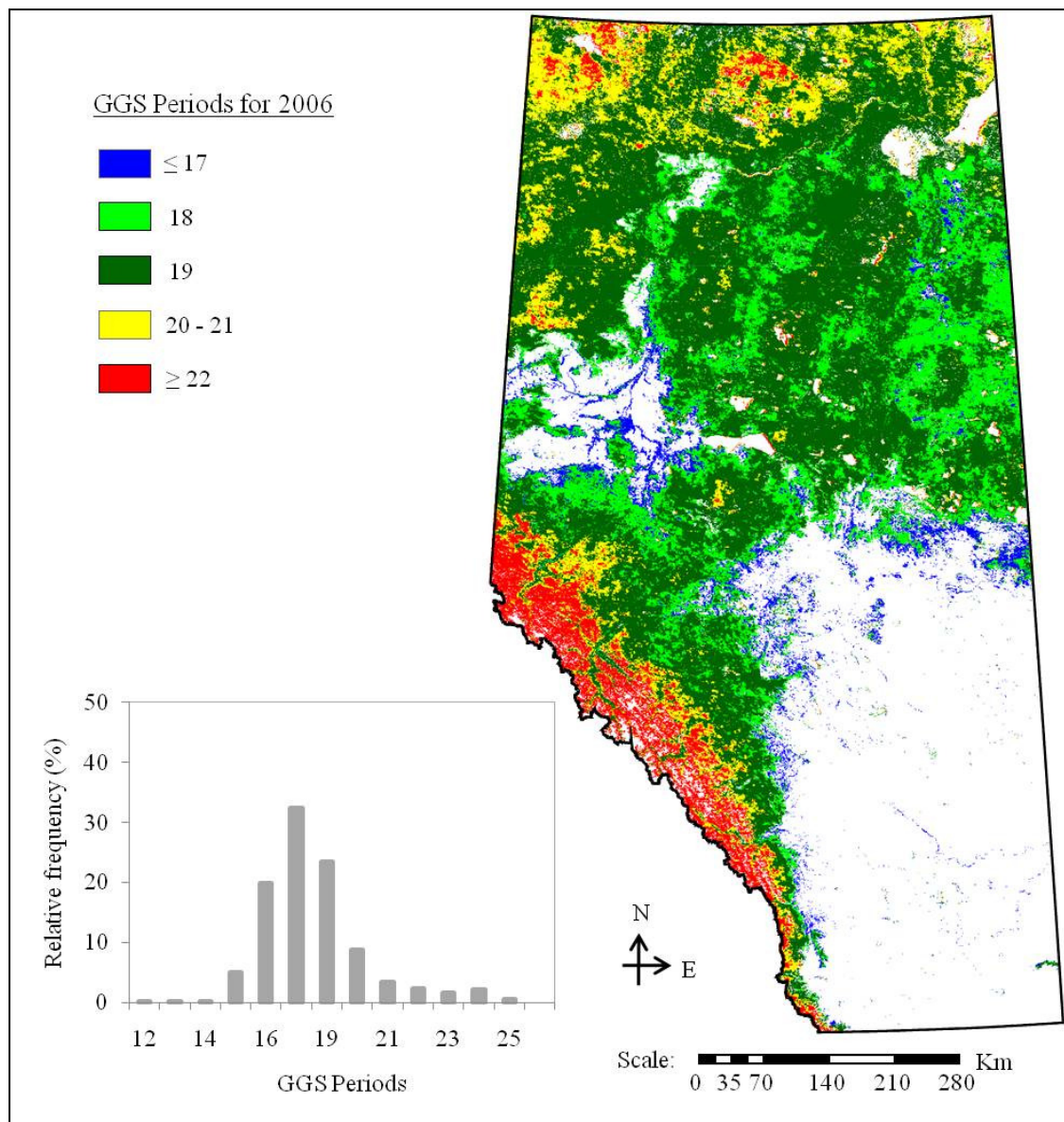


Figure 5.13: Spatial dynamics for the timing of GGS and its relative frequency during 2006.

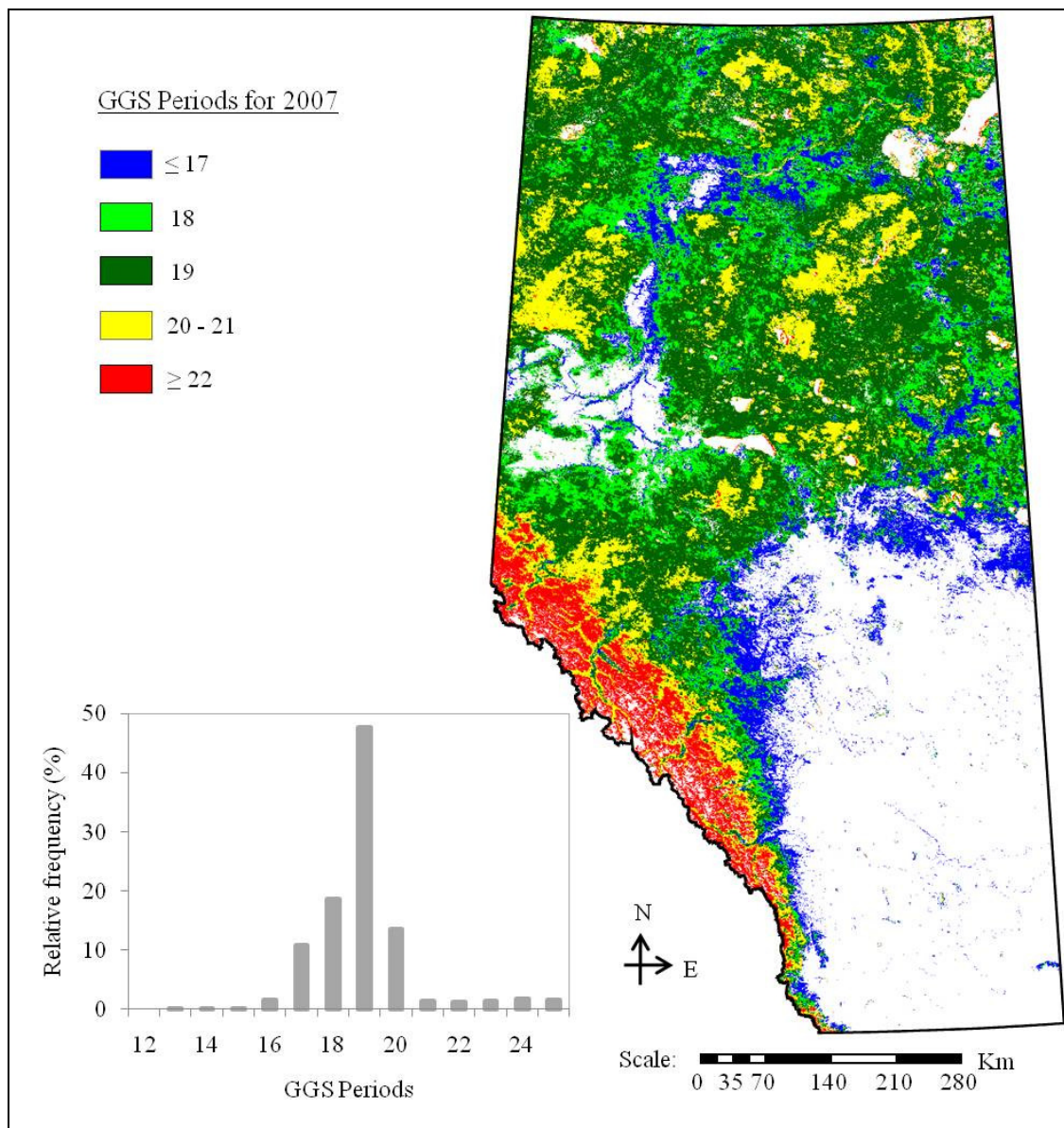


Figure 5.14: Spatial dynamics for the timing of GGS and its relative frequency during 2007.

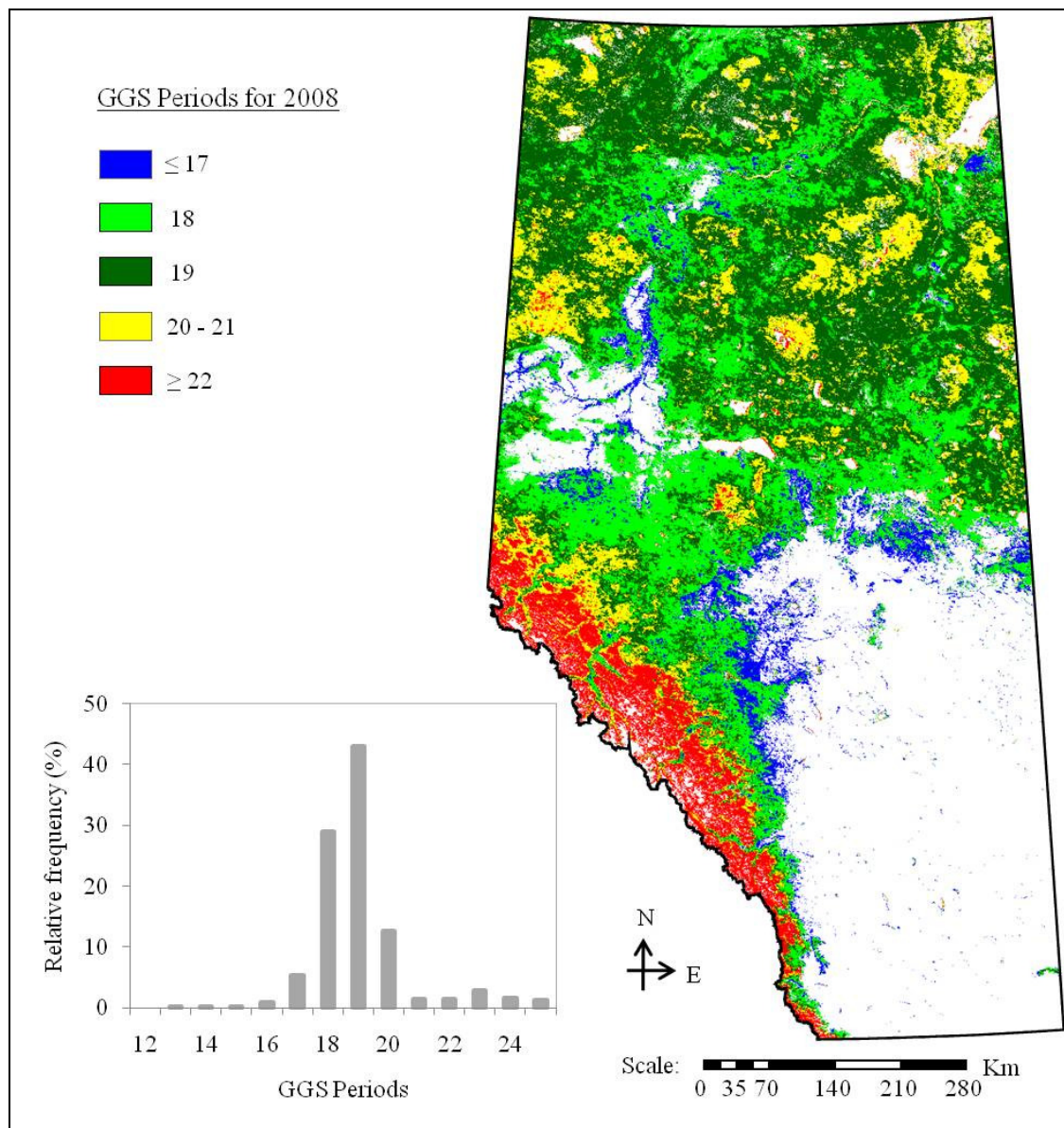


Figure 5.15: Spatial dynamics for the timing of GGS occurrence and its relative frequency distribution during 2008.

CHAPTER 6: CONCLUSIONS AND FUTURE WORK

6.1 Summary

In the scope of this thesis, a topical theme was studied, i.e., application of remote sensing in understanding vegetation phenology of DLO, DLF, and GGS. Here, the potential of MODIS-based AGDD, NDWI and equivalent \bar{T}_a were evaluated in determining the deciduous phenological stages of DLO and DLF and understory GGS over the boreal forested regions in Alberta. The comparison results was analyzed between the optimal thresholds of AGDD and NDWI for DLO/GGS and found that AGDD thresholds are more convincing than NDWI for the phenological stages determination. On the other hand, it was evaluated the MODIS-based equivalent air temperature threshold for DLF occurrence, which was acceptable. The findings indicated for the optimal thresholds that the DLO, DLF and GGS could be determined with reasonable agreements, such as, within ± 2 periods or ± 16 days of deviations for:

- ~91.9% of the cases for DLO during 2007-2008,
- ~94.2% of the cases for GGS during 2007-2008, and
- ~77.4% of the cases for DLF during 2008.

In general, the deciduous and understory vegetation phenology can be used to quantify the impact of climate change (Cleland et al. 2007). The proposed methods would be useful in delineating these phenological stages in the remote areas over a large geographical area, where the *in-situ* observations would be difficult. The general applications of this work could also be important for analysing the forest fire danger

conditions and potentially be incorporated in modelling of forest fire behaviour in the event of their occurrences.

6.2 Contributions

The major contribution of this research are summarised as follows:

- It would be worthwhile to note that the proposed methodology (i.e., integration of MODIS-based T_s and EVI products) that is the AGDD-based method is unique and new in mapping the DLO and GGS over boreal forested regions.
- The NDWI maps were used to delineate the DLO and GSS for the first time so far.
- The developments would be critical for Alberta SRD to map the dynamics of DLO, DLF, and GGS across the province, which would aid forest fire management related issues.

6.3 Further considerations

Despite the effectiveness of the proposed method of delineating the potential of MODIS-based AGDD, NDWI and equivalent \bar{T}_a in determining the deciduous/understory phenological stages, it requires to address more issues for enhancing the current study.

Those include:

- It would be worthwhile to incorporate some other influential climatic variables (that include , photosynthetically active radiation and water regimes);

- In the current study the analyzed images were in 500 m spatial resolution where in further study higher spatial resolution (i.e., 250 m) can be considered.
- The temporal resolution of the current study was 8-day where high temporal resolution (e.g., daily) can be employed in the future study.
- It will be recommended to calibrate and validate the methods before applying to other ecosystems.

References

- Ahl, D. E., Gower, S. T., Burrows, S. N., Shabanov, N. V. Myneni, R. B. & Knyazikhin, Y. 2006. Monitoring spring canopy phenology of a deciduous broadleaf forest using MODIS. *Remote Sensing of Environment*, 104: 88-95.
- Akther, M. S. & Hassan, Q. K. 2011. Remote sensing based estimates of surface wetness conditions and growing degree days over northern Alberta, Canada. *Boreal Environmental Research*, Vol. 16. (In press)
- Barbier, S., Gosselin, F. & Balandier, P. 2008. Influence of tree species on understory vegetation diversity and mechanisms involved-A critical review for temperate and boreal forests. *Forest Ecology and Management*, 254: 1-15.
- Baret, F., Clevers, J. G. P. W. & Steven, M. D. 1995. The robustness of canopy gap fraction estimates from red and near-infrared reflectances: a comparison of approaches. *Remote Sensing of Environment*, 54: 141-151.
- Barr, A. G., Black, T. A., Hogg, E. H., Kljun, N., Morgenstern, K. & Nesic, Z. 2004. Inter-annual variability in the leaf area index of a boreal aspen-hazelnut forest in relation to net ecosystem production. *Agricultural and Forest Meteorology*, 126: 237-255.

Barr, A., Black, T. A. & McCaughey, H. 2009. Climatic and phenological controls of the carbon and energy balances of three contrasting boreal forest ecosystems in western Canada. A. Noormets (Ed.), *Phenology of ecosystem processes*, (pp.3-34), New York: Springer Sciences+ Business Media.

Beaubien, E. G. & Hamann, A. 2011. Plant phenology networks of citizen scientists: recommendations from two decades of experience in Canada. *International Journal of Biometeorology*, (9 pages) DOI 10.1007/s00484-011-0457-y.

Butler, R., Montagnini, F. & Arroyo, P. 2008. Woody understory plant diversity in pure and mixed native tree plantations at La Selva Biological Station, Costa Rica. *Forest Ecology and Management*, 255: 2251-2263.

Chavez, V. & Macdonald, S. E. 2010. Understory species interactions in mature boreal mixedwood forests. *Botany*, 88: 912-922.

Chen, D., Huang, J. & Jackson, T.J. 2005. Vegetation water content estimation for corn and soybeans using spectral indices derived from MODIS near- and short-wave infrared bands. *Remote Sensing of Environment*, 98: 225-236.

Clark, R. N. 1999. Spectroscopy of Rocks and Minerals, and Principles of Spectroscopy. In A. N. Rencz (Ed.). *Manual of Remote Sensing, Volume 3, Remote Sensing for the Earth Sciences*, (pp. 3-58), New York: John Willey and Sons.

- Cleland, E. E., Chiune, I., Menzel, A., Mooney, H. A. & Schwartz M. D. 2007. Shifting plant phenology in response to global change. *Trends in Ecology and Evolution*, 22: 357-365.
- Colombo, R., Bellingeri, D., Fasolini, D. & Marino, C. M. 2003. Retrieval of leaf area index in different vegetation types using high resolution satellite data. *Remote Sensing of Environment*, 86: 120-13.
- Delbart, N., Toan, T. L., Kerogoats, L. & Fedotova, V. 2006. Remote sensing of spring phenology in boreal regions: A free of snow-effect method using NOAA-AVHRR and SPOT-VGT data (1982-2004). *Remote Sensing of Environment*, 101: 52-62.
- Delbart, N., Kergoata, L., Toana, T. L., Lhermittea, J. & Picard, G. 2005. Determination of phenological dates in boreal regions using normalized difference water index. *Remote Sensing of Environment*, 97: 26-38.
- Delbart, N., Picard, G., Toan, T. L., Kergoats, L., Quengan, S., Woodward, I., Dye, D. & Fedotava, V. 2008. Spring phenology in Boreal Eurasia over a nearly century time scale. *Global Change Biology*, 14: 603-614.

- Delpierre, N., Dufrene, E., Soudani, K., Ulrich, E., Cecchini, S., Boe, J. & Francois, C. 2009. Modelling interannual and spatial variability of leaf senescence for three deciduous tree species in France. *Agricultural and Forest Meteorology*, 149: 938-948.
- Dowing, D. J. & Pettapiece, W. W. (eds.) 2006. Natural regions and subregions of Alberta. Publication T/852, *Natural Regions Committee, Government of Alberta, Alberta, Canada.*
- Duchemin, B., Goubier, J. & Courier, G. 1999. Monitoring phenological key stages and cycle duration of temperate deciduous forest ecosystems with NOAA/AVHRR Data. *Remote Sensing of Environment*, 67: 68-82.
- Eriksson, H. M., Eklundh, L., Kuusk, A. & Nilson, T. 2006. Impact of understory vegetation on forest canopy reflectance and remotely sensed LAI estimates. *Remote Sensing of Environment*, 103: 408-418.
- Fisher, J. I., Richardson, A. D. & Mustard, J. F. 2007. Phenology model from surface meteorology does not capture satellite-based green up estimations. *Global Change Biology*, 13: 707-721.

- Fujii, Y., Kawahara, H., Suto, Y., Taruya, A., Fukuda, S., Nakajima, T. & Turner, E. L. 2010. Colors of a second earth: estimating the fractional areas of ocean, land, and vegetation of earth-like exoplanets. *The Astrophysical Journal*, 715: 866-880.
- Gao, B. C. 1996. NDWI a normalized difference water index for remote sensing of vegetation liquid water from space. *Remote Sensing of Environment*, 58: 257-266.
- Gilliam, F. S. 2007. The ecological significance of the herbaceous layer in temperate forest ecosystems. *Bioscience*, 57: 845-858.
- Gitelson, A. A. 2004. Wide Dynamic Range Vegetation Index for remote quantification of biophysical characteristics of vegetation. *Journal of Plant Physiology*, 161: 165-173.
- Gryning, S. E., Soegaard, H. & Batchvarova, E. 2009. Comparison of regional and ecosystem CO₂ fluxes. *Boreal Environmental Research*, 14: 204-212.
- Gu, Y., Brown, J. F., Miura, T., Leeuwen, W. J. D. V. & Reed, B. C. 2010. Phenological classification of the United States: a geographical framework for extending multi-sensor time series data. *Remote Sensing*, 2: 526-544.

- Hanes, J. M. & Schwartz, M. D. 2010. Modeling land surface phenology in a mixed temperate forest using MODIS measurements of leaf area index and land surface temperature. *Theoretical and Applied Climatology*, (14 pages) DOI 10.1007/s00704-010-0374-8.
- Hari, P. & Nojd, P. 2009. The effect of temperature and PAR on the annual photosynthetic production of Scots pine in northern Finland during 1906-2002. *Boreal Environmental Research*, 14: 5-18.
- Hart, S. A. & Chen, H. Y. H. 2006. Understory Vegetation Dynamics of North American Boreal Forests. *Critical Reviews in Plant Sciences*, 25: 381-397.
- Hassan, Q. K. & Bourque, C. P.-A. 2009. Potential species distribution of balsam fir based on the integration of biophysical variables derived with remote sensing and process-based methods. *Remote Sensing*, 1: 393-407.
- Hassan, Q. K. & Bourque, C. P.-A. 2010. Spatial enhancement of MODIS-based images of leaf area index: application to the boreal forest region of northern Alberta, Canada. *Remote Sensing*, 2: 278-289.
- Hassan, Q. K., Bourque, C. P.-A. & Meng F.-R. 2007b. Application of Landsat-7 ETM+ and MODIS products in mapping seasonal accumulation of growing degree days at an enhanced resolution. *Journal of Applied Remote Sensing*, 1: 013539.

- Hassan, Q. K., Bourque, C. P.-A., Meng F.-R. & Richards W. 2007a. Spatial mapping of growing degree days: an application of MODIS-based surface temperatures and enhanced vegetation index. *Journal of Applied Remote Sensing*, 1: 013511.
- Henebry, G. M., Vina, A. & Gitelson, A. A. 2004. The Wide Dynamic Range Vegetation Index and its potential utility for gap analysis. *GAP Analysis Program Bulletin*, 12: 50-56.
- Heidi, T. & Ari, V. 2008. The relationship between fire activity and fire weather indices at different stages of the growing season in Finland. *Boreal Environmental Research*, 13: 285-302.
- Hogg, E. H. 1999. Simulation of interannual responses of trembling aspen stands to climatic variation and insect defoliation in western Canada. *Ecological Modelling*, 114: 175-193.
- Huete, A. R. 1988. A soil adjusted vegetation index (SAVI). *Remote Sensing of Environment*, 25: 295-30
- Huete, A., Didan, K., Miura, T., Rodriguez, E.P., Gao, X. & Ferreira, L.G. 2002. Overview of the radiometric and biophysical performance of the MODIS vegetation indices. *Remote Sensing of Environment*, 83: 195-213.

- Kudo, G., Ida, T. Y. & Tani, T. 2008. Linkages between phenology, pollination, photosynthesis, and reproduction in deciduous forest understory plants. *Ecology*, 89: 321-331.
- Lawson, B.D., Armitage, O.B. 2008. Weather guide for the Canadian Forest Fire Danger Rating System; *Northern Forestry Centre, Canadian Forest Service, Natural Resources Canada: Edmonton, Alberta, Canada*, p.73.
- Lechowicz, M. J. & Koike, T. 1995. Phenology and seasonality of woody-plants an unappreciated element in global change research. *Canadian Journal of Botany*, 73: 147-148.
- Li, H., Wang, X. & Hamann, A. 2010. Genetic adaptation of aspen (*Populus tremuloides*) populations to spring risk environments: a novel remote sensing approach. *Canadian Journal of Forest Research*, 40: 2082-2090.
- Liang, L., & Schwartz, M. 2009. Landscape phenology: an integrative approach to seasonal vegetation dynamics. *Landscape Ecology*, 24: 465-472.
- Liang, L., Schwartz, M. D. & Fei, S. 2011a. Validating satellite phenology through intensive ground observations and landscape scaling in a mixed seasonal forest. *Remote Sensing of Environment*, 115: 143-157.

- Liang, L., Schwartz, M. D. & Fei, S. 2011b. Examining spring phenology of forest understory using digital photography. *Proceedings of the 17th Central Hardwood Forest Conference*. P-78.
- Lu, X.-T., Yin, J.-X. & Tang, J.-W. 2011. Diversity and composition of understory vegetation in the tropical seasonal rain forest of Xishuangbanna, SW China. *Revista de Biologia Tropical*, 59: 455-463.
- Macdonald, S. E. & Fenniak, T. E. 2007. Understory plant communities of boreal mixedwood forests in western Canada: natural patterns and response to variable retention harvesting. *Forest Ecology and Management*, 242: 34-48.
- McCloy, K. R. 2010. Development and evaluation of phenology changes indices derived from time series of image data. *Remote Sensing*, 2: 2442-2473.
- Morin, X., Lechowicz, M. J., Augspurger, C., O'Keefe, J., Viner, D. & Chuine, I. 2009. Leaf phenology in 22 North American tree species during the 21st century. *Global Change Biology*, 15: 961-975.
- Morisette, J.T., Richardson, A. D., Knapp, A. K., Fisher, J. I., Graham, E. A., Abatzoglou, J., Wilson, B. E., Breshears, D. D., Henebry, G. M., Hanes, J. M. & Liang, L. 2009. Tracking the rhythm of the seasons in the face of global

change: phenological research in the 21st century. *Frontiers in Ecology and the Environment*, 7: 253-260.

Nilsson, M. C. & Wardle, D. A. 2005. Understory vegetation as a forest ecosystem driver: evidence from the northern Swedish boreal forests. *Frontiers in Ecology and the Environment*, 3: 421-428.

Parry, D., Volney, W. J. A. & Currie, C.R. 1997. The relationship between trembling aspen phenology and larval development of the large aspen tortrix. *Nat. Resour. Can., Can. For. Serv., North. For. Cent.*, Edmonton, Alberta. Inf. Rep. NOR-X-350.

Parviainen, M., Luoto, M. & Heikkinen, R. K. 2010. NDVI-based productivity and heterogeneity as indicators of plant-species richness in boreal landscapes. *Boreal Environmental Research*, 15: 301-318.

Peckham, S. D., Ahl, D. E., Serbin, S. P. & Gower, S.T. 2008. Fire-induced changes in green-up and leaf maturity of the Canadian boreal forest. *Remote Sensing of Environment*, 112: 3594-3603.

Pellikka, P. 2001. Application of vertical skyward wide-angle photography and airborne video data for phenological studies of beech forests in the German Alps. *International Journal of Remote Sensing*, 22: 2675-2700.

- Reed, B. C., Schwartz, M. D. & Xiao, X. 2009. Remote sensing phenology: status and the way forward. A. Noormets (Ed.), *Phenology of ecosystem processes*, (pp. 231-246), New York: Springer Sciences+ Business Media.
- Richardson, A. D. & O’Keefe, J. 2009. Phenological differences between understory and overstory: A case study using the long-term Harvard forest records. A. Noormets (Ed.), *Phenology of ecosystem processes*. DOI 10.1007/978-1-4419-0026-5_4, New York: Springer Sciences+ Business Media.
- Richardson, A. J. & Wiegand, C. L. 1977. Distinguishing vegetation from soil-background information. *Photogrammetric Engineering & Remote Sensing*, 43: 1541-1552.
- Roberts, M. R. 2004. Response of the herbaceous layer to natural disturbance in North American Forests. *Canadian Journal of Botany*, 82: 1273-1283.
- Rouse, J., Haas, R., Schell, J. & Deering, D. 1974. Monitoring vegetation systems in the Great Plains with ERTS. In S. C. Freden, E. P. Marcanti, & M. A. Becker (Eds.), *Proceedings of the 3rd Earth Resources Technology Satellite-1 Symposium, 10-14 Dec. 1973, Washington, D.C.*, (pp. 309–317).

- Sekhon, N. S., Hassan, Q. K. & Sleep R.W. 2010. Evaluating potential of MODIS-based indices in determining "snow gone" stage over forest-dominant regions. *Remote Sensing*, 2: 1348-1363.
- Serbin, S. P., Gower, S.T. & Ahl, D. E. 2009. Canopy dynamics and phenology of a boreal black spruce wildfire chronosequence. *Agricultural and Forest Meteorology*, 149: 178-204.
- Soudani, K., Maire, G. L., Dufrene, E., Francois, C., Delpierre, N., Ulrich, E. & Cecchini, S. 2008. Evaluation of the onset of green-up in temperate deciduous broadleaf forests derived from Moderate Resolution Imaging Spectroradiometer (MODIS) data. *Remote Sensing of Environment*, 12: 2643-2655.
- Tuanmu, M.-N., Vina, A., Bearer, S., Xu W., Ouyang, Z., Zhang, H. & Liu, J. 2010. Mapping understory vegetation using phenological characteristics derived from remotely sensed data. *Remote Sensing of Environment*, 14: 1833-1844.
- Urgenson, L. S., Reichard, S. H. & Halpern, C. B. 2009. Community and ecosystem consequences of giant knotweed (*Polygonum sachalinense*) invasion into riparian forests of western Washington, USA. *Biological Conservation*, 142: 1536-1541.

- Vitasse, Y., Porte, A. J., Kremer, A., Michalet, R. & Delzon, S. 2009. Responses of canopy duration to temperature changes in four temperate tree species: relative contributions of spring and autumn leaf phenology. *Oecologia*, 161: 187-198.
- Wang, C., Lu, Z., & Haithcoat, T. L. (2007). Using Landsat images to detect oak decline in the Mark Twain National Forest, Ozark Highlands. *Forest Ecology and Management*, 240, 70-78.
- White, M. A., De Beurs, K. M., Didan, K., Inouye, D. W., Richardson, A. D., Jensen, O. P., O'Keefe, J., Zhang, G., Nemani, R. R., Van Leeuwen, W. J. D., Brown, J. F., De Wit, A., Schaepman, M., Lin, X., Dettinger, M., Bailey, A. S., Kimball, J., Schwartz, M. D., Baldocchi, D. D., Lee, J. T. & Lauenroth, W. K. 2009. Intercomparison, interpretation, and assessment of spring phenology in North America estimated from remote sensing for 1982-2006. *Global Change Biology*, 15: 2335-2359.
- Wilfong, B. N., Gorchoy, D. L. & Henry, M. C. 2009. Detecting an invasive shrub in deciduous forest understories using remote sensing. *Weed Science*, 57: 512-520.
- Wilson, K. B. & Baldocchi, D. D. 2000. Seasonal and interannual variability of energy fluxes over a broadleaved temperate deciduous forest in North America. *Agricultural and Forest Meteorology*, 100: 1-18.

- Xiao, X., Zhang, J., Yan, H., Wu, W. & Biradar, C. 2009. Land Surface Phenology: Convergence of Satellite and CO₂ Eddy Flux Observations. A. Noormets (Ed.), *Phenology of ecosystem processes*, (pp. 247-270), New York: Springer Sciences+ Business Media.
- Yauschew-Raguenes, N., Guyon, D., Kruszewski, A., Hagolle, O. & Wigneron, J. P. 2008. Discrimination of the respective contributions of understory and tree canopy to the seasonal dynamics of reflectance of maritime pine forest in southwest France. *Proceedings of IEEE International Geoscience & Remote Sensing Symposium*, 3: 808-811.
- Zhang, X., Friedl, M. A., Schaff, C. B., Strahler, A. H., Hodges, J. C. F., Gao, F., Reed, B. C. & Huete, A. 2003. Monitoring vegetation phenology using MODIS. *Remote Sensing of Environment*, 84: 471-475.
- Zhang, X., Friedl, M. A., Schaff, C. B. & Strahler, A. H. 2004. Climate controls on vegetation phenological patterns in northern mid- and high latitudes inferred from MODIS data. *Global Change Biology*, 10: 1133-1145.

Web References

CBI, 2011. Canadian Boreal Initiative. <http://www.borealcanada.ca/research-maps-e.php>, last accessed on 10 August, 2011.

EC,2010.EnvironmentCanada.http://www.climate.weatheroffice.gc.ca/climateData/canada_e.html, last accessed on 25 May 2010.

ERDAS, 2011. <http://www.erdas.com/products.aspx>, last accessed on 15 July, 2011.

Forest Fire Management Terms.1999. Forest Protection Division, Alberta Land and Forest Service:Alberta,Canada,p.77.Availableonline:<http://www.srd.alberta.ca/MapsFormsPublications/Publications/documents/ForestFireManagementTerms-AbbrevGlossary> (accessed on 11 October 2010).

LP DAAC, 2010. The Land Processes Distributed Active Archive Center, https://lpdaac.usgs.gov/lpdaac/products/modis_products_table, last accessed on 15 June 2010.

MRT,2010.MODISReprojectionTool,https://lpdaac.usgs.gov/lpdaac/tools/modis_reprojection_tool, last accessed on 25 September 2010

NRC, 2010. Natural Resource Canada, The state of Canada's forest, Annual report 2010.

<http://cfs.nrcan.gc.ca/pubwarehouse/pdfs/31835.pdf>, last accessed on, 2011

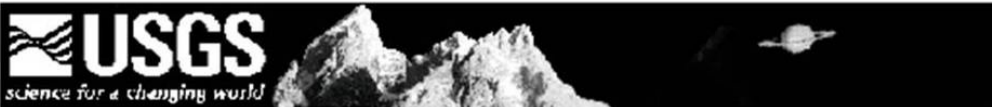
SRD, 2011. Sustainable Resource Development, Government of Alberta,

<http://www.srd.alberta.ca/UpdatesFireAlerts/WildfireStatus/10->

[YearStatisticalSummary.aspx](http://www.srd.alberta.ca/UpdatesFireAlerts/WildfireStatus/10-YearStatisticalSummary.aspx), last accessed on 02 February, 2011.

Appendix

Appendix-I

Copyright permission document for Clark et al. (1999):

**Spectroscopy of Rocks and Minerals, and
Principles of Spectroscopy**

by
Roger N. Clark

U.S. Geological Survey, MS 964
Box 25046 Federal Center
Denver, CO 80225-0046

(303) 236-1332
(303) 236-1371 FAX

<http://speclab.cr.usgs.gov>

rclark@speclab.cr.usgs.gov

Derived from Chapter 1 in:
Manual of Remote Sensing

John Wiley and Sons, Inc
A. Rencz, Editor
New York
1999

This book chapter was produced by personnel of the US Government
therefore it can not be copyrighted and is in the public domain

This Web Page last revised June 25, 1999

<http://speclab.cr.usgs.gov/PAPERS.refl-mrs/refl4.html>

Appendix-II

A Step-by-Step modeling with ERDAS Imagine image processing system

In this study, the “Spatial Modeller” module of the ERDAS Imaging Software (ERDAS 2011) was used. There were 9 (nine) major models developed and their descriptions are as follows:

- 1. Mosaicking:** The four scenes of Geo-TIFF images per period for each of the data set (i.e., T_s , EVI, NDWI, and land cover type) were mosaicked together using the following model. For example:

Input image:

n1_1, n2_2, n3_3, and n4_4 are Tiff Images (.tif) of MOD11A2 of the desired study area of Alberta.

Output image:

n10_surface temperatures at 1 km resolution, Imagine Image (.img) file type.

The following equations were used in Mosaicking:

EITHER \$n2_2 IF (\$n1_1==255) OR \$n1_1 OTHERWISE * 2

EITHER \$n3_3 IF (\$n4_4==255) OR \$n4_4 OTHERWISE *2

EITHER \$n7_memory IF (\$n8_memory==255) OR \$n8_memory OTHERWISE

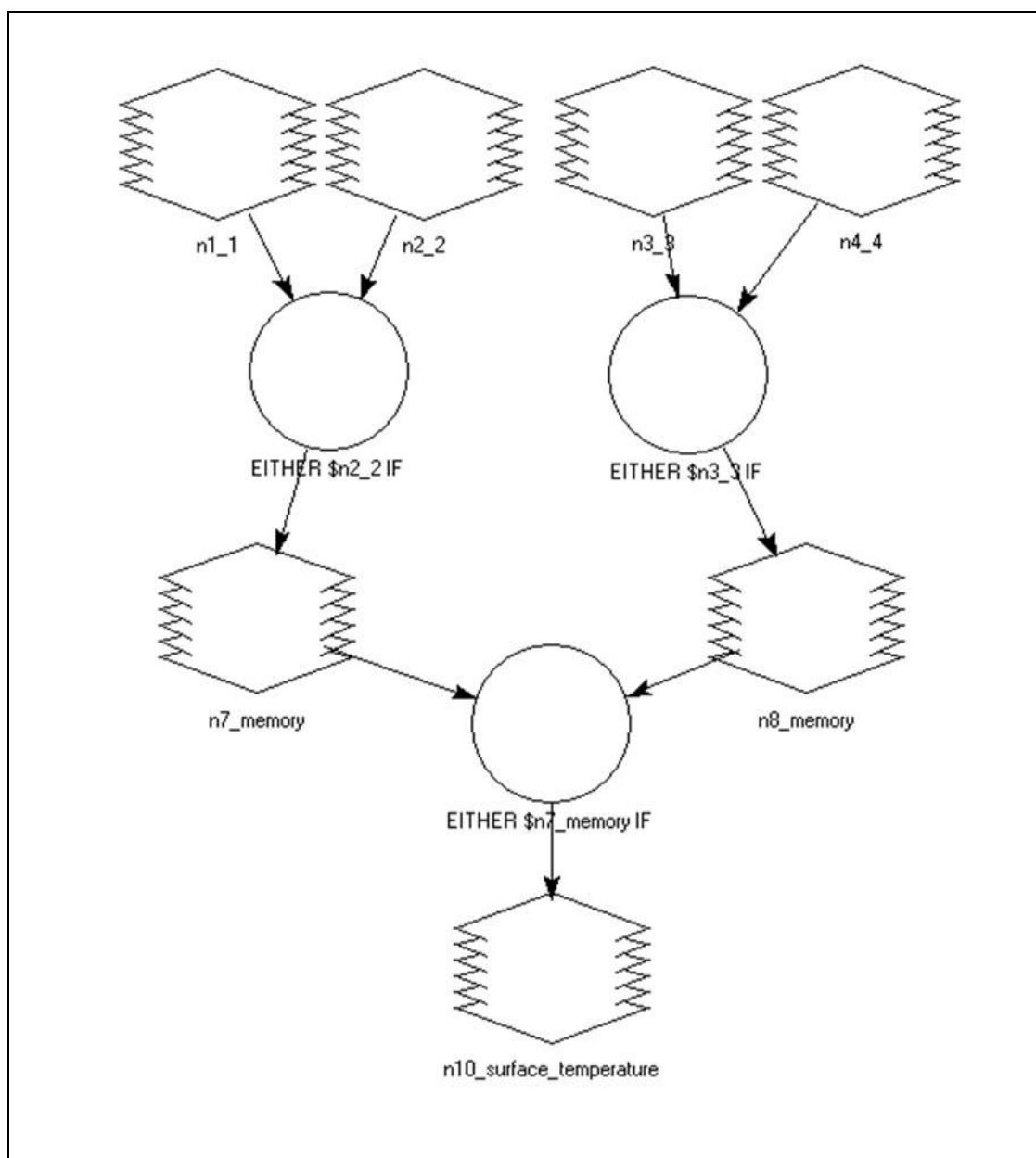


Figure AII.1: Graphical interface for Mosaicking Geo-TIFF images.

The data type of the input/output file was “Integer Unsigned 16 bit” and it set “Ignore zero” in the stats calculation. The images were mosaicked for the periods from 12 to 38 (i.e., 89 to 297 DOY) and this Mosaicking was done for all the data sets.

2. **Stack Layer:** In this process the images were stacked which, includes 27 images for each of the respective data sets.

Input image:

n7_ spots and n15_dmtm, (Images from 89 to 297 DOY)

Output image: n17_stacklayer

The following equation was used for stack layer:

STACKLAYERS (\$n7_spots (1), \$n15_dmtm (2: NUMLAYERS (\$n15_dmtm)))

(Variable LAYERSTACK using Spatial Modeler syntax)

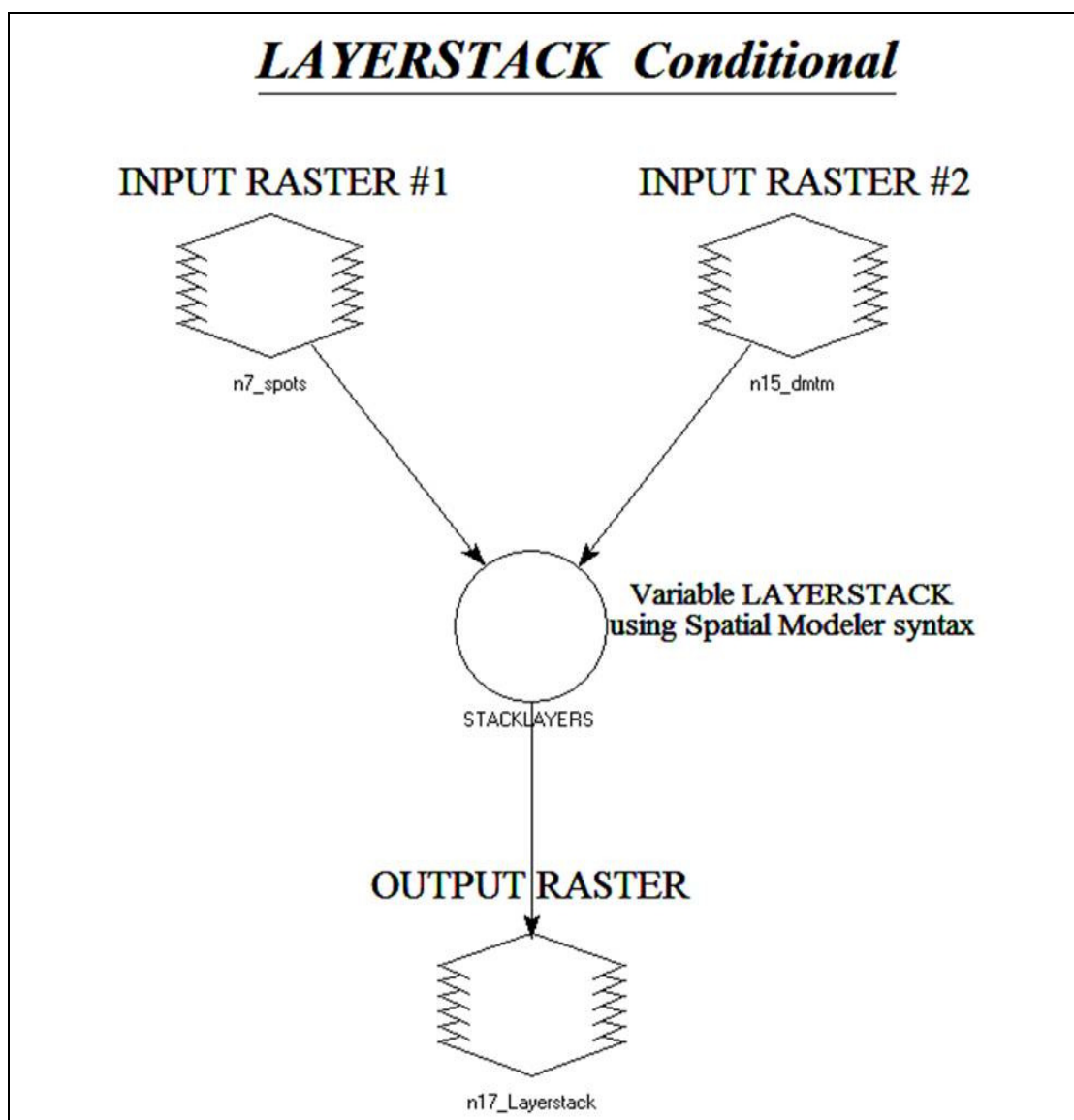


Figure AII.2: Graphical interface for generating layer-stack images.

The data type of the input/output file was “Integer Unsigned 16 bit” and it set “Ignore zero” in the stats calculation. The stack layers for each of the data sets consists of 27 images for the periods from 12 to 38 (i.e., 89 to 297 DOY).

3. Cloud contamination correction: Some of the pixels of the images were found cloud contaminated and used the following corrections of modeling:

(i) Conversion to binary number:

Input image: n17_stacklayer

Output image: Convert_0_1

The following equation was used for binary conversion:

EITHER 0 IF (\$n1_stack_89_297 ==0) OR 1 OTHERWISE

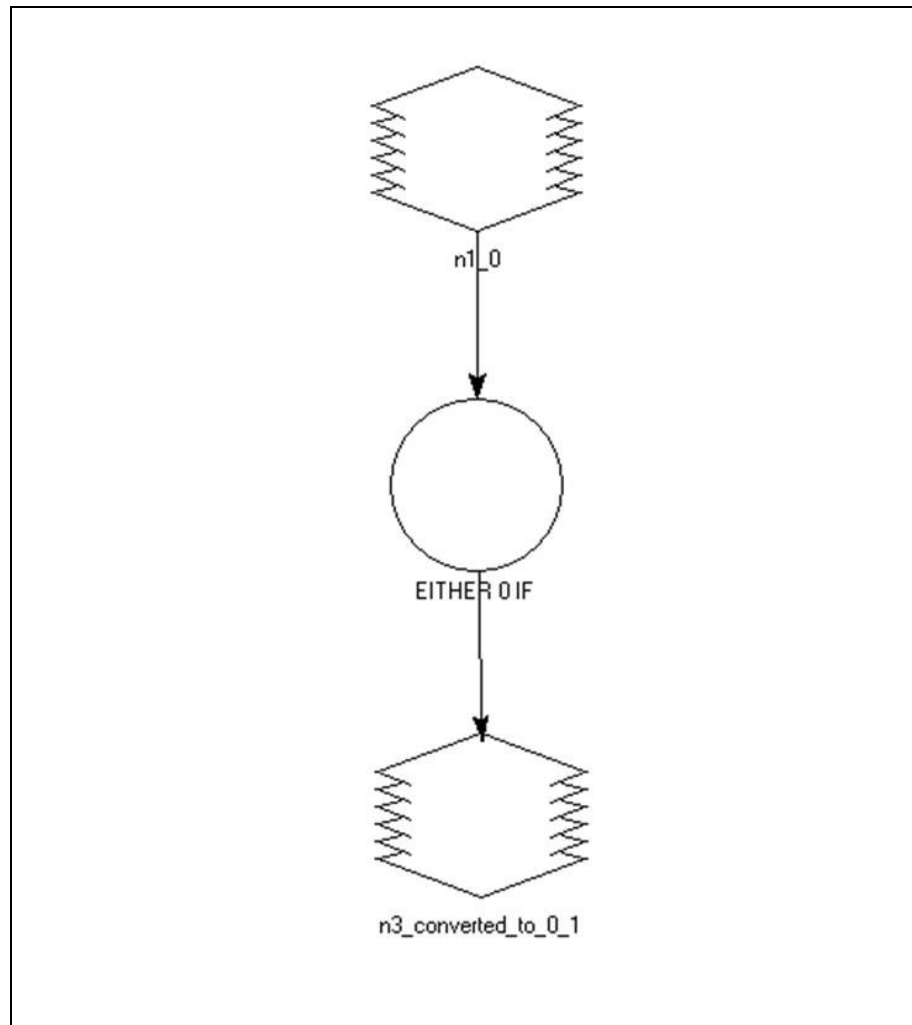


Figure AII.3: Graphical interface for converting to binary number.

The data type of the output file was “Integer Unsigned 1 bit” and it set “Ignore zero” in the stats calculation. This binary conversion was done for all the data sets as required.

(ii) Total cloud free number (m) calculation:

Input image: n17_stacklayer

Output image: n_3_3

The following equation was used for total cloud free number (m) calculation:

STACK SUM (\$n1_convert_0_1)

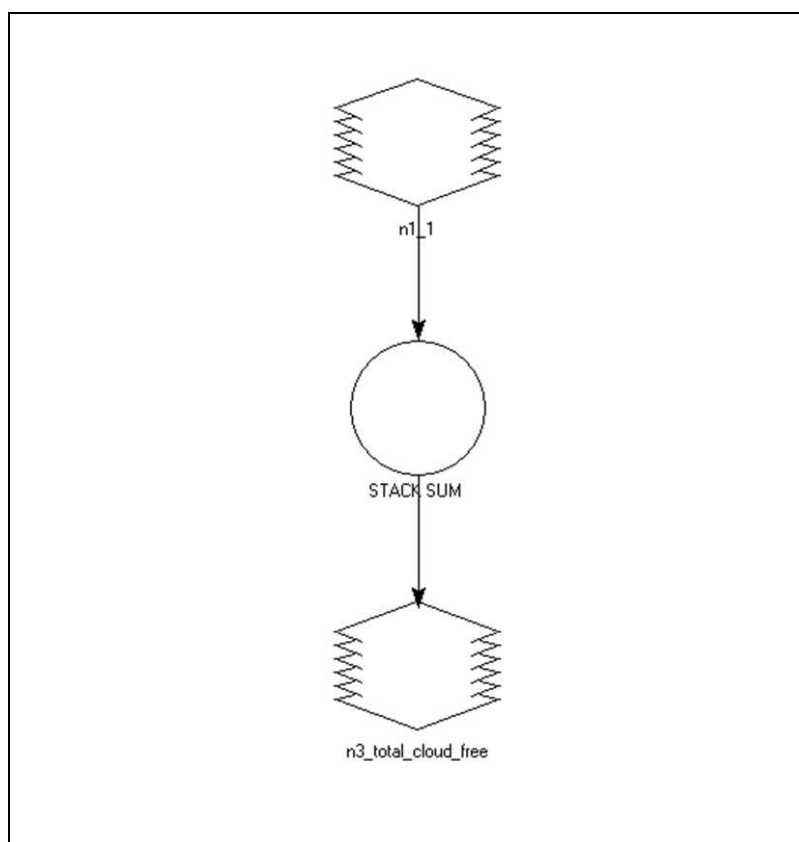


Figure AII.4: Graphical interface for calculating total cloud free number.

The data type of the output file was “Integer Unsigned 8 bit” and it set “Ignore zero” in the stats calculation. This modelling was done for all the data sets as required for cloud correction.

(iii) Mean & sum of mean deviation calculation:

Input image: n_stacklayer_89-297 & Custom-integer

Output image: Mean diff & sum of mean diff

The following equation was used for this modeling:

EITHER 0 IF (\$n1_stack_lst_089 ==0) OR (\$n2_Custom_Integer -
\$n1_stack_lst_089) OTHERWISE

STACK SUM (\$n4_mean)

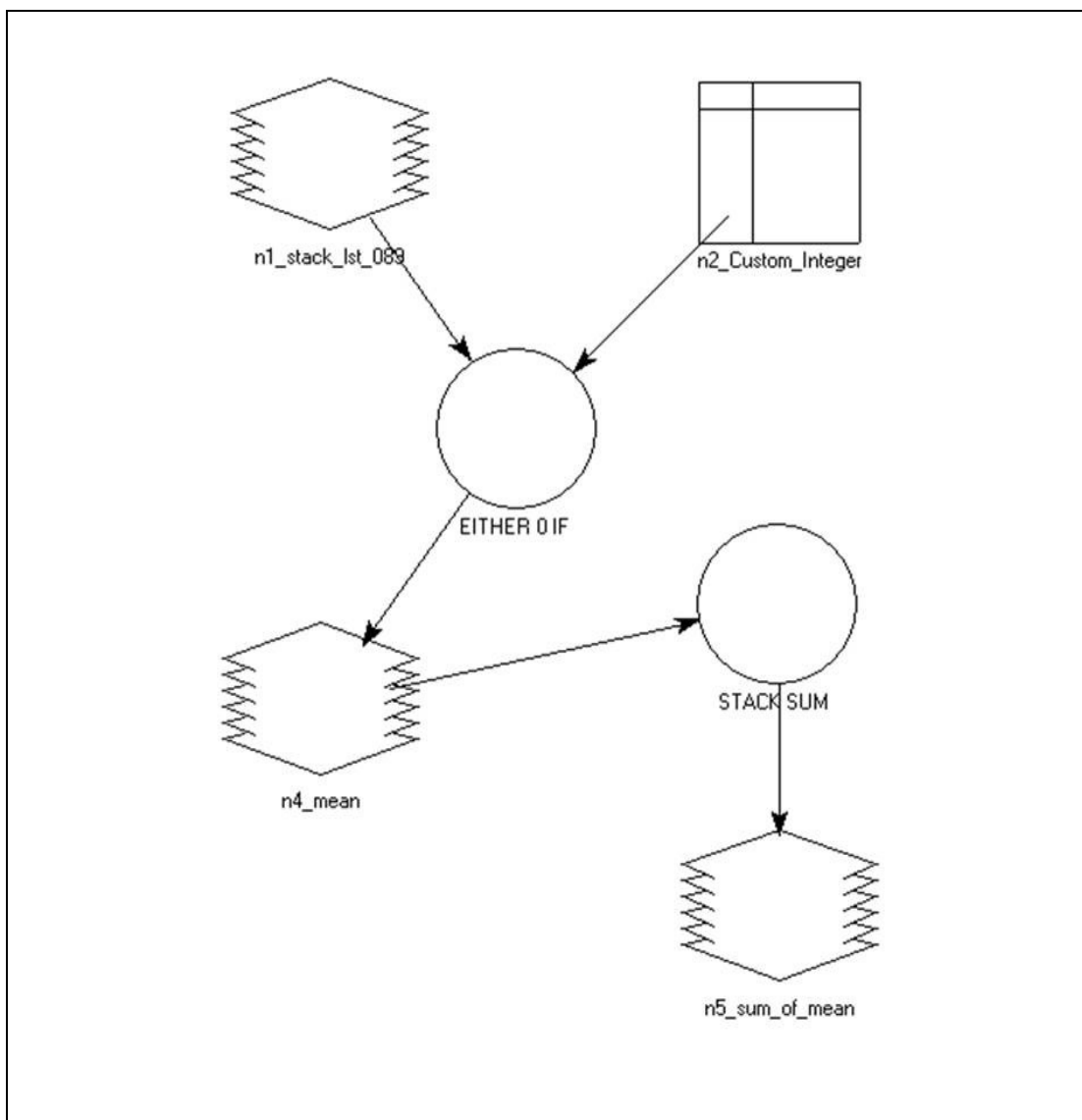


Figure AII.5: Graphical interface for calculating mean & sum of mean deviation.

The data type of the output files were “Signed 16 bit” and it set “Ignore zero” in the stats calculation. This modelling was done for all the data sets as required for cloud correction.

(iv) Average diff. calculation:

Input image: sum-mean-diff & total cloud free number

Output image: Average diff

The following equation was used for this modeling:

EITHER 0 IF ((\$n1_sum_of_mean ==0) or (\$n2_total_cloud_free ==0)) OR
\$n1_sum_of_mean/\$n2_total_cloud_free OTHERWISE

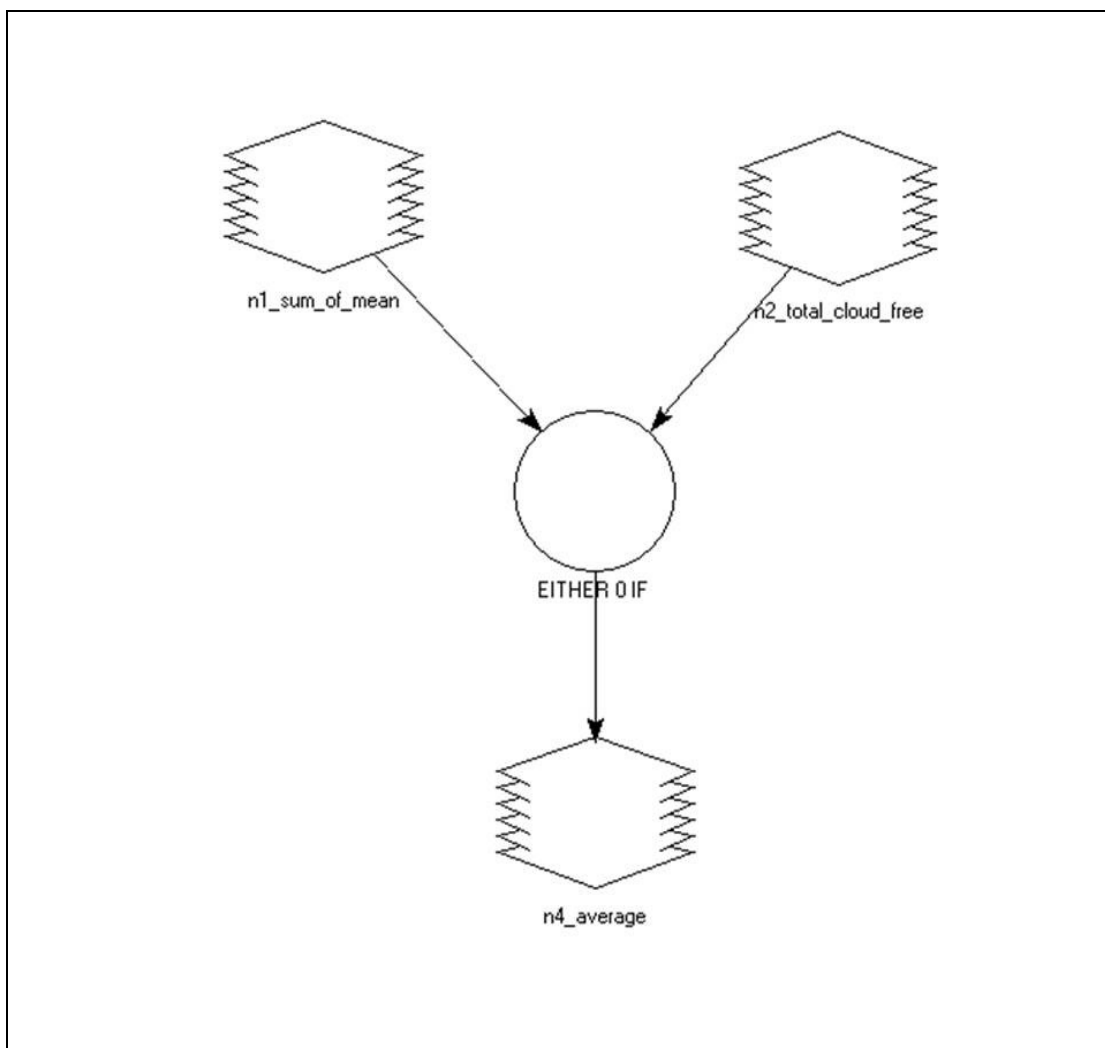


Figure AII.6: Graphical interface for calculating average deviation.

The data type of the output file was “Float single” and it set “Ignore zero” in the stats calculation. This modelling was done for all the data sets as required for cloud correction.

(v) Corrected (Gap filled) calculation:

Input image: Custom-integer, avg.-diff, clod-free, stack-layer

Output image: Corrected gap-filled-1st

The following equation was used for this modeling:

```
CONDITIONAL {($n1_total_cloud_free ==0) 0,  
($n8_stack_89 ==0) ($n2_Custom_Integer - $n7_avg_from_sum_mean),  
($n8_stack_89 >0) $n8_stack_89}
```

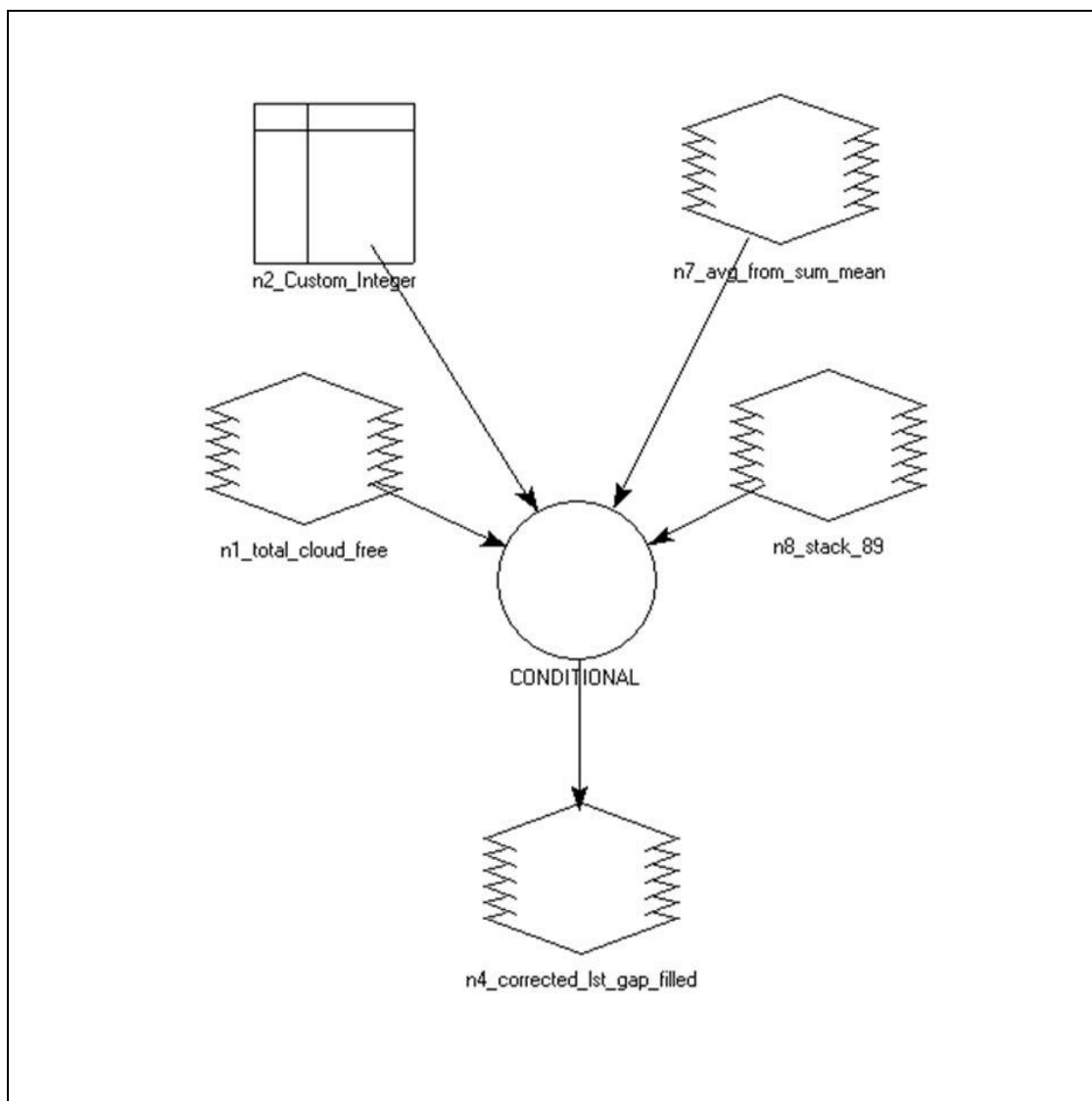



Figure AII.7: Graphical interface for estimating the corrected gap-filled pixel values due to cloud contamination.

The data type of the output files were “Un-signed 16 bit” and it set “Ignore zero” in the stats calculation. This modelling was done for all the data sets as required for cloud correction.

4. **MODIS-based equivalent \bar{T}_a calculation:** this modeling was used in converting the MODIS-based T_S images into equivalent \bar{T}_a .

Input image: corrected_lst_gap_filled.img

Output image: converted_to_daily_air_mean_temp.img

The following equation was used for this calculation:

EITHER 0 IF (\$n1_corrected_lst_gap_filled ==0) OR

10366+ (0.6146*\$n1_corrected_lst_gap_filled) OTHERWISE

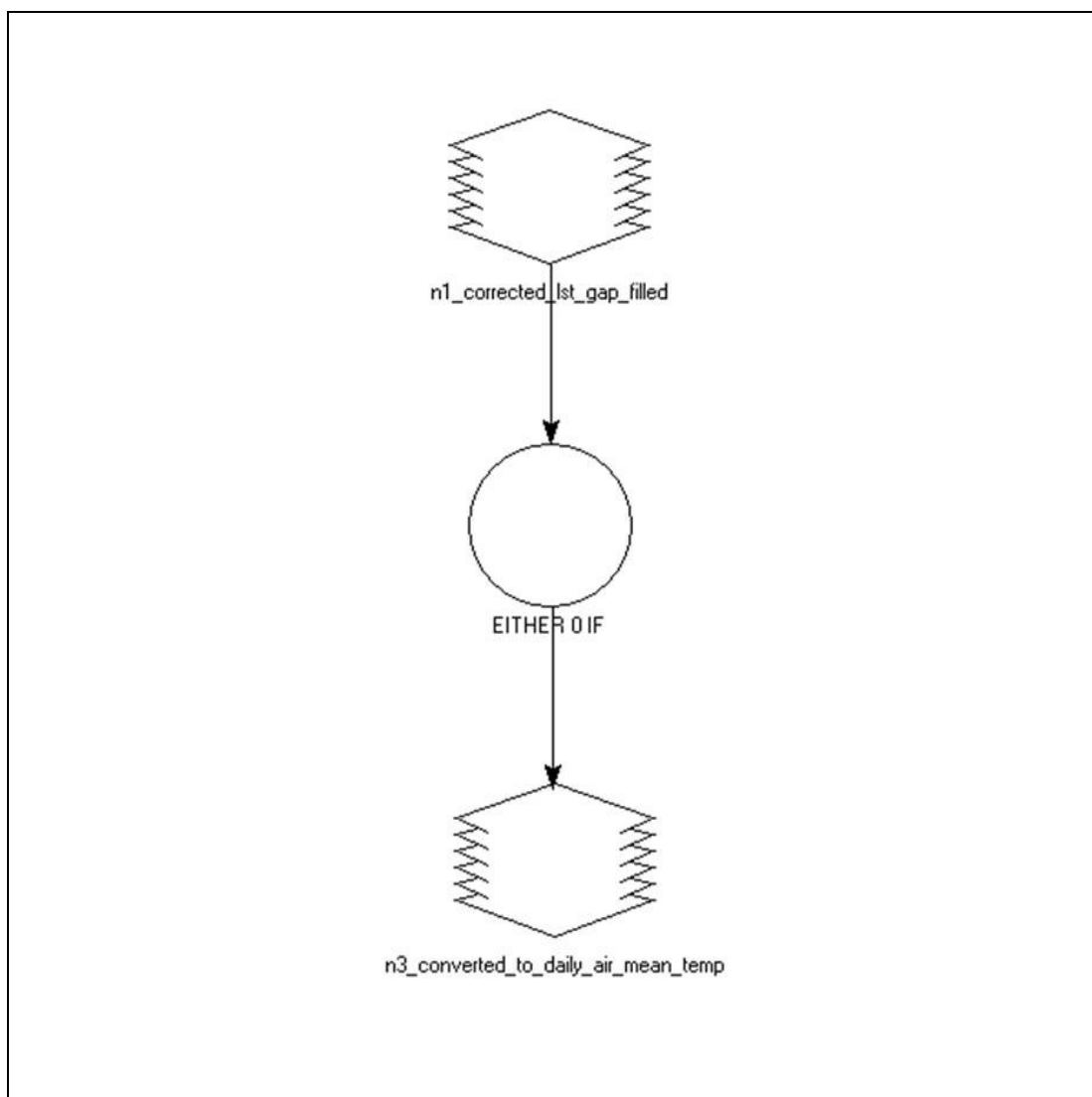


Figure AII.8: Graphical interface for converting T_s into \bar{T}_a .

The data type of the output files were “Un-signed 16 bit” and it set “Ignore zero” in the stats calculation. This modelling was done for MODIS-based equivalent air temperature calculation.

5. Daily & 8-day GDD calculation: Using the \bar{T}_a and the base temperature, daily and 8-day GDD was calculated as follows:

Input image: converted_to_daily_air_mean_temp.img

Output image: Daily & 8-day GDD

The following equation was used for this calculation:

EITHER 0 IF (\$n1_converted_to_daily_air_mean_temp <=27815) OR
 (\$n1_converted_to_daily_air_mean_temp - 27815) OTHERWISE

(STACK SUM (\$n3_daily_gdd) *8)/100

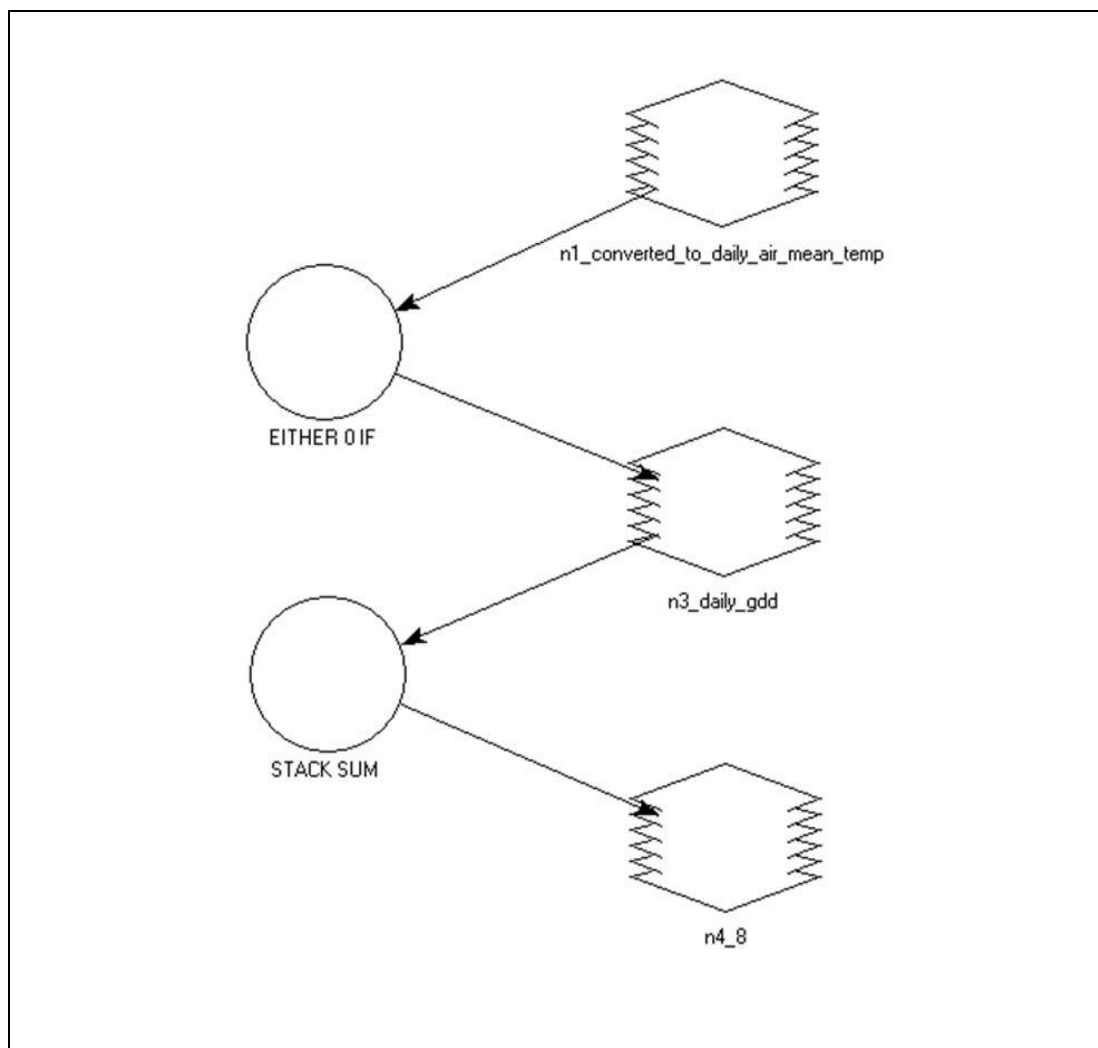


Figure AII.9: Graphical interface for GDD calculation.

The data type of the output files were “Un-signed 16 bit” and it set “Ignore zero” in the stats calculation. This modelling was done for GDD calculation.

6. Enhanced GDD calculation: Using the data fusion technique, GDD was enhanced from 1 km to 500 m spatial resolution as follows:

Input image: Low-pass filtering, stack_EVI, stack_GDD

Output image: Enhanced GDD

The following equation was used for this calculation:

FOCAL MEAN (\$n1_stack_evi (38), \$n2_Low_Pass)

EITHER 0 IF ((\$n6_memory ==0) or (\$n1_stack_evi (38) ==0)) OR
\$n1_stack_evi (38)/\$n6_memory OTHERWISE

CONDITIONAL {(((\$n16_memory ==0) or (\$n13_stack_gdd_of_8day (27) ==0))
0,
(\$n13_stack_gdd_of_8day (27) >0) \$n13_stack_gdd_of_8day
(27)*\$n16_memory}

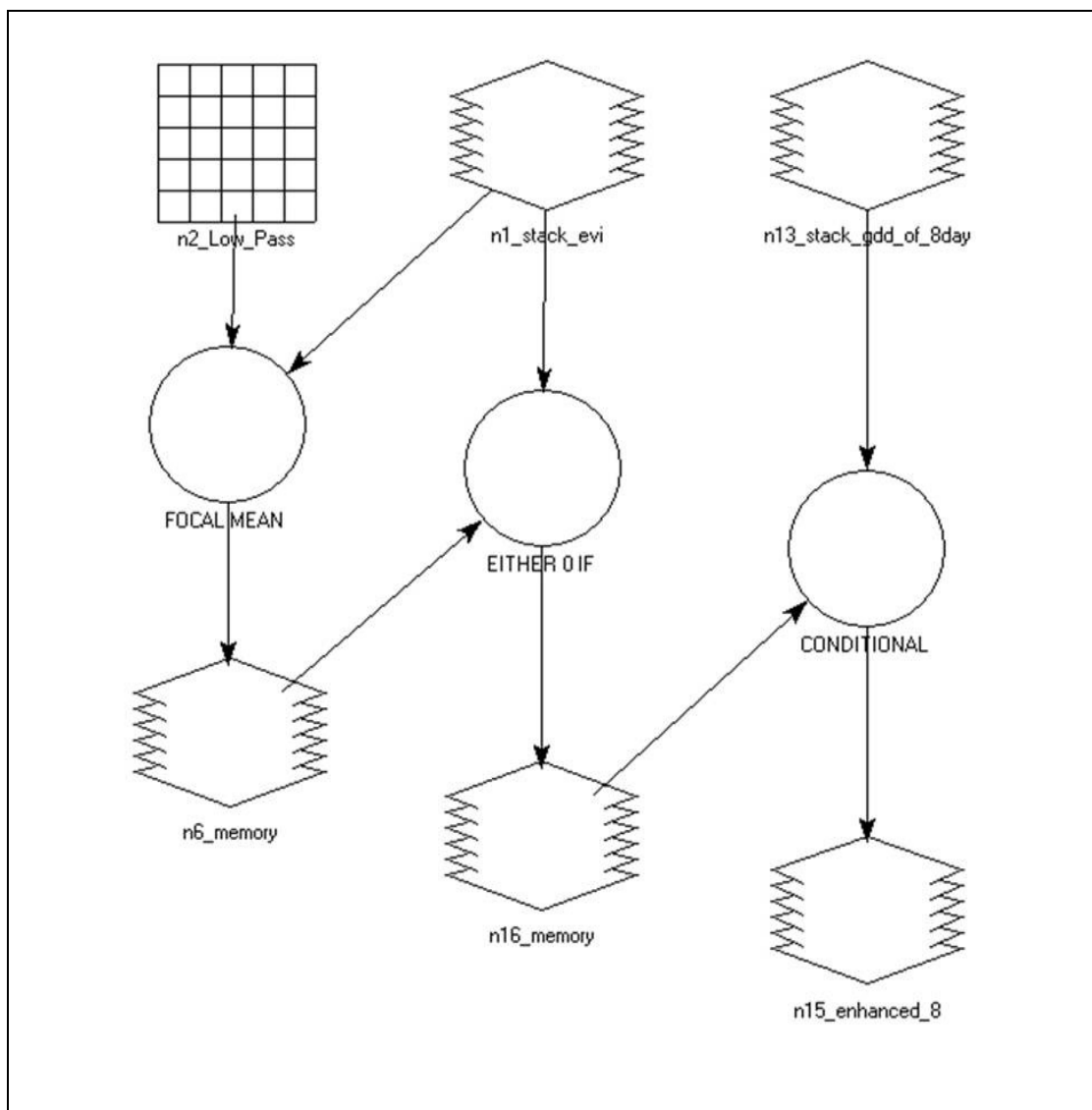


Figure AII.10: Graphical interface for enhancing 1 km GDD into 500 m spatial resolution.

The data type of the output files were “Un-signed 16 bit” and it set “Ignore zero” in the stats calculation. This modelling was done for enhanced GDD calculation.

7. Accumulated GDD calculation: Using the enhanced GDD, AGDD was calculated at 500 m spatial resolution throughout the growing season as follows:

Input image: Stack_8-day_gdd_089-297_500m_07.img, all successive accumulated 8-day GDD layers

Output image: cumulative accumulated_gdd_stack.img

The following equation was used for this calculation:

\$n1_stack_8 (27) + \$n53_temp

STACKLAYERS (\$n3_temp, \$n5_temp, \$n7_temp, \$n9_temp, \$n11_temp, \$n13_temp, \$n15_temp, \$n17_temp, \$n19_temp, \$n21_temp, \$n23_temp, \$n25_temp, \$n27_temp, \$n29_temp, \$n31_temp, \$n33_temp, \$n35_temp, \$n37_temp, \$n39_temp, \$n41_temp, \$n43_temp, \$n45_temp, \$n47_temp, \$n49_temp, \$n51_temp, \$n53_temp, \$n55_memory)

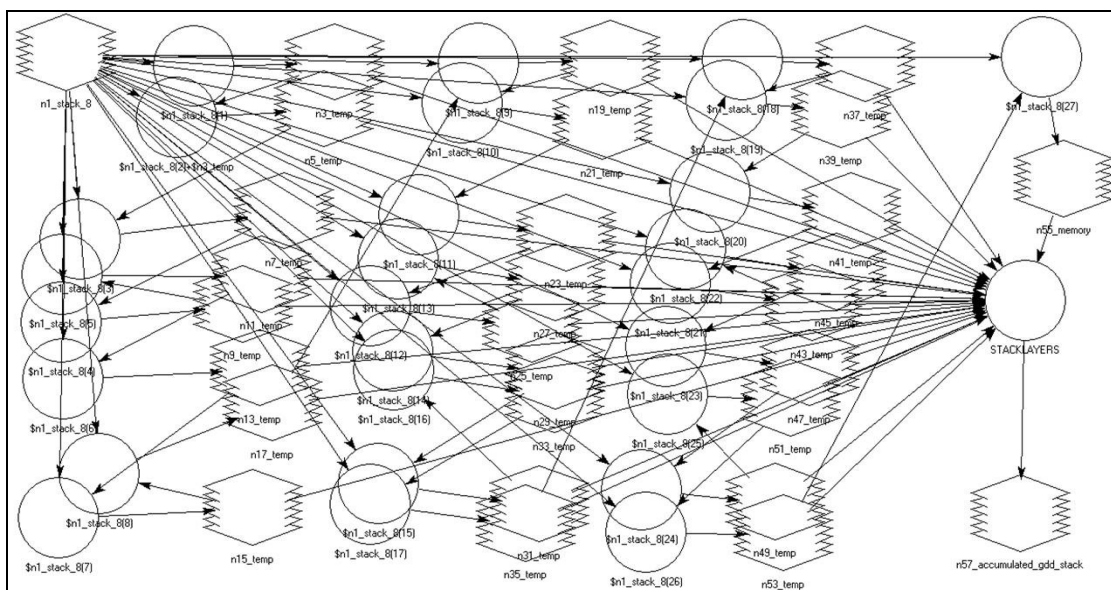


Figure AII.11: Graphical interface for cumulative AGDD calculation.

The data type of the output files were “Un-signed 32 bit” and it set “Ignore zero” in the stats calculation. This modelling was done for AGDD calculation.

8. Generating DLO/GGS spatial maps: Using the AGDD thresholds, the spatial dynamics of DLO/GGS were modeling as following equations:

(i) Stack min on the basis of AGDD threshold:

Input image: cumltv_lyrs_8-day_gdd_089-297_500m

Output image: stack_min_agdd_value

The following equation was used for this calculation:

EITHER 3000000 IF (\$n1_cumltv_lyrs_8 < 7999) OR \$n1_cumltv_lyrs_8

OTHERWISE

STACK MIN (\$n3_memory)

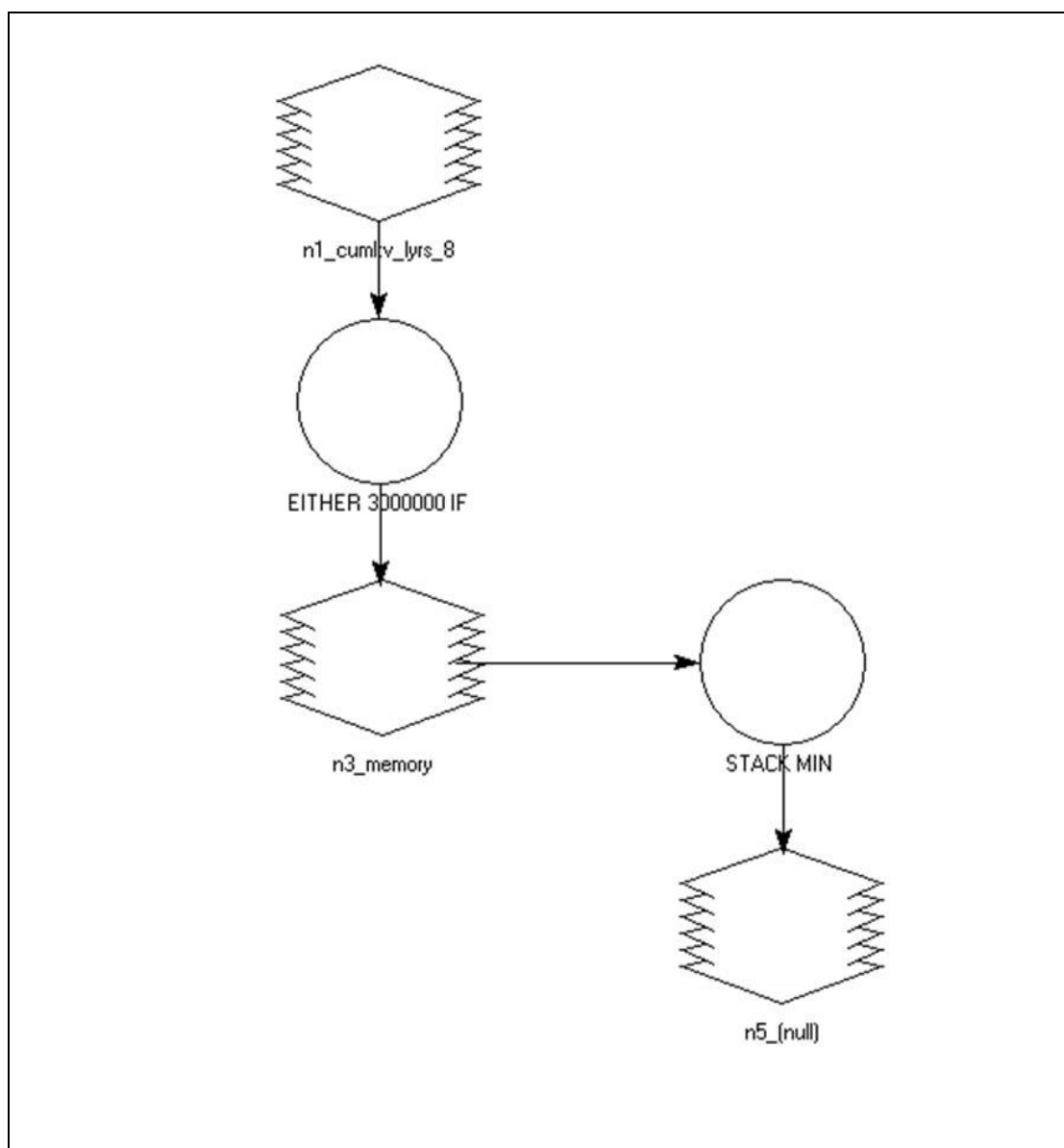


Figure AII.12: Graphical interface for calculating the stack min on the basis of AGDD threshold.

The data type of the output files were “Un-signed 32 bit” and it set “Ignore zero” in the stats calculation. This modelling was done for DLO/GGS spatial maps generation.

(ii) Indexing on the basis of stack min:

Input image: cumltv_lyrs_8-day_gdd_089-297_500m, stack_min_agdd_value.img

Output image: index_dlo/ggs.img

The following equation was used for this calculation:

$$\text{INDEX} \left(\$n1_stack_min_agdd_value \right) \{ \$n2_cumltv_lyrs_8(1) , \\ \$n2_cumltv_lyrs_8(2) , \$n2_cumltv_lyrs_8(3) , \$n2_cumltv_lyrs_8(4), \\ \$n2_cumltv_lyrs_8(5), \$n2_cumltv_lyrs_8(6), \$n2_cumltv_lyrs_8(7), \\ \$n2_cumltv_lyrs_8(8), \$n2_cumltv_lyrs_8(9), \$n2_cumltv_lyrs_8(10), \\ \$n2_cumltv_lyrs_8(11), \$n2_cumltv_lyrs_8(12), \$n2_cumltv_lyrs_8(13), \\ \$n2_cumltv_lyrs_8(14), \$n2_cumltv_lyrs_8(15), \$n2_cumltv_lyrs_8(16), \\ \$n2_cumltv_lyrs_8(17), \$n2_cumltv_lyrs_8(18), \$n2_cumltv_lyrs_8(19), \\ \$n2_cumltv_lyrs_8(20), \$n2_cumltv_lyrs_8(21), \$n2_cumltv_lyrs_8(22), \\ \$n2_cumltv_lyrs_8(23), \$n2_cumltv_lyrs_8(24), \$n2_cumltv_lyrs_8(25), \\ \$n2_cumltv_lyrs_8(26), \$n2_cumltv_lyrs_8(27) \}$$

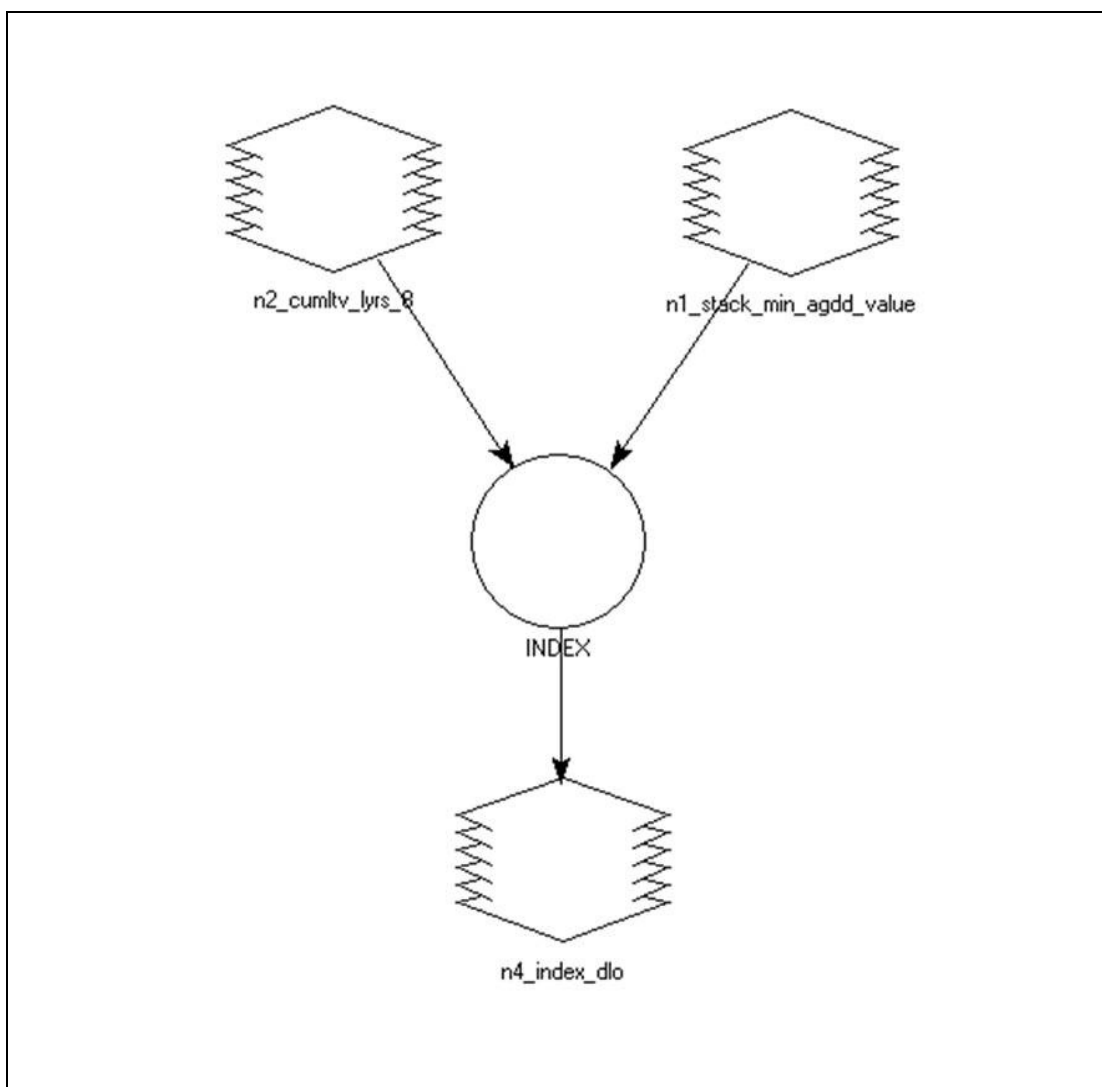


Figure AII.13: Graphical interface for indexing on the basis of stack min.

The data type of the output files were “Un-signed 8 bit” and it set “Ignore zero” in the stats calculation. This modelling was done for DLO/GGS spatial maps generation.

(iii)DLO/GGS Spatial maps:

Input image: index_dlo/ggs.img

Output image: dlo/ggs_periodic_map.img

The following equation was used for this calculation:

EITHER 0 IF (\$n1_index_dlo==0) OR (\$n1_index_dlo+11) OTHERWISE

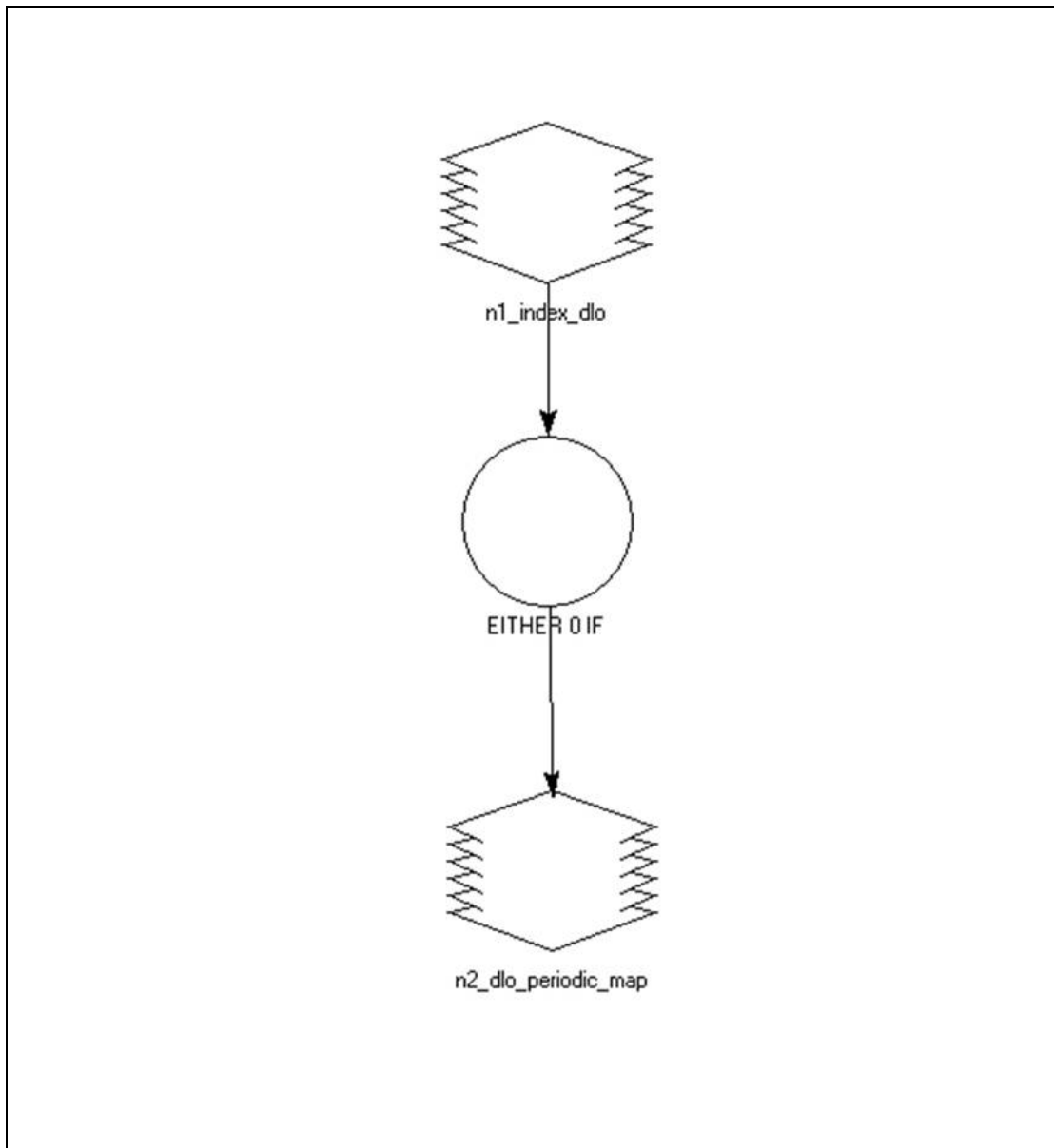


Figure AII.14: Graphical interface for generating the spatial dynamics for DLO and GGS.

The data type of the output files were “Un-signed 8 bit” and it set “Ignore zero” in the stats calculation. This modelling was done for DLO/GGS spatial maps generation.

9. Generating DLF spatial maps: Using the \bar{T}_a threshold, the spatial dynamics of DLF was modeling as following equations:

(i) Stack min on the basis of \bar{T}_a threshold:

Input image: converted_air-mean-temp.img

Output image: stack_min_temp_value_dlf.img

The following equation was used for this calculation:

```
EITHER 3000000 IF ($n1_converted_air < 27715) OR $n1_converted_air  
OTHERWISE
```

```
STACK MIN ($n3_memory)
```

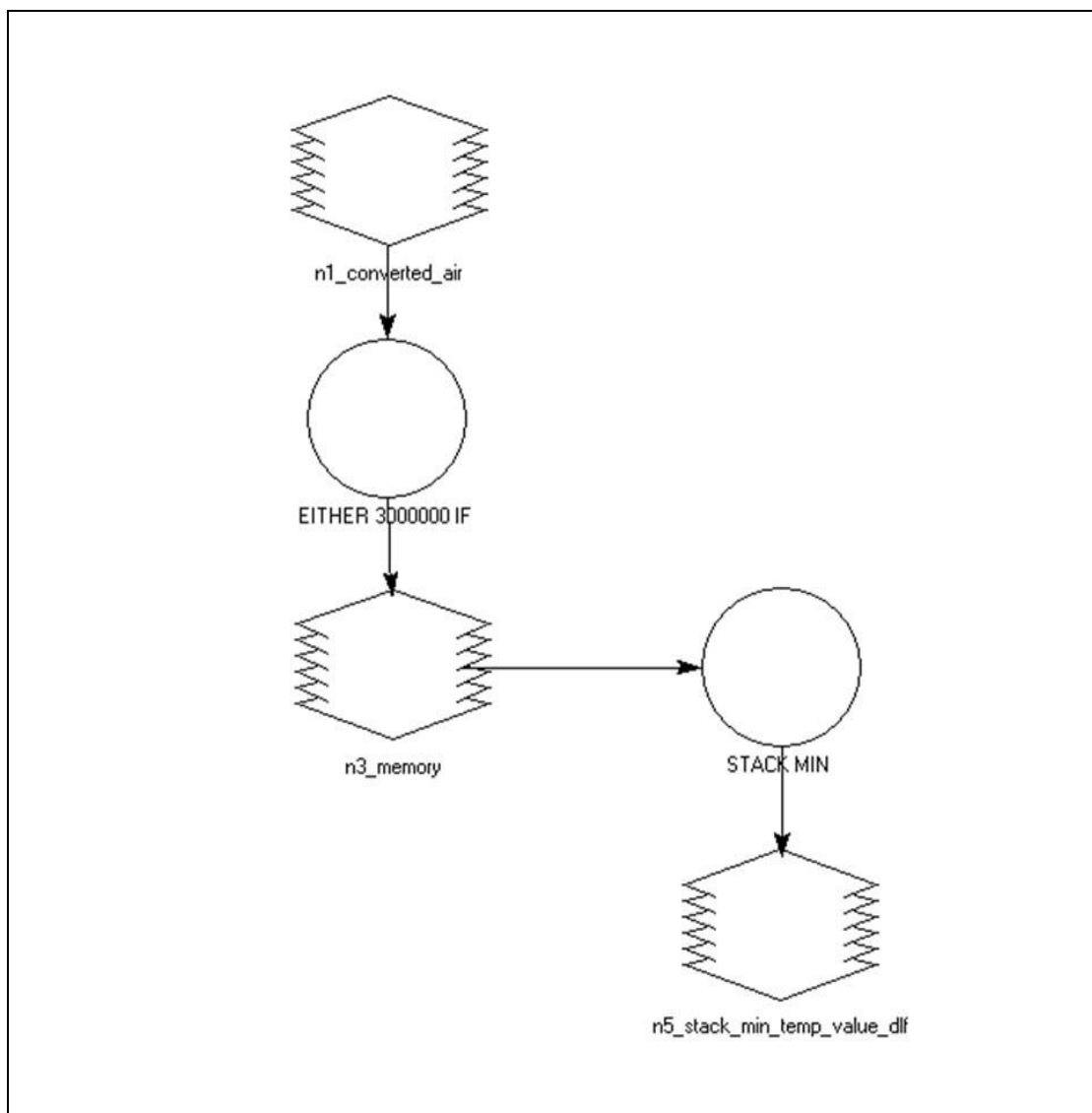



Figure AII.15: Graphical interface for calculating the stack min on the basis of \bar{T}_a threshold.

The data type of the output files were “Un-signed 32 bit” and it set “Ignore zero” in the stats calculation. This modelling was done for DLF spatial map generation.

(ii) Indexing on the basis of stack min:

Input image: converted_air-mean-temp.img, stack_min_ \bar{T}_a _value.img

Output image: index_dlf.img

The following equation was used for this calculation:

INDEX (\$n1_stack_min_) { \$n2_converted_air(1) , \$n2_converted_air(2) ,
 \$n2_converted_air(3) , \$n2_converted_air(4), \$n2_converted_air(5),
 \$n2_converted_air(6), \$n2_converted_air(7), \$n2_converted_air(8),
 \$n2_converted_air(9), \$n2_converted_air(10), \$n2_converted_air(11),
 \$n2_converted_air(12), \$n2_converted_air(13) }

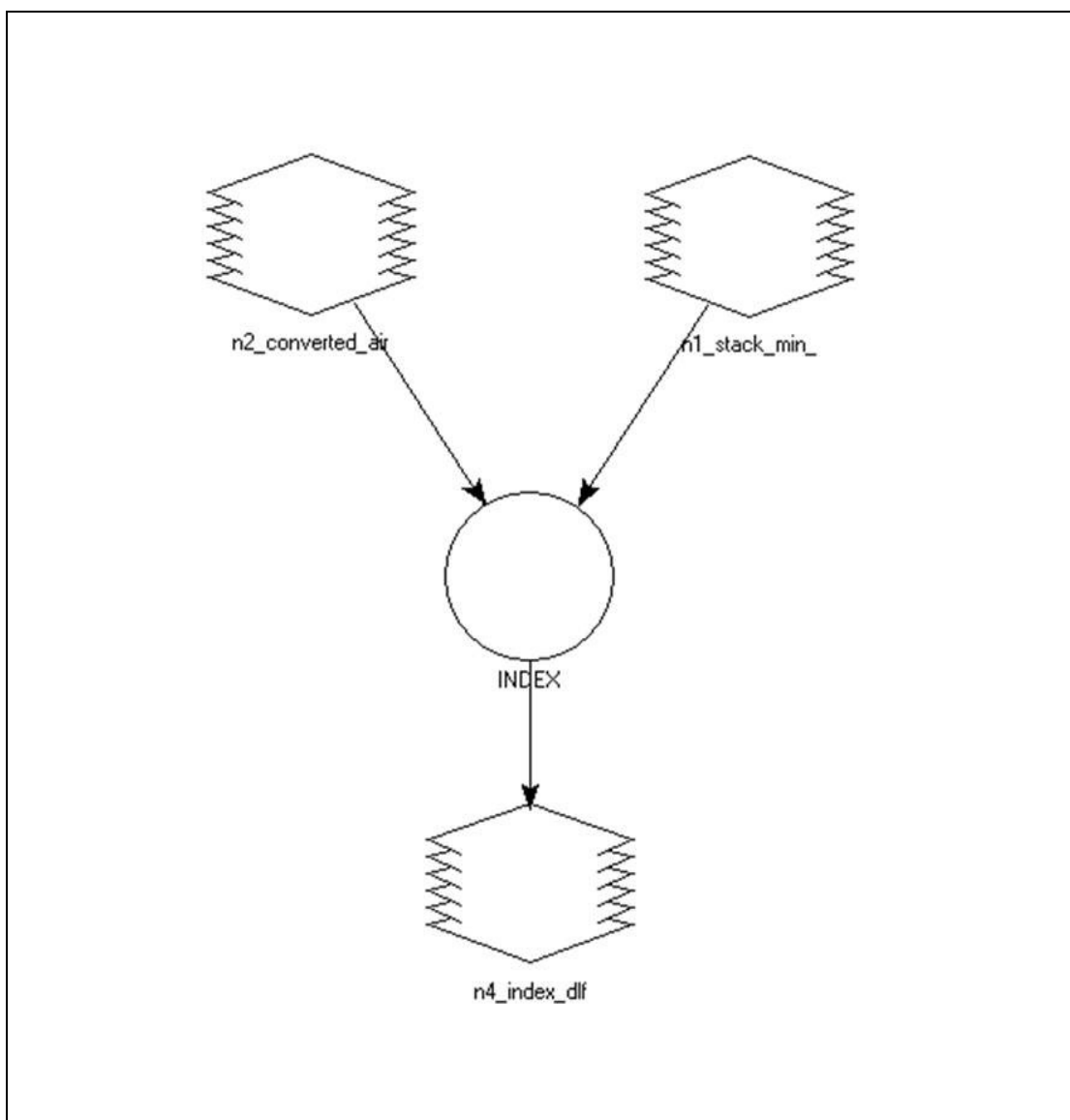


Figure AII.16: Graphical interface for Indexing on the basis of stack min for DLF.

The data type of the output files were “Un-signed 8 bit” and it set “Ignore zero” in the stats calculation. This modelling was done for DLF spatial map generation.

(iii)DLF Spatial map:

Inputimage: index_dlf.img

Output image: dlf_periodic_map.img

The following equation was used for this calculation:

EITHER 0 IF (\$n1_index_dlf==0) OR (\$n1_index_dlf+25) OTHERWISE

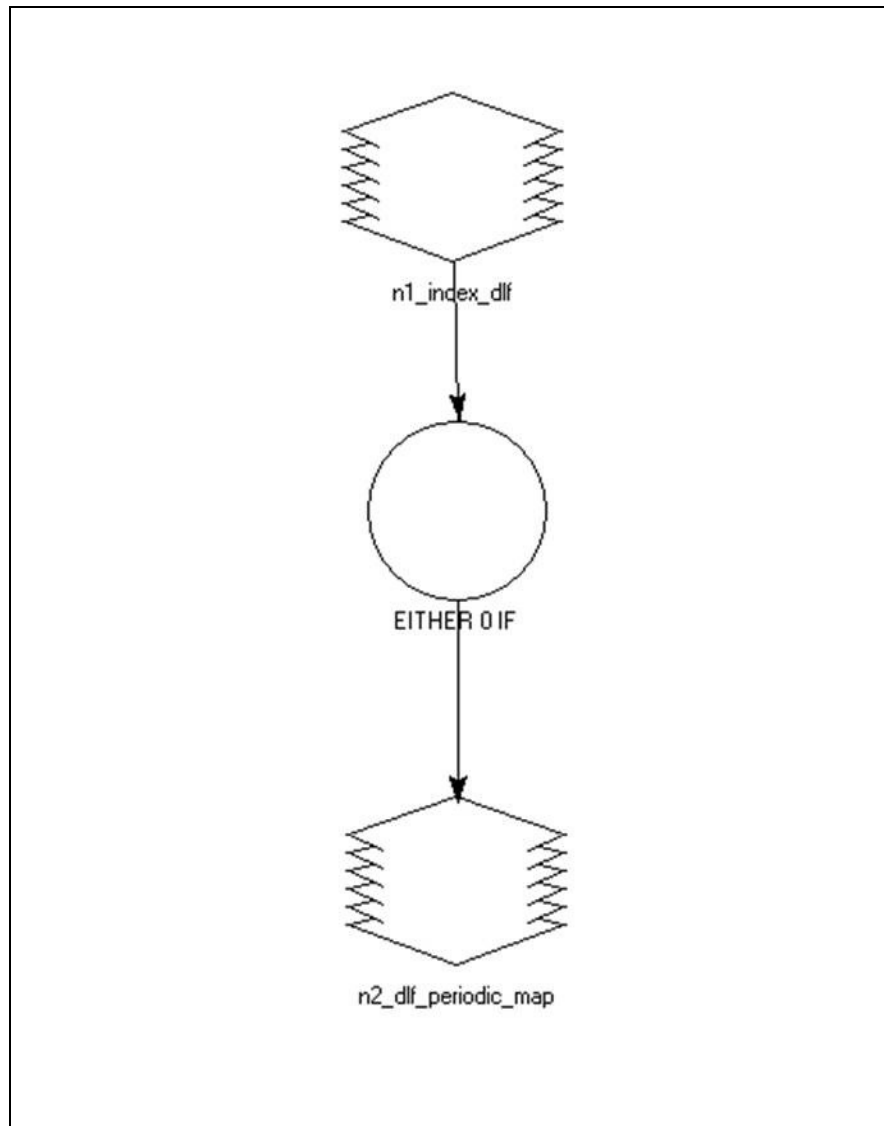


Figure AII.17: Graphical interface for generating the spatial dynamics for DLF.

The data type of the output files were “Un-signed 8 bit” and it set “Ignore zero” in the stats calculation. This modelling was done for DLF spatial map generation.

10. Classified spatial dynamics: According to Alberta SRD classified map for DLO/DLF and MODIS-based land cover map for GGS for the forest area. For example:

Input image: dlo_periodic_map and classified map for dlo/dlf

Output image: final_dlo/dlf/ggs_spatial_dynamics_map

The following equation was used for this calculation:

```
EITHER $n1_2 IF ($n2_re == 5 OR $n2_re == 55 OR $n2_re == 57 OR $n2_re  
== 58 OR $n2_re == 155 OR $n2_re == 157 OR $n2_re == 158) OR 0  
OTHERWISE
```

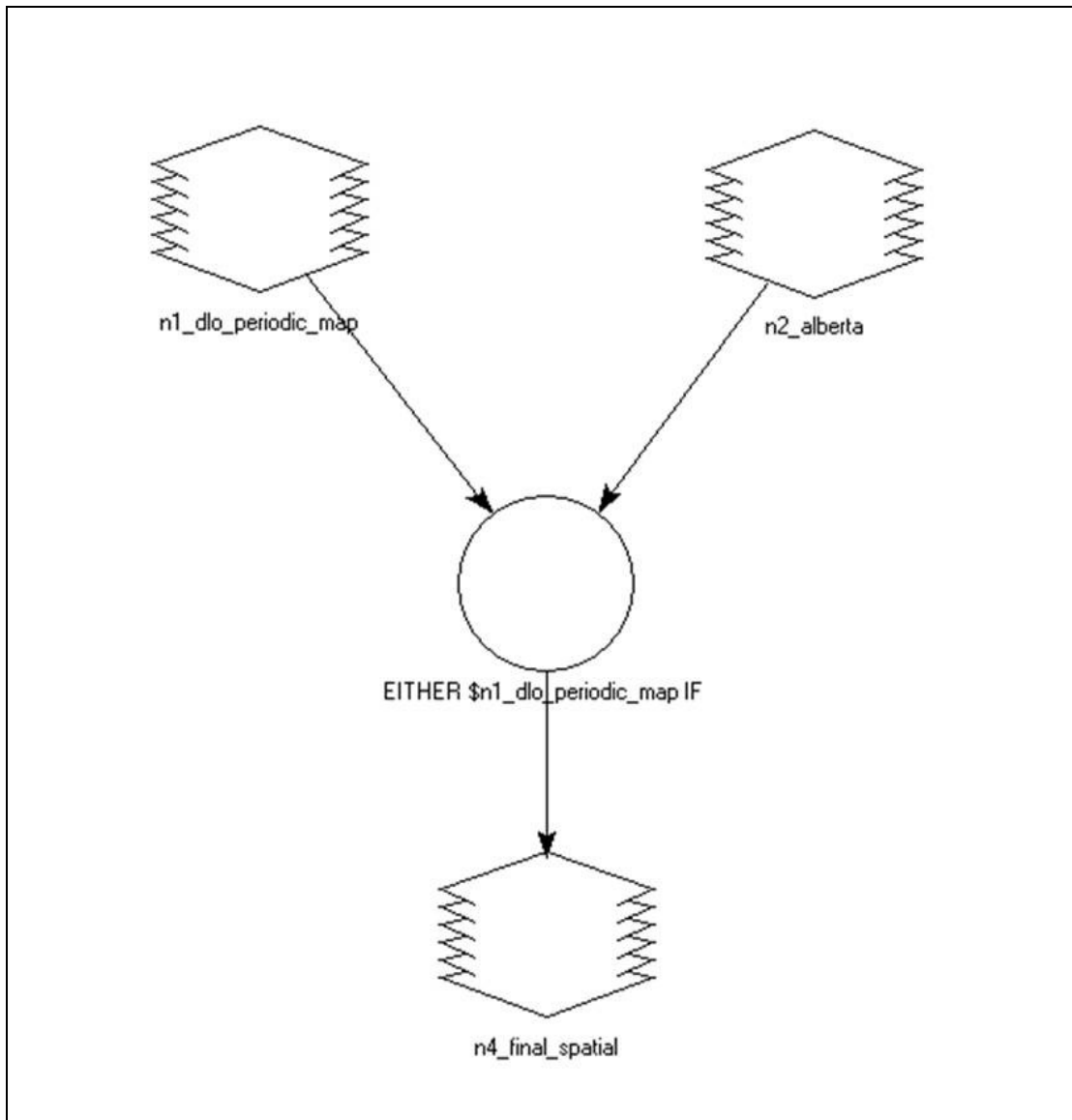


Figure AII.18: Classified map of generating the spatial dynamics for DLO/DLF/GGS.

The data type of the output files were “Un-signed 8 bit” and it set “Ignore zero” in the stats calculation. This modelling was done for classify the DLO/DLF/GGS stands for spatial map generation.